available at www.sciencedirect.com

ScienceDirect

www.elsevier.com/locate/brainres

BRAIN RESEARCH

Research Report

Spikes, synchrony, and attentive learning by laminar thalamocortical circuits

*Stephen Grossberg**, *Massimiliano Versace*[1]

Department of Cognitive and Neural Systems, Center for Adaptive Systems, Center of Excellence for Learning in Education, Science, and Technology, Boston University, 677 Beacon Street, Boston, MA 02215, USA

ARTICLE INFO

Article history:
Accepted 4 April 2008
Available online 22 April 2008

Keywords:
Attention
Learning
STDP
Bottom-up filter
Top-down expectation
Match
Prediction
Mismatch
LGN
Pulvinar
V1
V2
Spikes
Gamma oscillations
Beta oscillations
Synchronization
Local field potentials
Mismatch negativity
Acetylcholine
Cortical layers
Adaptive Resonance Theory

ABSTRACT

This article develops the Synchronous Matching Adaptive Resonance Theory (SMART) neural model to explain how the brain may coordinate multiple levels of thalamocortical and corticocortical processing to rapidly learn, and stably remember, important information about a changing world. The model clarifies how bottom-up and top-down processes work together to realize this goal, notably how processes of learning, expectation, attention, resonance, and synchrony are coordinated. The model hereby clarifies, for the first time, how the following levels of brain organization coexist to realize cognitive processing properties that regulate fast learning and stable memory of brain representations: single-cell properties, such as spiking dynamics, spike-timing-dependent plasticity (STDP), and acetylcholine modulation; detailed laminar thalamic and cortical circuit designs and their interactions; aggregate cell recordings, such as current source densities and local field potentials; and single-cell and large-scale inter-areal oscillations in the gamma and beta frequency domains. In particular, the model predicts how laminar circuits of multiple cortical areas interact with primary and higher-order specific thalamic nuclei and nonspecific thalamic nuclei to carry out attentive visual learning and information processing. The model simulates how synchronization of neuronal spiking occurs within and across brain regions, and triggers STDP. Matches between bottom-up adaptively filtered input patterns and learned top-down expectations cause gamma oscillations that support attention, resonance, learning, and consciousness. Mismatches inhibit learning while causing beta oscillations during reset and hypothesis testing operations that are initiated in the deeper cortical layers. The generality of learned recognition codes is controlled by a vigilance process mediated by acetylcholine.

* *Corresponding author*. Department of Cognitive and Neural Systems, Boston University, 677 Beacon Street, Boston, MA 02215, USA. Fax: +1 617 353 7755.
E-mail addresses: steve@bu.edu, steve@cns.bu.edu (S. Grossberg), versace@cns.bu.edu (M. Versace).
URL: http://cns.bu.edu/~steve (S. Grossberg), http://cns.bu.edu/~versace (M. Versace).

[1] Authors in alphabetical order. MV was supported in part by the Air Force Office of Scientific Research (AFOSR F49620-01-1-0397), the National Science Foundation (NSF SBE-0354378), and the Office of Naval Research (ONR N00014-01-1-0624). SG was supported in part by the National Science Foundation (NSF SBE-0354378) and the Office of Naval Research (ONR N00014-01-1-0624).

0006-8993/$ – see front matter © 2008 Elsevier B.V. All rights reserved.
doi:10.1016/j.brainres.2008.04.024

1. Introduction

1.1. *The link between learning, expectation, attention, resonance, and synchrony*

This article proposes how the brain coordinates multiple levels of thalamocortical and corticocortical processing to rapidly learn, and stably remember, important information about the world. The Synchronous Matching Adaptive Resonance Theory (SMART) model that is presented here shows how bottom-up and top-down pathways work together to accomplish this goal by coordinating processes of learning, expectation, attention, resonance, and synchrony. In particular, SMART explains how attentive learning requirements are realized by detailed brain circuits, notably the layered organization of cells in neocortical circuits and how they interact with first-order (e.g., the lateral geniculate nucleus, LGN) and higher-order (e.g., the pulvinar nucleus, PULV; Sherman and Guillery, 2001; Shipp, 2003), and nonspecific thalamic nuclei (van Der Werf et al., 2002).

Corticothalamocortical pathways work in parallel with corticocortical routes (Maunsell and Van Essen, 1983; Salin and Bullier, 1995; Sherman and Guillery, 2002). Specific first-order thalamic nuclei relay sensory information to the cerebral cortex, whereas specific second-order thalamic nuclei receive their main input from layer 5 of lower-order cortical areas and relay this information to higher-order cortical areas (Sherman and Guillery, 2002, Fig. 1a).

The SMART model clarifies how a *match* at the specific first-order and higher-order thalamic nuclei may induce fast learning and stable memory of neural representations in the thalamocortical system (cf., Gove et al., 1995; Grossberg, 1980, 2003). Such a match may occur, for example, at LGN cells in response to bottom-up driving retinal inputs and top-down modulatory expectations from layer 6 of cortical area V1 (Sillito et al., 1994). At a higher level of brain organization, a match may occur at pulvinar cells in response to driving bottom-up inputs from layer 5 of V1 (Rockland et al., 1999) and top-down modulatory cortical inputs from layer 6 of V2. The model proposes how this bottom-up/top-down matching process can allow bottom-up and top-down feedback loops to cause a persistent resonant state which supports spike synchronization in the gamma frequency range (20–70 Hz). Such an oscillation frequency is fast enough to support spike-timing-dependent plasticity (STDP; Levy and Steward, 1983; Markram et al., 1997; Bi and Poo, 2001), since STDP is maximal when pre-synaptic and post-synaptic cells fire within 10–20 ms of each other (Traub et al., 1998; Wespatat et al., 2004). In contrast, during a mismatch, slower beta frequency (4–20 Hz) oscillations are caused. STDP is disabled at this lower frequency. The model hereby proposes how thalamocortical matching, resonant feedback, synchronous oscillations, and STDP learning may be coordinated, notably how match-sensitive differences in oscillation frequency can enable or disable learning.

The matching process is carried out by a top-down, modulatory on-center, off-surround circuit (Grossberg and

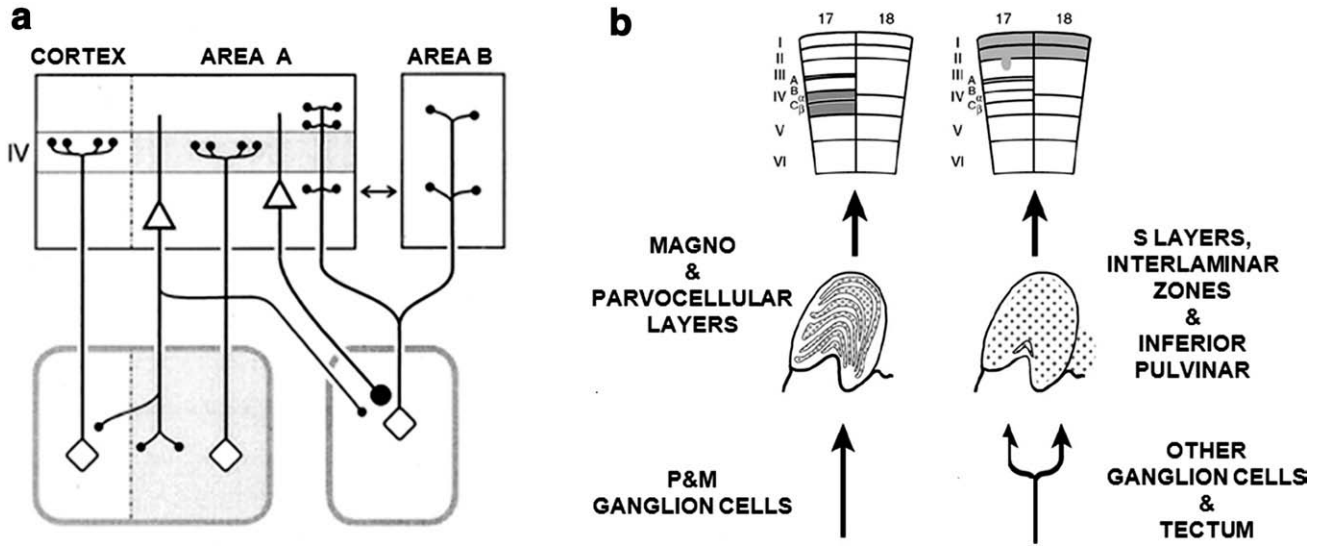

Fig. 1 – (a) A cortical area A receives thalamocortical inputs from the corresponding thalamic sector (thalamocortical neuron in the gray zone). Layer 6 neurons from cortical area A send modulatory feedback projections (small endings) to the corresponding and to nearby thalamic sectors, as well as a modulatory projection to the thalamic nucleus of a higher-order thalamocortical loop (area B), where driving connections (giant endings) originating in layer 5 neurons of cortical area A are found. These driving connections can activate the thalmocortical pathway to layer IV in area B. This corticothalamocortical indirect pathway supplements the direct corticocortical pathway (double-headed arrow) from A to B. Dashed lines correspond to the border of each thalamocortical loop. [Modified and reprinted with permission from Rouiller and Welker (2000)]. (b) Schematic views of the diffuse and specific subcortical inputs that terminate in the matrix and core compartments of the dorsal lateral geniculate nuclei of macaque monkeys, and the layer-specific and diffuse or focused projections of these compartments to the cerebral cortex. Cortical areas are indicated by schematic vertical sections with the layers indicated. [Modified and reprinted with permission from Jones (2002)].

Stone, 1986; Carpenter and Grossberg, 1987, 1991; Grossberg, 1995, 1999a) which selects a *critical feature pattern* of attended features, while inhibiting unattended features. This process clarifies how attention carries out a form of "biased competition" (Desimone and Duncan, 1995; Desimone, 1998). The attended feature patterns are the ones that can be rapidly learned in the adaptive weights of bottom-up adaptive filters and top-down expectations. In the case of a partial mismatch, there may simultaneously be cells at which matching and learning occurs, as well as other cells at which mismatch, inhibition, and suppression of learning occurs. Thus, in describing match vs. mismatch states, one needs to understand that there may be cells at which bottom-up and top-down signals mismatch, even though there is a good enough partial match for a synchronous resonant state to persist long enough for STDP to occur at the matched features.

If a mismatch between bottom-up and top-down signal patterns is large enough, it prevents such a synchronous resonant state from developing. Within the model, resonance is prevented when mismatch causes a rapid *reset* of ongoing information processing, and triggers a memory search, or hypothesis testing, for uncommitted cells, or an already familiar recognition category that can better match bottom-up data. In particular, such a memory search can enable either a totally new recognition category to be learned, or a learned refinement of the critical features that can activate an already familiar recognition category. Thus, the model proposes that there are cycles of resonance and reset, with resonance supporting learning, and reset driving hypothesis testing that leads away from poorly matched states to better ones.

START clarifies how such a memory search may be controlled by an interaction between specific thalamic nuclei, nonspecific thalamic nuclei, and the cerebral cortex. The SMART model (Figs. 2 and 3) predicts how a big enough mismatch at a specific thalamic nucleus can generate a novelty-sensitive burst of activation at a nonspecific thalamic nucleus. Nonspecific thalamic nuclei, such as the midline and intralaminar nuclei (van Der Werf et al., 2002), as well as "matrix" cells in the specific thalamic nuclei (Jones, 2002), derive their name from the fact that they receive diffuse innervations from the sensory periphery and the reticular

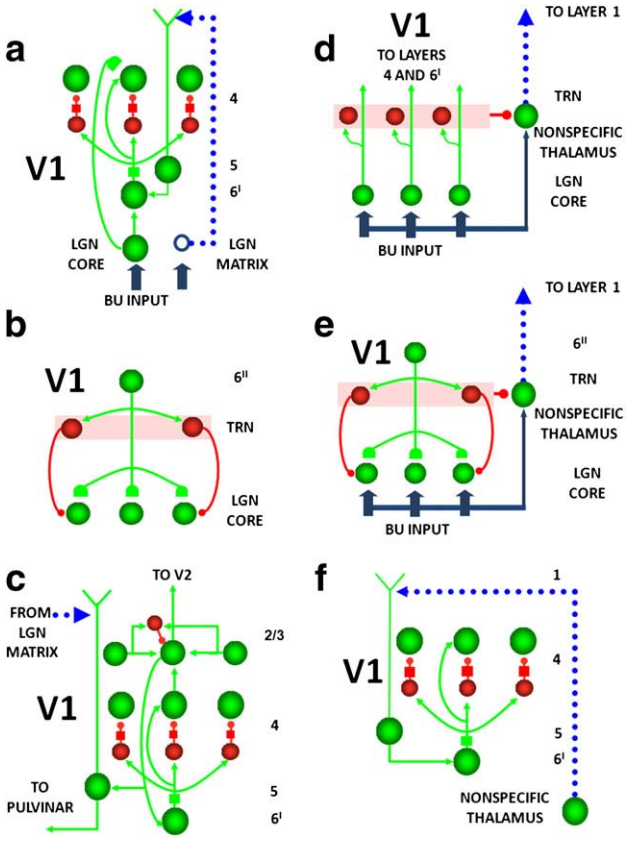

Fig. 2 – (a) LGN core cells in the specific pathway activate layer 4. LGN core cells also send axons to layer 6^I cells, and thereby also activate layer 4 via a $6^I \rightarrow 4$ modulatory on-center, off-surround network that implements divisive contrast normalization of LGN inputs in layer 4. Layer 4 cells, in turn, activate cells in layer 2/3. In parallel, LGN matrix cell activation in the nonspecific pathway primes layer 5 cortical cells via excitatory connections to cortical layer 1, where layer 5 apical dendrites terminate. Layer 5 cells fire only when *both* matrix cells and layer 2/3 cells fire. Matrix cells hereby enable layer 5 cells to fire in response to layer 2/3 inputs, thereby closing closes the intracortical $4 \rightarrow 2/3 \rightarrow 5 \rightarrow 6^I \rightarrow 4$ resonant loop while activating driving inputs from layer 5 to the PULV. (b) Top-down feedback from V1 layer 6^{II} has a dual effect on LGN core cells: excitation via adaptive synapses (hemi-disks at ends of axonal pathways) and broad inhibition via the thalamic reticular nucleus (TRN) pathway. (c) Layer 2/3 cell outputs feed back to layer 5 cells, which can fire if matrix cells also input to the layer 1 apical dendrites of layer 5 cells. Layer 5 cell firing can, in turn, activate layer 6^I cells that activate layer 4 cells. Matrix cells hereby enable layer 5 cells to close the intracortical $4 \rightarrow 2/3 \rightarrow 5 \rightarrow 6^I \rightarrow 4$ resonant loop, even while they activate driving inputs from layer 5 to the PULV. (d) During bottom-up processing, bottom-up inputs send convergent excitatory signals to the nonspecific thalamus. In parallel, LGN core cells send specific inputs to layers 4 and 6^I of the cortex, as well as to TRN cells. The TRN cells, in turn, send convergent inhibition to the nonspecific thalamus. During bottom-up processing, the total excitatory and inhibitory signals are balanced, so that the nonspecific thalamus is not activated by the bottom-up input. (e) During top-down matching, layer 6^{II} cells excite TRN cells which, in turn, send inhibitory signals via a broad off-surround to LGN core cells. This inhibition helps to prevent cells that receive only bottom-up or top-down signals from firing, but not cells that receive both. Only LGN cells that receive *matching* bottom-up input and top-down cortical feedback cross the spiking threshold and propagate their activity to V1, while also (see (d)) exciting the TRN and inhibiting the nonspecific thalamus. (f) If a bottom-up/top-down mismatch is too great, then the decrease of LGN excitation reduces TRN inhibition to the nonspecific thalamus. The firing rate of the nonspecific thalamus hereby increases, which propagates via the apical dendrites of layer 5 cortical cells to cause a reset of active coding cells in layer 4 (see text).

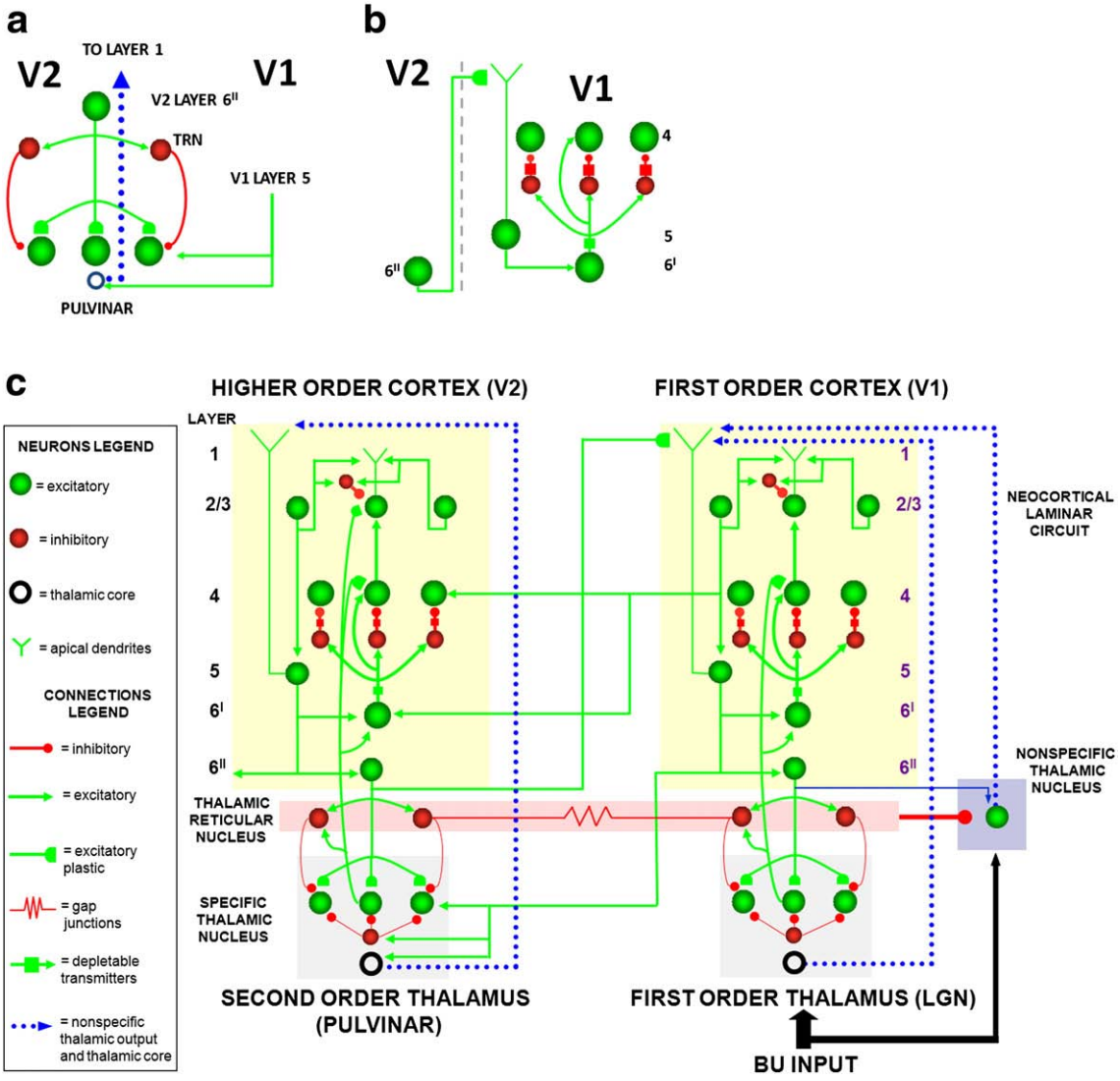

Fig. 3 – (a) Layer 5 of V1 provides a driving bottom-up input to the pulvinar (PULV), which is matched against top-down signals from layer 6^{II} of V2. This circuit is homologous to the bottom-up driving input from the retina to the LGN, which is matched against top-down signals from layer 6^{II} of V1 (see Fig. 2). Layer 5 of V1 also excites PULV matrix cells, which provide nonspecific priming input to layer 5 cells in V2. (b) Layer 6^{II} of V2 also provides top-down corticocortical feedback to layer 4 of V1 via layer 1 apical dendrites of layer 5 cells that project to layer 6^{I} and then to 4 via a modulatory on-center, off-surround circuit. (c) The entire SMART model circuit includes thalamic nuclei and laminar cortical circuits. The thalamus is subdivided into specific first-order and second-order nuclei, nonspecific nucleus, and thalamic reticular nucleus (TRN). The first-order thalamic matrix cells (1 cell population at each specific thalamic nucleus, shown as an open ring) provide nonspecific excitatory priming to layer 1 in response to bottom-up input, priming layer 5 cells and allowing them to respond to layer 2/3 input. This allows layer 5 to close the intracortical loop and activate the PULV. V1 layer 4 receives inputs from two parallel bottom-up thalamocortical pathways: a direct LGN→4 excitatory input, and a 6^{I}→4 modulatory on-center, off-surround network that contrast-normalizes the pattern of layer 4 activation via the recurrent 4→2/3→5→6^{I}→4 loop. V1 activates the bottom-up V1→V2 corticocortical pathways from V1 layer 2/3 to V2 layers 6^{I} and 4, as well as the bottom-up corticothalamocortical pathway from V1 layer 5 to the PULV, which projects to V2 layers 6^{I} and 4. In V2, as in V1, the layer 6^{I}→4 pathway provides divisive contrast normalization to V2 layer 4 cells. Corticocortical feedback from V2 layer 6^{II} reaches V1 layer 1, where it activates apical dendrites of layer 5 cells. Layer 5 cells, in turn, activate the modulatory 6^{I}→4 pathway in V1, which projects a V1 top-down expectation to the LGN. TRN cells of the two thalamic sectors are linked via gap junctions, which synchronize activation across the two thalamocortical sectors when processing bottom-up stimuli. The nonspecific thalamic nucleus receives convergent bottom-up excitatory input from specific thalamic nuclei and inhibition from the TRN, and projects to layer 1 of the laminar cortical circuit, where it regulates mismatch-activated reset and hypothesis testing in the cortical circuit (see text). Corticocortical feedback connections from layer 6^{II} of the higher cortical area terminate in layer 1 of the lower cortical area, whereas corticothalamic feedback from layer 6^{II} terminates in its specific thalamus and on the TRN. This corticothalamic feedback is matched against bottom-up input in the specific thalamus.

formation, and project diffusely to the superficial layers of the cerebral cortex (Fig. 1b).

In particular, the nonspecific thalamic nuclei are predicted to generate reset signals in the form of novelty-sensitive bursts of activation during mismatch episodes. Such a burst is broadcast nonspecifically to the superficial layers of the cerebral cortex, notably layer 1. The nonspecific burst is sensed by dendrites in layer 1 of cortical layer 5 cells. The model explains how the burst leads to a reset event by propagating from layer 1 dendrites via their layer 5 cells to layer 6 and then on to layer 4, shutting down previously active cells there, and thereby enabling a different pattern of activation to take hold in layer 4. This reset event causes a slower beta oscillation frequency in the model. Thus the reset event prevents learning of poorly matched bottom-up and top-down information, both by inhibiting the active learned categorical representations whose top-down expectations led to the mismatch, and also by creating a slower oscillation frequency to which STDP is insensitive. The details of how this works will be described below.

As noted above, the SMART model predicts that the reset event is expressed in the deeper layers of cerebral cortex, such as layers 4 to 6, and may thereby initiate slower beta oscillations in these layers. The more superficial cortical layers (e.g., layers 2/3) may, in contrast, express faster gamma oscillations. The model supports its proposal about how match-sensitive differences in oscillation frequency can enable or disable learning by quantitatively simulating data about single-cell biophysics, pharmacology, and neurophysiology; laminar neuroanatomy; aggregate cell recordings, such as current source densities and local field potentials; large-scale oscillations at beta and gamma frequencies; and functionally links them all to requirements about how to achieve fast attentive learning and stable memory. It is also suggested below how to directly test this prediction.

Many authors have examined synchronous oscillations within and across brain regions as one way in which behaviorally significant brain states are organized (Engel et al., 2001). Aggregate and single-cell recordings from multiple thalamic and cortical levels of mammals have shown high-frequency and low-frequency rhythmic synchronous activity correlated with cognitive, perceptual and behavioral tasks. In addition, large-scale neuronal population models have been proposed to model oscillatory dynamics (Bazhenov et al., 1998; Lumer et al., 1997; Destexhe et al., 1999; Siegel et al., 2000). However, these models do not link brain spikes, oscillations,

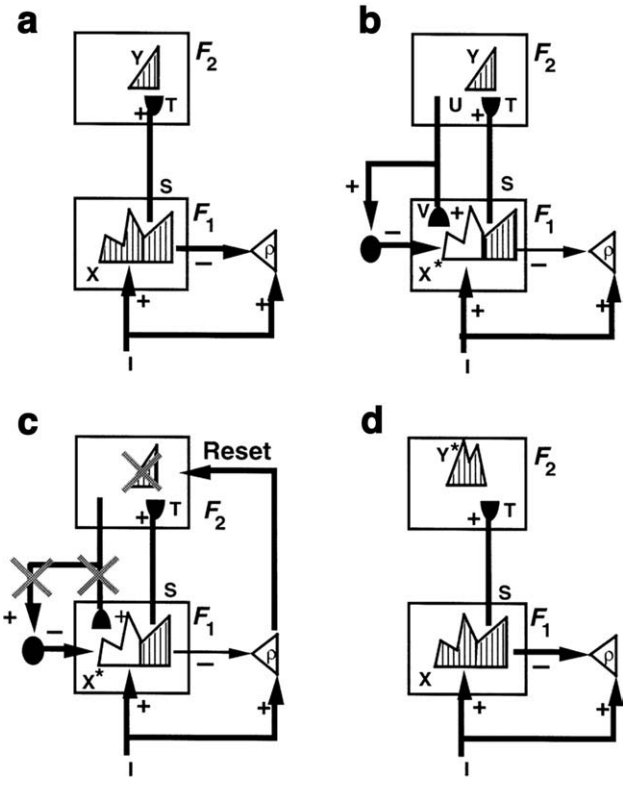

Fig. 4 – Search for a recognition code within an ART learning circuit: (a) The input pattern *I* is instated across the feature detectors at processing stage F_1 as a short term memory (STM) activity pattern X. Input *I* also nonspecifically activates the orienting system with a gain that is called *vigilance* (ρ); that is, all the input pathways converge with gain ρ onto the orienting system and try to activate it. STM pattern X is represented by the hatched pattern across F_1. Pattern X both inhibits the orienting system and generates the output pattern S. Pattern S is multiplied by learned adaptive weights, also called long-term memory (LTM) traces. These LTM-gated signals are added at F_2 cells to form the input pattern T, which activates the STM pattern Y across the recognition categories coded at level F_2. (b) Pattern Y generates the top-down output pattern *U* which is multiplied by top-down LTM traces and added at F_1 cells to form a *prototype* pattern V that encodes the learned expectation of the active F_2 nodes. Such a prototype represents the set of commonly shared features in all the input patterns capable of activating Y. If V mismatches I at F_1, then a new STM activity pattern X^* is selected *at* F_1. X^* is represented by the hatched pattern. It consists of the features of *I* that are confirmed by *V*. Mismatched features are inhibited. The inactivated cells corresponding to unconfirmed features of *X* are unhatched. The reduction in total STM activity which occurs when X is transformed into X^* causes a decrease in the total inhibition from F_1 to the orienting system. (c) If inhibition decreases sufficiently, the orienting system releases a nonspecific arousal wave to F_2; that is, a wave of activation that equally activates all F_2 cells. This wave instantiates the intuition that "novel events are arousing". This arousal wave resets the STM pattern Y at F_2 by inhibiting Y. (d) After Y is inhibited, its top-down prototype signal is eliminated, and X can be reinstated at F_1. The prior reset event maintains inhibition of Y during the search cycle. As a result, X can activate a different STM pattern Y at F_2. If the top-down prototype due to this new Y pattern also mismatches *I* at F_1, then the search for an appropriate F_2 category continues until a better-matching one is selected. Such a search cycle represents a type of non-stationary hypothesis testing. When search ends, an attentive resonance develops and learning of the attended data is initiated. [Adapted with permission from Carpenter and Grossberg (1993).]

and self-stabilizing STDP with the brain states that subserve attentive cognitive information processing.

1.2. *ART, LAMINART and SMART*

The SMART model fills this gap. It clarifies data about how bottom-up processing and learned tuning of adaptive filters is modulated by top-down attentive learned expectations that embody predictions or hypotheses that focus attention on expected bottom-up stimuli (Salin and Bullier, 1995; Engel et al., 2001; Gao and Suga, 1998; Krupa et al., 1999; Desimone, 1998; Ahissar and Hochstein, 2002; Herrmann et al., 2004). These data support predictions of Adaptive Resonance Theory, or ART (Grossberg, 1980, 2003; Carpenter and Grossberg, 1987, 1991, 1993; Carpenter et al., 1991) that top-down expectations regulate predictive coding and matching and thereby help to focus attention, synchronize and gain-modulate attended feature representations, and trigger fast learning that is dynamically buffered against catastrophic forgetting. The goal of achieving fast stable learning without catastrophic forgetting is often summarized as the *stability–plasticity dilemma* (Grossberg, 1980). The stability–plasticity dilemma must be solved by every brain system that needs to rapidly, yet stably, learn about the flood of signals that subserves even the most ordinary experiences. If the brain's design is parsimonious, then we should expect to find similar principles operating in all the brain systems that can stably learn an accumulating knowledge base in response to changing conditions throughout life.

ART has predicted that some fundamental properties of human and animal perception and cognition are part of the brain's solution of the stability–plasticity dilemma. In particular, humans are *intentional* beings who learn expectations about the world and make predictions about what is about to happen. Humans are also *attentional* beings who focus processing resources upon a restricted amount of incoming information at any time. Why are we both intentional and attentional beings, and are these two types of processes related? The stability–plasticity dilemma and its solution using resonant states provides a unifying framework for understanding these issues.

In particular, ART predicted that there is an intimate connection between the mechanisms that enable us to learn quickly and stably about a changing world, and the mechanisms that enable us to learn expectations about such a world, test hypotheses about it, and focus attention upon information that we find interesting. ART also proposes that, in order to solve the stability–plasticity dilemma, only resonant states can drive rapid new learning, which gave the theory its name. Fig. 4 illustrates these ART ideas in a simple two-level example whose anatomical, physiological, and pharmacological substrates are clarified by SMART. Here, a bottom-up input pattern, or vector, I activates a pattern X of activity across the feature detectors of the first processing stage F_1. For example, a visual scene may be represented by the features comprising its boundary and surface representations (Cao and Grossberg, 2005; Grossberg, 1994; Grossberg and Yazdanbakhsh, 2005). This feature pattern represents the relative importance of different features in the inputs pattern I. In Fig. 4a, the pattern peaks represent more active feature detector cells, the troughs less activated feature detectors. This feature pattern sends signals S through an adaptive filter to the second level F_2 at which a compressed representation Y (also called a recognition category, or a symbol) is activated in response to the distributed input T. Input T is computed by multiplying the signal vector S by a matrix of adaptive weights that can be altered through learning. The representation Y is compressed by competitive interactions across F_2 that allow only a small subset of its most strongly activated cells to remain active in response to T. The pattern Y in the figure indicates that a small number of category cells may be activated to different degrees. These category cells, in turn, send top-down signals U to F_1 (Fig. 4b). The vector U is converted into the top-down expectation V by being multiplied by another matrix of adaptive weights. When V is received by F_1, a matching process takes place between the input vector I and V which selects that subset X^* of F_1 features that were "expected" by the active F_2 category Y. The set of these selected features is the emerging "attentional focus".

If the top-down expectation is close enough to the bottom-up input pattern, then the pattern X^* of attended features reactivates the category Y which, in turn, reactivates X^*. The network hereby locks into a resonant state through a positive feedback loop that dynamically links, or binds, the attended features across X^* with their category, or symbol, Y. Figs. 4c and d shows how such an ART circuit can search for a novel or better marching recognition category if there is not a good enough match.

This *match-based learning* process is the foundation of the stability of learned memories, both bottom-up categories and top-down expectations, in an ART model. Match-based learning allows memories to change only when input from the external world is close enough to internal expectations, or when something completely new occurs. This feature makes ART systems well suited to problems that require online learning of large and evolving databases. For example, ART systems have been applied in fields ranging from technological solutions in industrial design and manufacturing, to the

Table 1 – ART operations and their new implementation in the SMART circuitry

ART operations	SMART implementation
Arousal	Intralaminar/midline nonspecific thalamic nuclei projections to layer 5 apical dendrites in layer 1
Reset and search	Layer 5 → 6^I → 4 and layer 6^I → 4 habituative synapses respond to arousal increases with graded reset of previously active cells
Vigilance regulation	Intralaminar/midline nonspecific thalamic nuclei → Nucleus basalis of Meynert → Layer 5
Resonance/learning enabled	Gamma (γ) oscillations
Reset/learning disabled	Beta (β) oscillations

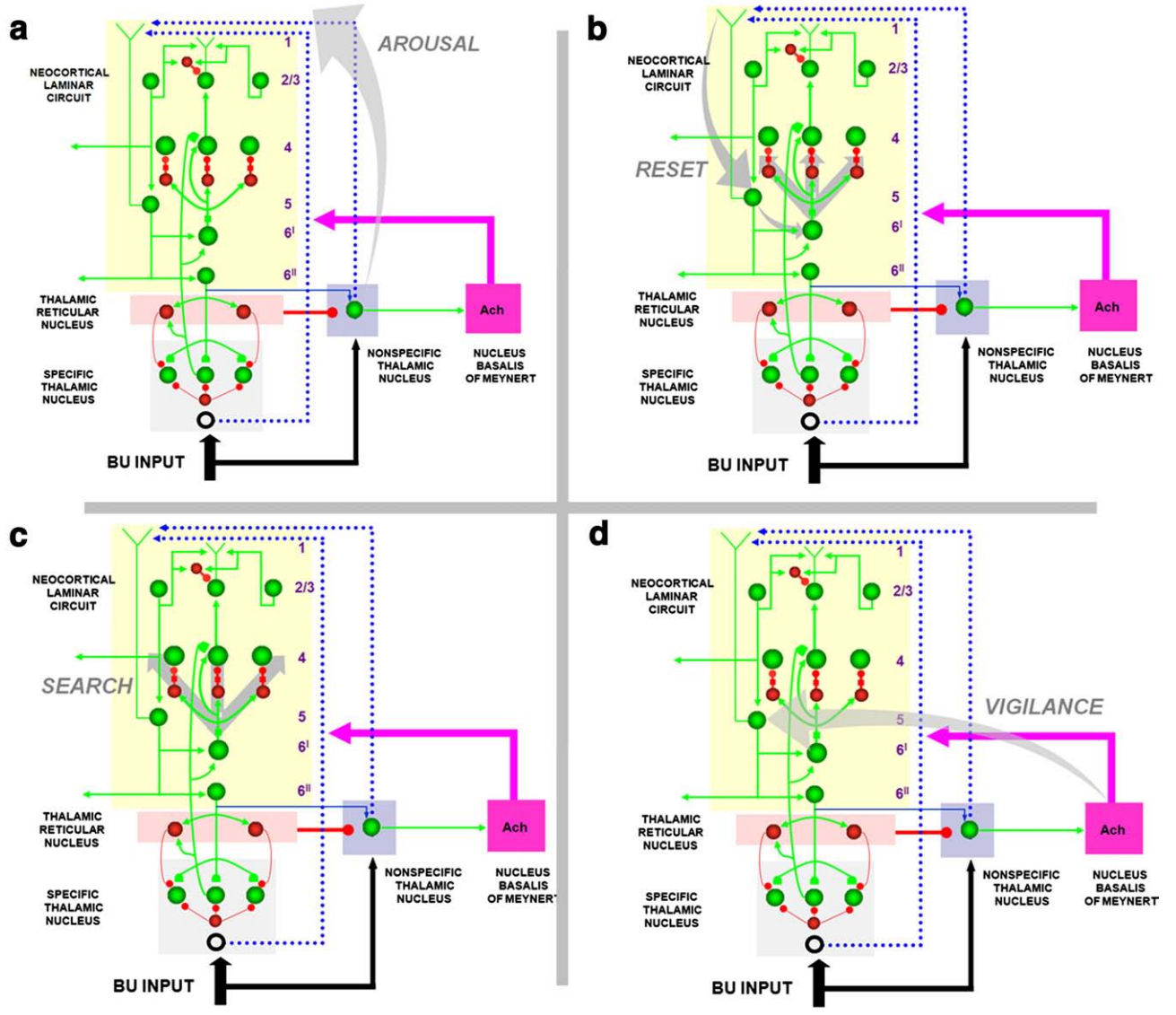

Fig. 5 – The large shaded gray arrows in the figure indicate the SMART pathways involved in the generation of the (a) *AROUSAL* burst, (b) *RESET*, (c) *SEARCH*, and (d), *VIGILANCE* control. See text for details.

control of mobile robots, to remote sensing land cover classification (see Carpenter et al., 2005 for a review).

Reconciling distributed and symbolic representations using resonance. ART models also clarify fundamental issues concerning symbol grounding, in addition to intentional and attentional aspects of primate cognition. The individual features at F_1 have no meaning on their own, just like the pixels in a picture are meaningless one-by-one. The bottom-up category, or symbol, in F_2 is sensitive to the global patterning of these features, but it cannot represent the "contents" of the experience, including their conscious qualia, due to the very fact that a category is a compressed, or "symbolic" representation. The bottom-up/top-down resonance between these two types of information converts the *pattern* of attended features into a coherent context-sensitive state that is linked to its category through feedback. It is this coherent state, that joins together distributed features and symbolic categories, that can enter consciousness. ART predicts that *all conscious states are resonant states*. In particular, such a resonance binds spatially distributed features into either a synchronous equilibrium or oscillation, until it is dynamically reset. Such synchronous states were predicted in the 1970's in the articles which introduced ART (see Grossberg, 1999b, 2003 for data reviews). The SMART model simulates finer properties of synchronous oscillations and their reset in the form of gamma and beta oscillations.

Recent ART models, called LAMINART, began to show how ART predictions may be embodied in laminar cortical circuits (Grossberg, 1999a, 2003; Raizada and Grossberg, 2003). These LAMINART models unify properties of visual development, learning, perceptual grouping, attention, and 3D vision. They did not, however, incorporate spiking dynamics, higher-order specific thalamic nuclei and nonspecific thalamic nuclei, control mechanisms for regulating resonance vs. reset, or pharmacological modulation of learning. The SMART model goes beyond ART and LAMINART models by showing how

Table 2 – Major simulated anatomical pathways

Model connections	Type	Functional interpretation	References
First-order thalamic relay cells → Layer 4 cells V1	D	Primary thalamic relay cells drive layer 4.	Blasdel and Lund (1983)
First-order thalamic relay cells → Layer 6^{I} cells V1	D	Primary thalamic relay cells prime layer 4 via the 6 → 4 modulatory circuit.	Blasdel and Lund (1983) for LGN → 6; LGN input to 6 is weak (Callaway, 1998, page 56); Layer 5 projects to 6 [Note 1]
First-order thalamic relay cells → TRN	D	Recurrent inhibition to primary and secondary thalamic relay cells.	Sherman and Guillery (2001); Jones (2002)
TRN → First-order thalamic relay cells	I	Off-surround to primary and secondary thalamic relay cells, synchronization of thalamic relay cells.	Pinault and Deschenes (1998); Sherman and Guillery (2001)
TRN → TRN	I	Normalization of inhibition.	Jones (2002); Sohal and Huguenard (2003)
TRN → TRN	GJ	Synchronize TRN and thalamic relay cells.	Landisman et al. (2002)
TRN → Nonspecific thalamic cells	I	Inhibition of nonspecific thalamic cells, participates in the reset mechanism.	Kolmac and Mitrofanis (1997); van der Werf et al. (2002)
Nonspecific thalamic cells → Layer 5 cells V1	M	To 5 through apical dendrites in 1, participates in the reset mechanism.	van der Werf et al. (2002)
Layer 4 cells V1 → Layer 4 inhibitory interneurons V1	D	Lateral inhibition in layer 4.	Markram et al. (2004)
Layer 4 inhibitory interneurons V1 → Layer 4 cells V1	I	Lateral inhibition in layer 4.	Markram et al. (2004)
Layer 4 inhibitory cells V1 → Layer 4 inhibitory interneurons V1	I	Normalization of inhibition in layer 4.	Ahmed et al. (1997), Markram et al. (2004)
Layer 4 cells V1 → Layer 2/3 cells V1	D	Feedforward driving output from 4 to 2/3.	Fitzpatrick at al. (1985); Callaway and Wiser (1996)
Layer 2/3 cells V1 → Layer 2/3 cells V1	D	Recurrent connections (grouping) in 2/3.	Bosking et al. (1997); Schmidt et al. (1997); Raizada and Grossberg (2003)
Layer 2/3 cells V1 → Layer 2/3 inhibitory interneurons V1	D	Avoid outward spreading (bipole) in 2/3.	McGuire et al. (1991); Raizada and Grossberg (2003)
Layer 2/3 inhibitory cells V1 → Layer 2/3 inhibitory interneurons V1	I	Normalization of inhibition.	Tamas et al. (1998); Raizada and Grossberg (2003)
Layer 2/3 cells V1 → Layer 4 cells V2	D	Feedforward output from cortical Area A to cortical Area B.	Van Essen et al. (1986)
Layer 2/3 cells V1 → Layer 6^{II} cells V2	D	Feedforward output from cortical Area A to cortical Area B.	Van Essen et al. (1986)
Layer 2/3 cells V1 → Layer 5 cells V1	D	Conveys layer 2/3 output to layer 5.	Callaway and Wiser (1996)
Layer 2/3 cells V1 → Layer 6^{II} cells V1	D	Conveys layer 2/3 output to layer 6^{II}.	Callaway (1998)
Layer 5 cells V1 → Pulvinar	D	Feedforward connections from cortical Area A to cortical Area B through secondary thalamic relay neurons.	Sherman and Guillery (2001).
Layer 5 cells V1 → Layer 6^{I} cells V1	D	Delivers corticocortical feedback to the 6^{I} → 4 circuit from higher cortical areas, sensed at the apical dendrites of 5 branching in 1.	Callaway (1998); Callaway and Wiser (1996, "class B" cells) [Note 2]
Layer 6^{I} cells V1 → Layer 4 cells V1	M	On-center to 4. Mediated by habituative synapses.	Stratford et al. (1996); Callaway (1998); Raizada and Grossberg (2003)
Layer 6^{I} cells V1 → Layer 4 inhibitory interneurons V1	D	Off-surround to 4.	McGuire et al. (1984); Ahmed et al. (1997); Callaway (1998);
Layer 6^{II} cells V1 → First-order thalamic relay cells	M	On-center to primary thalamic relay cells.	Sillito et al. (1994); Callaway (1998);
Layer 6^{II} cells V1 → TRN	D	Off-surround to primary thalamic relay cells mediated by thalamic TRN.	Guillery and Harting (2003); Sherman and Guillery (2001)
Layer 6^{II} cells V2 → Layer 5 cells V1 → Layer 6^{II} cells V1→ Layer 4 cells V1	M	Intercortical feedback from 6^{II} Area B to 1 area A, where it synapses on layer 5 cells apical dendrites branching in 1, resulting in subliminar priming of layer 4 cells via 5 → 6^{I}→ 4 on-center/off-surround circuit.	Rockland and Virga (1989); Salin and Bullier (1995)

Abbreviations: TRN = thalamic reticular nucleus; D = driving connections; M = modulatory connections; I = inhibitory connections; GJ = gap junctions. [Note 1]: Callaway (1998) subdivides cortical layer 6 neurons in 3 classes: *Class I:* project to 4C, also receive input from LGN, and project to LGN; *Class IIa:* dendrites in layer 6, receive projections from 2/3, project back to 2/3 with modulatory connections; *Class IIb:* dendrites in 5, project exclusively to deep layers (5 and 6) and claustrum. In the model, these populations are clustered in 2 classes, layer 6^{I} and 6^{II}, which provide feedback to thalamic relay cells and layer 4, respectively. [Note 2]: Callaway (1998) subdivides Layer 5 neurons in 3 classes: *Class A:* dendrites in 5, axons from 2/3, project back to 2/3 with modulatory connections; *Class B:* dendrites in 5, axons from 2/3, project laterally to 5 and the pulvinar; *Class C:* dendrites in 1, project to SC. In the model, layer 5 neurons receive input from 2/3 (Classes A and B), as well modulatory input from nonspecific thalamic nucleus (Class C, apical dendrites in layer 1), and provides output to 6^{I} and second-order thalamic nuclei.

these properties naturally coexist in the LAMINART framework. In particular, SMART explains and simulates how laminar cortical circuits may interact with specific primary and higher-order thalamic nuclei and nonspecific thalamic nuclei to control match vs. mismatch processes that regulate recognition learning and dynamically buffer learned memories against catastrophic forgetting; how spiking dynamics are incorporated into synchronous oscillations whose oscillation frequencies can provide an additional degree of freedom for controlling cognitively-mediated operations such as matching and fast learning; and how acetylcholine-based processes may embody predicted properties of vigilance control that regulate the generality of learned recognition categories in a way that is sensitive to changing environmental statistics, using only locally computed signals in the network. Table 1 illustrates the new ART operations implemented in the SMART circuitry. Fig. 5 depicts anatomical pathways that are predicted to subserve the arousal, reset, search, and vigilance operations.

What is vigilance and why is it needed? It is not enough to just regulate the stability of learned memories in a changing world. Survival requires that a human or animal learn to correctly discriminate, recognize, and predict important objects and events. An effective learner must be sensitive to changing environmental statistics and feedback that determine how specific or general learned knowledge must be to control and predict the external environment. How does the brain determine how specific (concrete) or general (abstract) a learned recognition category should be in a given situation? If matches trigger learning, then a flexible, situationally-sensitive, criterion of matching is needed to control specific vs. general learning. Such a criterion has been called *vigilance* (Carpenter and Grossberg, 1987, 1991), corresponding to the intuition that higher vigilance enables finer discriminations to be made. In all ART models, including SMART, high vigilance triggers reset and search for a new category when even small mismatches occur, thereby leading to concrete learning. Low vigilance allows even coarse matches to trigger resonance, and to thereby learn abstract categories that respond to many input variations. What is new in SMART is the prediction that neuromodulation by acetylcholine (ACh) may regulate the level of vigilance through time.

1.3. *Specific and nonspecific interactions control attention, learning, reset, and memory search*

The remainder of this section specifies in greater detail how SMART model circuits work. SMART clarifies how retinal inputs activate the thalamus, and from there, the cortex, through two separate pathways, a *specific* pathway targeting middle cortical layers (LGN core cells to layers 4 and 6^I cells, a subdivision of layer 6, see Table 2), and a *nonspecific* pathway targeting superficial layers (LGN matrix cells and nonspecific thalamic nucleus to layer 1 of V1). These two pathways are treated separately due to the different functional roles that were outlined in the previous section.

1.3.1. *The specific pathway*

The SMART specific pathway includes both specific first-order and second-order thalamic nuclei projecting to the middle layers of the cerebral cortex (Jones, 2002). Specific thalamic nuclei are often divided into first-order relays, such as the LGN, which receive inputs from the sensory periphery, and second-order relays, which receive their main inputs from the cerebral cortex (Sherman and Guillery, 2002). Although the largest part of the thalamus consists of second-order relays, the most widely studied structures are the first-order thalamic nuclei. As a consequence, thalamic nuclei are usually seen as relay stations of information from the sensory periphery to the cerebral cortex. This picture is misleading. For instance in the LGN, a first-order relay nucleus, the retina contributes only 5–10% of the total afferents (Sherman and Guillery, 2001). The pulvinar (PULV), one of the largest second-order thalamic nuclei, receives only minimal afferents from the sensory periphery. Most of its inputs originate from the cerebral cortex and the superior colliculus (SC). The LGN receives a massive cortical projection from V1 cortical layer 6, and the PULV receives afferents from layers 5 and 6 of several cortical areas (Rockland, 1998; Wang et al., 2002; Shipp, 2003).

Driving vs. modulatory pathways: Round-large vs. round-small terminals. In the primate, synaptic terminals in the thalamus can be roughly subdivided into two classes (Rockland, 1996; Sherman and Guillery, 2001): (a) round-large (RL) synapses, such as retinogeniculate synapses. These synapses are believed to be driving; (b) round-small (RS) terminations, such as the corticothalamic synapses from V1 layer 6 to the LGN. These synapses are believed to be modulatory. Terminations arising from layer 5 to a second-order thalamic nucleus are similar to retinogeniculate RL synapses, or driving, connections, often found in more proximal segments of the dendrites. This dual pattern of connectivity seems to be constant across species (Rouiller and Welker, 2000). A functional correlate of the distinction between RL and RS synapses is that, whereas lesioning a cortical area that innervates the thalamus through layer 6 alone does not change the receptive field property of the thalamic cell, lesioning an area that innervates the thalamus through layer 5 *does* abolish the receptive field of the cell (in, for example, areas 17, 18 and 19; Sherman and Guillery, 2002; Soares et al., 2004). In addition, the observed receptive fields in the PULV resemble those of complex cells in visual cortex (binocular and direction selective).

In the SMART specific pathway, LGN core cells are driven by bottom-up sensory inputs and excite both layer 4 and layer 6^I (Fig. 2a). Layer 6^I, in turn, contrast-normalizes layer 4 cell activities in response to bottom-up input patterns (Grossberg, 1980; Heeger, 1992; Douglas et al., 1995) via a modulatory on-center, driving off-surround network (Carpenter and Grossberg, 1987; Grossberg, 1980, 2003) whose off-surround is mediated by layer 4 inhibitory interneurons (Grieve and Sillito, 1991). The direct pathway from LGN to layer 4 enables the cortex to fire despite the modulatory nature of the on-center from layer 6^I to 4. The on-center off-surround of the LGN→6^I→4 pathway biases the emergence of orientation sensitivity in layer 4 cells that spike after the arrival of the LGN input within the STDP learning window (see Section 2.1).

Top-down matching, attention, and learning. Top-down feedback pathways coexist with bottom-up pathways in the brain. SMART proposes that top-down feedback from layer 6^{II} of V1 to the LGN controls attention and plasticity in both the bottom-up adaptive filter pathways from LGN to V1 and in

the top-down expectation pathways (Fig. 2b). As in previous ART models, SMART corticothalamic feedback is realized by a top-down, modulatory on-center, driving off-surround circuit whose on-center helps to create an attentional focus that selects, enhances, and synchronizes behaviorally relevant, bottom-up sensory inputs (match), and whose off-surround suppresses inputs that are irrelevant (mismatch).

The processing that goes on between LGN and V1 has homologs in the processing by PULV and V2, and beyond. Bottom-up driving inputs to higher-order specific thalamic nuclei, such as the PULV, arise from layer 5 of V1, as indicated in Fig. 3a (Salin and Bullier, 1995; Callaway, 1998). Top-down feedback from layer 6^{II} (see Table 2) of V2 to PULV can match the bottom-up input pattern from V1 layer 5 in a manner similar to how top-down feedback from layer 6^{II} of V1 matches retinal input in the LGN (Figs. 3a and 2a, respectively).

Accumulating experimental evidence supports the ART prediction (Carpenter and Grossberg, 1987; Grossberg 1980, 1999a, 2003) that that top-down attentional signals are mediated by a modulatory on-center, off-surround network. Both V2→V1 feedback (Bullier et al., 1988) and V1→LGN feedback (Sillito et al., 1994) possess this structure. A similar modulatory on-center, off-surround architecture has been observed in feedback interactions from auditory cortex to the medial geniculate nucleus (MGN) and the inferior colliculus (IC) (Zhang et al., 2004; Gao and Suga, 1998). Consistent with the ART prediction of the role of attention in controlling adult plasticity, Gao and Suga (1998) found that acoustic stimuli caused plastic changes in the IC of bats only when the IC received top-down feedback from auditory cortex. Moreover, plasticity is enhanced with behaviorally relevant auditory stimuli, consistent with the ART proposal that top-down feedback allows matched, and therefore attended, critical feature patterns to be learned, while suppressing mismatched, and thus unattended, features. Nicolelis and colleagues have shown that cortical feedback also controls thalamic plasticity in the somatosensory system (Krupa et al., 1999).

ART also predicted that matching synchronizes the firing patterns of cells coding matched stimuli and thereby facilitates fast stable learning (cf., Engel et al., 2001; Fries et al., 2001; Grossberg, 1976, 1980, 1999a; Pollen, 1999; Usrey, 2002). SMART further develops that proposal to include spiking neurons and the role of the higher-order specific and nonspecific thalamic nuclei.

SMART clarifies how the thalamic reticular nucleus (TRN) mediates the off-surround that helps to select thalamic cells during the matching process (Fig. 2b). The TRN forms a shell around the lateral and dorsal portions of the thalamus, lying in the axonal path connecting the specific and nonspecific thalamus and the cortex (Guillery and Harting, 2003). Afferents to the TRN are mainly branches of bottom-up axons from a specific thalamus to its target cortex, or branches of top-down axons from cortical layer 6 to its specific thalamic nucleus. Notably, the TRN does not receive projections from layer 5. The TRN has a rather uniform local structure. TRN cells are GABAergic, and are reciprocally linked both by chemical inhibitory projections and by electrical synapses (Landisman et al., 2002). Top-down inhibitory feedback from the TRN to specific thalamic nuclei helps to balance top-down cortical layer 6 excitatory signals at their shared target cells (Figs. 2b and 3a), and thereby enables the excitatory signals to have only a modulatory effect on these cells (Guillery and Harting, 2003) when these are the only active inputs. In addition to projecting to first-order and higher-order specific thalamic nuclei (Guillery and Harting, 2003), the TRN also projects to the nonspecific intralaminar and midline thalamic nuclei (Kolmac and Mitrofanis, 1997); see Figs. 2e and 3c. TRN projections to the intralaminar and midline nuclei are more diffuse than the reticular projection to the specific dorsal thalamic nuclei. The TRN is known to influence a number of important brain processes. In particular, it influences the sleep/wake cycle (Steriade et al., 1993), the efficacy of thalamic inputs to the cortex (Nicolelis and Fanselow, 2002; Swadlow et al., 2002), and attention (Sherman and Guillery, 2001). The current article focuses on the latter two processes, which are clearly relevant to the sleep/wake cycle, while suggesting an additional role for the TRN in suppressing unmatched features in recognition and learning.

Both V1 layer 2/3 and PULV inputs are required to fully activate the SMART V2 area. V1 layer 2/3 and PULV can drive V2 layer 4, which in turns activates V2 layers 2/3, 5 and 6^{II}, whose axons project to the PULV, where V1 input from layer 5 is attentively matched against the layer 6^{II} feedback (Figs. 3a and c). Layer 5 of V1 excites the matrix cells (see below), whose input is necessary for V2 layer 5 cells to close the intracortical resonant loop in V2 that is capable of driving fast self-stabilizing learning in V2; see Section 1.3.2.

V2 layer 6^{II} can also influence attentive top-down cortico-cortical feedback to layer 4 of V1 via layer 1 apical dendrites of layer 5 cells that project to layer 6^{I} and then to 4 via a modulatory on-center, off-surround circuit (Fig. 3b). See Section 2.2 for simulation results.

In summary, the SMART specific pathway is responsible for attentively matching bottom-up and top-down information in the specific thalamus, and creating attentive and synchronous resonant states that can support fast stable learning of bottom-up oriented filters and top-down oriented modulatory expectations. When the specific pathway interacts with the nonspecific pathway, it can also experience reset and memory search for better-matching filters and expectations, as the following section clarifies.

1.3.2. *The nonspecific pathway*

The thalamic nonspecific pathway includes both the "matrix" cells in the specific thalamic nuclei (Fig. 2a; Jones, 2002) and the nonspecific thalamic nuclei (Figs. 2d–f). Both pathways project to the superficial layers of the cerebral cortex. The term *nonspecific*, as opposed to *specific*, thalamic nuclei (both first-order and second-order nuclei), refers to the midline thalamic and the intralaminar nuclei. The term *nonspecific* derives from three characteristics of these nuclei, namely: (1) their diffuse innervation from pontine, medullary and mesencephalic reticular formation; (2) the signature of their stimulation in the cortical mantle (somnolence for low-frequency stimulation, arousal for high-frequency); and (3) the anatomical observation that they project to cerebral cortex in a fairly uniform fashion (van Der Werf et al., 2002). Most of the nonspecific thalamic nuclei are characterized by a high degree of convergent cortical input, widespread projections to large portions of neocortical layer 1, inhibition from the thalamic reticular nucleus (TRN), and strong neuromodulatory input from several brainstem centers (van Der Werf et al., 2002).

Neuropsychological and neurological evidence has demonstrated the importance of the intralaminar and midline nuclei for cortical functioning (Llinas and Pare, 1991; Llinas et al., 2002). Midline lesions of the thalamus affect general cognition, resulting in lethargy or coma (Facon et al., 1958) or unilateral hemineglect (Heilman et al., 1993), despite the fact that the specific sensory stimuli are relayed to the cortex.

Core vs. matrix cells. Recent studies have shed additional light on the dichotomy between specific and nonspecific thalamic nuclei, showing how the distinction between patterns of cortical termination (superficial vs. deep layers) not only characterizes cells between nuclei, but also cells within specific thalamic nuclei. Cytological studies on thalamocortical relay cells in monkeys conducted with the use of immunoreactivity for the calcium binding proteins parvalbumin and calbindin have shown a "core" of parvalbumin-rich cells projecting to the middle layers of their cortical targets, surrounded by a "matrix" of calbindin-rich cells projecting to the superficial layers (Jones, 2002). This matrix extends to all specific thalamic nuclei irrespective of nuclear borders, and differs from the core also by the nature of its input.

Core cells receive subcortical afferents that are highly ordered topographically, and a similarly ordered pattern is maintained at the site of cortical terminations of core cell axons at layer 4 (Jones 2002). Matrix cells receive subcortical input which tends to terminate in multiple thalamic nuclei, show a less precise stimulus–response relationship, have receptive fields that are not easily definable, and project to superficial cortical layers. For instance, in the medial geniculate complex, core cells receive tonotopically-ordered inputs from the central nucleus of the inferior colliculus, representing the most direct ascending pathway from the cochlea. Matrix cells are instead innervated by a less direct auditory pathway which ascends in the midbrain tegmentum and terminates diffusely in most of the nuclei that form part of the medial geniculate complex. Similar patterns of terminations are repeated in somatosensory and visual sections of the thalamus (ventral posterior complex and dorsal lateral geniculate nucleus, respectively). The results of Jones (2002) suggest that a functional microarticulation similar to the one observed in the specific and nonspecific thalamic nuclei may be mirrored by the core/matrix cell dichotomy in the specific thalamic nuclei. Both the matrix cells and nonspecific thalamic cells in the nonspecific pathway terminate on apical dendrites of layer 5 cells, mirroring the anatomical and functional similarities between matrix cells in specific nuclei and nonspecific thalamic cells (Jones, 2002).

Priming vs. reset. As noted above, in the SMART model, the matrix cells in the nonspecific pathway provide a priming input that allows the cortical hierarchy to fully process a

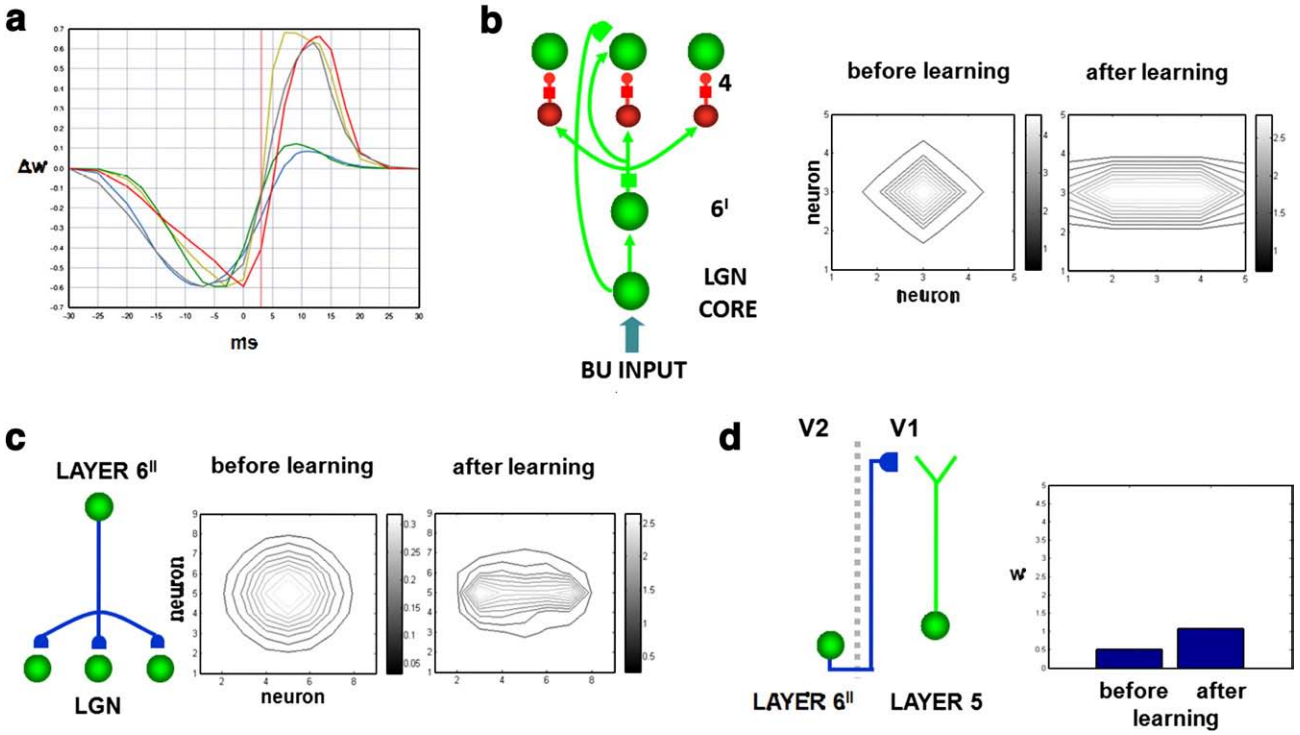

Fig. 6 – (a) STDP curves obtained by varying the time interval between presynaptic and postsynaptic spikes between [−30, 30] ms for five gating functions: grey (no gating), blue (dual OR gating), red (presynaptic gating), green (postsynaptic gating), yellow (dual AND gating), modified from Gorchetchnikov et al. (2005b). For a discussion of all gating functions, see Methods section and Gorchetchnikov et al. (2005a). (b) Presentation of a horizontal bar to a untrained thalamocortical circuit causes changes in the bottom-up synaptic weights of LGN→layer 4 synapses (postsynaptic gating, 100 ms episode). (c) At the same time, TD layer 6^{II}→LGN weights change by adapting to the BU input shape (presynaptic gating). (d) Top-down synaptic weights at the connections from V2 layer 6^{II} to the layer 1 apical dendrites of layer 5 cells change during learning when layer 6^{II} feedback is active (dual AND gating). Episodes of asynchronous activities can occur at learnable synaptic stages in different cortical areas. Dual AND gating prevents learning when only V2 layer 6^{II} cells are active and no activity is present in V1 layer 5.

bottom-up input (Fig. 2a). Sudden increments in activity within the nonspecific thalamic nucleus are also responsible for generating reset signals and memory search during predictive mismatch episodes. The model cell population in this nucleus is excited by converging bottom-up input (Fig. 2d), and sends excitatory connections to layer 1 of the cerebral cortex (Jones, 2002; Miller and Benevento, 1979), where its collaterals contact apical dendrites of layer 5 pyramidal cells (Vogt, 1991; Cauller, 1995; Cauller and Connors, 1994, 2001; Larkum et al., 2002, 2004). The nonspecific thalamus is also inhibited by the thalamic reticular nucleus, or TRN (Fig. 2e), and the balance between bottom-up excitation and TRN inhibition is controlled by the matching process. If a mismatch is large enough, the decrease of excitation in the LGN due to the misalignment of bottom-up and top-down input will decrease LGN firing and, thus, TRN inhibition to the nonspecific thalamus, while the excitatory bottom-up input will remain unchanged. Thus the total excitatory input to the TRN from layer 6^{II} and LGN is, all else being equal, larger in cases of match, when many LGN cells are excited, than in cases of mismatch, when only a smaller subset or no LGN cells are allowed to fire. The net result is an increase in firing rate in the nonspecific thalamus (see Section 2.3) that causes a spatially diffuse arousal burst to layer 1 of the cortex.

Arousal, reset, and search. How does a spatially diffuse arousal burst from the nonspecific thalamic nucleus *selectively* reset the cortical codes that caused a mismatch? At the moment when a mismatch occurs, the brain does not know which cortical areas caused the predictive failure (Grossberg, 1980). Despite this lack of information in the nonspecific thalamus, the mismatch there needs to be able to selectively reset active representations throughout the cortical hierarchy.

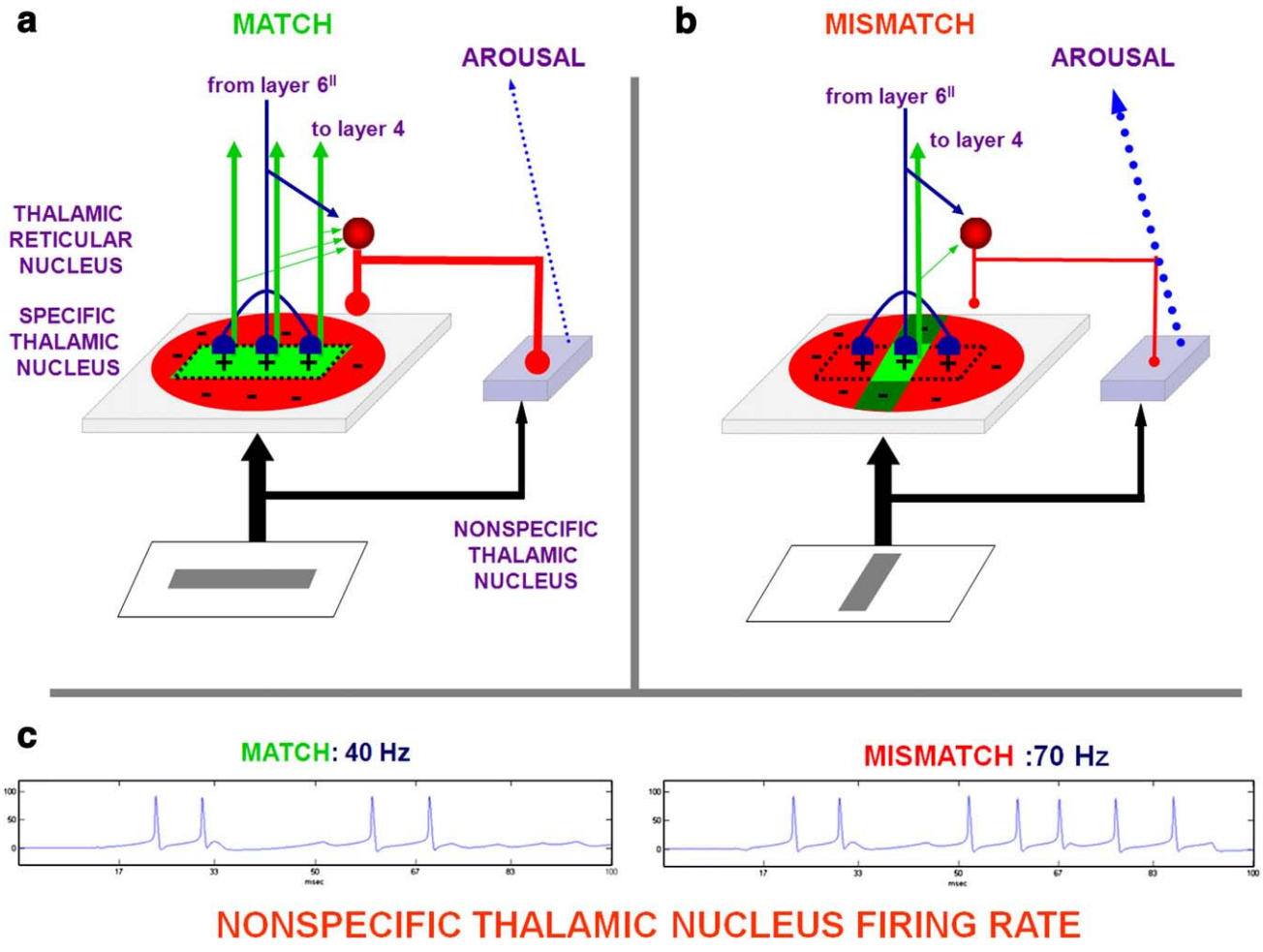

Fig. 7 – Regulation of nonspecific thalamic nucleus firing rate by the amount of match in the specific thalamic nucleus. (a) A bottom-up input pattern (horizontal bar, in green) is matched with a top-down expectation from layer 6^{II} (dotted horizontal bar) in the on-center (layer 6^{II}→specific thalamus) off-surround (layer 6^{II}→TRN→specific thalamus) corticothalamic loop. The convergent bottom-up excitation to the nonspecific thalamus is (partially or totally) cancelled by convergent TRN inhibition to the nonspecific thalamus. A spatial match (green horizontal area) allows specific thalamic cells to fire, excite their cortical target, and inhibit the nonspecific thalamus via the TRN. (b) A spatial mismatch between a bottom-up input pattern (vertical bar) and a top-down expectation (horizontal dotted bar) causes only a subset of specific thalamic cells to fire (bright green square area), excite their cortical target, and inhibit the nonspecific thalamus via the TRN. (c) Since the total, convergent bottom-up input to the nonspecific thalamus does not change in a match vs. a mismatch episode, the lower TRN firing rate during a mismatch triggers a higher firing rate in the nonspecific thalamus.

SMART proposes, in accord with known anatomical and physiological data both *in vivo* and *in vitro* (Larkum et al., 1999; Larkum and Zhu, 2002), that layer 5 pyramidal cell firing rate is jointly controlled by nonspecific thalamic inputs *and* specific layer 2/3 inputs, thus explaining how layer 5 cells exhibit two distinct firing modes (Williams and Stuart, 1999): Layer 5 cells that receive layer 2/3 inputs *and* nonspecific thalamic inputs during a mismatch episode fire in bursts at high rates (see Section 2.6 for experimental and simulation results). Active 2/3 cells represent cortical codes that caused the mismatch. In contrast, single spikes are produced in layer 5 cells when only one of these sources is activated, either during a match, or during a mismatch when layer 2/3 cells are inactive.

As noted above, layer 5 pyramidal cells send *driving* inputs directly to higher cortices through the thalamus (e.g., the pulvinar; Sherman and Guillery, 2002; Shipp, 2003; see Fig. 3a), indirectly control corticothalamic feedback at their own cortical level through layer 6^{II} (Figs. 2b and 3a), and also control corticocortical feedback to layer 4 at their own cortical level via layer 6^{I} (Figs. 2c and 3c). Layer 5 can hereby generate widespread bursts of synchronized activity throughout the neocortex mediated by driving layer 5 terminations on higher-order thalamic nuclei (including pathological epileptogenic activity; Williams and Stuart, 1999), and selectively reset multiple cortical areas by relaying from the nonspecific thalamus layer 5 bursts to layer 4 via the $6^{I}\rightarrow 4$ pathway. In particular, model layer 6^{I} cells are predicted to respond to a thalamic mismatch with selective cortical reset and search for a more predictive cortical code in layers 4 and 2/3 (see Section 2.6 for simulation results).

The nonspecific pathway may also help to regulate modality-specific attention during reset episodes (Crick, 1984; Guillery et al., 1998; Montero, 1997; Weese et al., 1999). SMART predicts how cortical areas that experience strong predictive mismatches in a given modality may reduce priming of the cortical area of a competing modality by inhibiting the corresponding nonspecific thalamic nucleus. In particular, Crabtree and Isaac (2002) have shown that nonspecific thalamic nuclei which subserve different modalities are linked by mutually inhibitory interactions. SMART simulates how TRN-mediated (van Der Werf et al., 2002) inhibitory interactions (Crabtree and Isaac, 2002) between nonspecific thalamic nuclei can cause a pause in firing of one nonspecific thalamic nucleus that can transiently down-regulate layer 5 pyramidal cells of the competing cortical area (see simulations in Section 2.9). SMART further predicts that competing *specific* nuclei, not only nonspecific nuclei as shown by Crabtree and Isaac (2002), might be inhibited by the TRN in cases of strong mismatches, therefore being a possible thalamic substrate for competitive allocation of attention.

Learned generalization, vigilance, and acetylcholine. How is the generality of recognition categories regulated to represent statistical properties of the environment? As noted above, ART predicts that resonance and learning occur when the degree of match between bottom-up and top-down representations is greater than a gain parameter, called *vigilance* (see Fig. 4). Vigilance can change due to internal factors, such as fatigue,

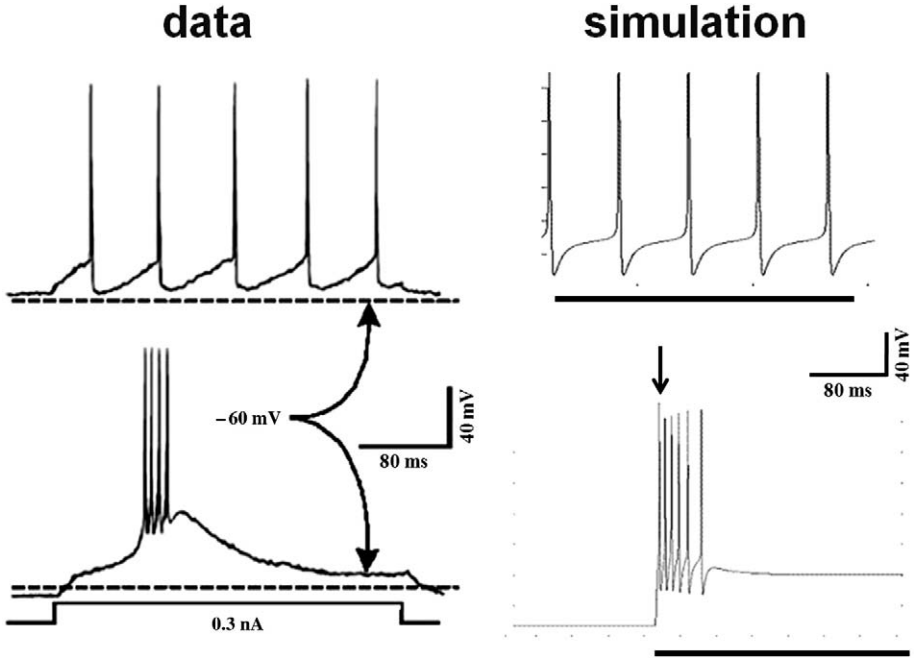

Fig. 8 – Burst and tonic firing in thalamic relay cells. *Data*: intracellularly *in vitro* recording illustrating the voltage dependency of the low threshold spike for a geniculate relay cell. The same depolarizing current pulse administered at two different initial holding potentials causes either tonic firing (top, cell depolarized, I_T inactivated) or burst firing (bottom, cell hyperpolarized, I_T de-inactivated). Modified and reprinted with permission from Sherman and Guillery, 2002. *Simulation*: a 0.3 nA current (horizontal bar) is injected in a simulated LGN cell in the absence (top) or presence (bottom) of a hyperpolarizing voltage clamp. The hyperpolarization of the cell and the presence of low-threshold Ca^{++} currents (see Eqs. (21)–(27) in Methods) causes the de-inactivation of the I_T current, inducing burst firing.

or external factors, such as predictive mismatch or punishment. A baseline vigilance determines how big a mismatch is initially tolerated before cortical representations are reset. When a predictive error causes a mismatch to occur, the vigilance level is predicted to increase just enough to drive a memory search for a new recognition code. This process is called *match tracking* (Carpenter and Grossberg, 1987; 1991; Carpenter et al., 1992). Match tracking realizes a kind of minimax learning rule; namely, it enables a learning system to minimize predictive error while maximizing generalization. Choosing a low baseline vigilance leads to the learning of general categories and thus a minimum use of memory resources. Match tracking increases this baseline vigilance just enough to learn the most general categories that are consistent with predictive success.

The SMART model predicts that one way to control vigilance may be to modify the excitability of layer 5 cells during mismatch episodes (Fig. 5). Anatomical studies in monkeys, cats and rats have established that the nonspecific thalamus (in particular, the midline and central lateral thalamic nuclei), whose activation is sensitive to the degree of mismatch, projects to the cholinergic nucleus basalis of Meynert (van Der Werf et al., 2002), one of the main sources of cholinergic innervations of the cerebral cortex. The nucleus basalis of Meynert is also influenced by noxious stimulation and cortical control (Zhang et al., 2004). Saar et al. (2001) have shown that ACh release reduces the after-hyperpolarization (AHP) current and increases cell excitability in layer 5 cortical cells (see Section 2.8). In SMART, this increased layer 5 excitability due to predictive mismatch may cause reset via the layer 5-to-6^{I}-to-4 circuit, even in cases where top-down feedback may earlier have partially matched bottom-up input, which is a key property of vigilance control. The increase of ACh might therefore promote search for finer recognition categories in response to environmental feedback, even when bottom-up and top-down signals have a pretty good match in the nonspecific thalamus based on similarity alone.

Fig. 3c summarizes all of the simulated SMART circuitry. Table 2 summarizes the main anatomical features simulated, their functional interpretation, and supportive experimental literature. The Methods section provides a detailed description of the model equations and parameters.

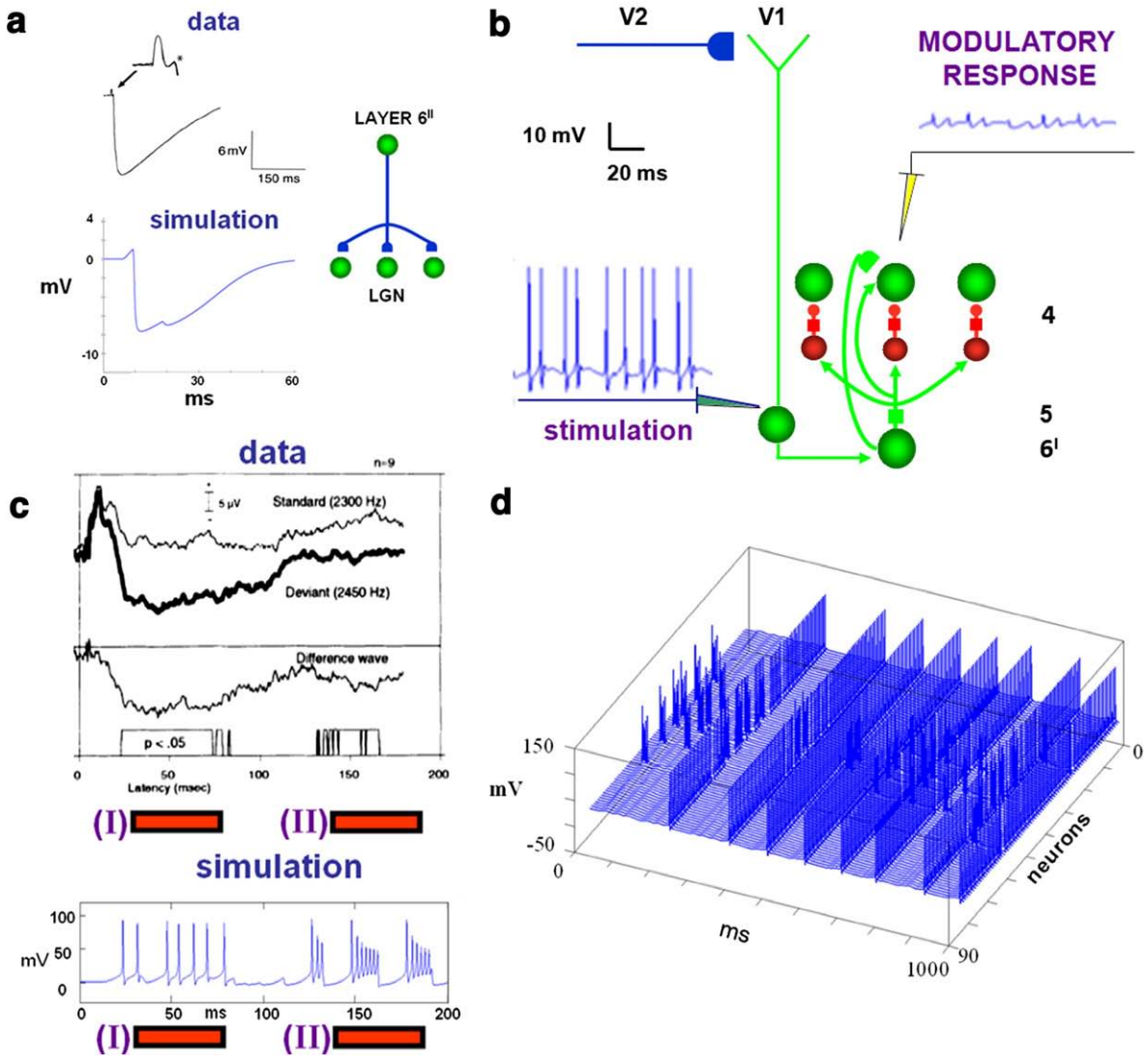

2. Results

2.1. *Learning bottom-up oriented filters in the specific pathway*

In both the brain and the model, LGN parvalbumin-rich "core" cells receive topographically highly ordered bottom-up sensory input and project to layers 6^{I} and 4 of cortical area V1 (Jones 2002, Fig. 1b) in a manner that is sensitive to stimulus orientation (Reid and Alonso, 1995). SMART simulates how adaptive synapses may become orientationally tuned in the pathways from LGN core relay cells to V1 layer 4 and layer 6^{I} cortical neurons (Fig. 2a) via postsynaptically gated STDP (Fig. 6a) during synchronous match-mediated gamma oscillations.

Fig. 6b illustrates the development of orientation sensitivity in a layer 4 cell that wins the competition with its neighboring cells. It spikes within a few milliseconds after the arrival of the LGN input, while nearby cells are suppressed and their spiking delayed by the on-center off-surround layer $6^{I}\rightarrow4$ network. This delay reduces or completely suppresses learning in cells other than the winning neurons. The gamma oscillations (see Section 2.10) during match episodes allow layer 4 cells to fire a few ms after LGN cells, and thus within the STDP window. The orientation selectivity is expressed in terms of LGN→4 synaptic weights (cf., Alonso et al., 2001) before and after a 100 ms exposure to a horizontally-oriented stimulus. Orientationally selective cells in layer 4 of V1 excite layer 2/3 cells, which in turn project to layer 5 of V1. Layer 5 projects to layers 6^{I} and 6^{II} of the same area (Callaway, 1998). Layer 6^{I} closes the layer $2/3\rightarrow6^{I}\rightarrow4\rightarrow2/3$ intracortical modulatory excitatory loop that helps select the most activated cells in layer 4, while strongly suppressing less active cells and noise. Layer 6^{II} closes the thalamocorticothalamic loop by projecting with top-down modulatory connections to the specific thalamic nuclei (Figs. 2b, 3a, and 3c) and nonspecific thalamic nuclei (Figs. 2e and 3c), and with driving connections to the TRN (Figs. 2b, 3a, and c), as detailed below.

2.2. *Top-down attention and STDP learning*

V1 layer 6^{II} cells send top-down modulatory excitatory glutamatergic signals to thalamic relay cells in LGN (Sherman and Guillery, 2001; Murphy et al., 1999; Ichinohe et al., 2003). Although LGN neurons respond to unoriented visual stimuli, oriented spatial arrays of LGN neurons can respond to oriented contours in an image or scene, and corticothalamic feedback comes from oriented cortical cells. SMART simulates how top-down feedback signals from V1 layer 6^{II} are matched and mismatched in LGN, and thereby help to stabilize learning in both bottom-up adaptive filters and top-down modulatory expectations. Learning during a match state encodes top-down orientation sensitivity, which has also been reported in neurophysiological experiments (Murphy et al., 1999). Fig. 6c illustrates the learned oriented shaping of model corticothalamic synaptic weights using an STDP rule with presynaptic gating (see Methods) before and after 100 ms presentation of a horizontal bar. The oriented synaptic weights are learned in a gamma oscillation regime (see Fig. 14b below) and allow subsequent attentive top-down signals to subliminally prime the consistent learned bottom-up stimulus, and match it or mismatch it with incoming bottom-up inputs. In particular, the oriented top-down expectation supports competitive selection, synchronization, and gain modulation of matched LGN cells, which has been reported in neurophysiological experiments (Sillito et al., 1994).

Fig. 9 – (a) Top-down corticothalamic feedback exerts a subthreshold excitatory effect on the membrane potential of thalamic relay cells. *Data (upper left panel):* whole-cell recording from a relay neuron in the somatosensory ventral posterior nucleus of a mouse thalamocortical slice *in vitro*. A single weak electrical stimulus (arrow) applied to a corticothalamic fiber elicits a small monosynaptic EPSP (asterisk in enlarged inset) followed by a deep and long-lasting disynaptic IPSP resulting from collateral corticothalamic excitation of the TRN (Jones, 2002). *Simulation (lower left panel):* a complete corticothalamic module is used in this simulation. Stimulation via current injection is provided to a central layer 6^{II} neuron, which has previously learned a bottom-up stimulus, until a single spike is produced, and the somatic membrane potential of the cell which coded the learned bottom-up stimulus is recorded in the absence of external stimulation. (b) Electrical stimulation of model layer 5 apical dendrites, simulating the top-down feedback excitation exerted by layer 6^{II} of V2, induces layer 4 priming via the 6^{I} modulatory on-center, off-surround network. (c) The nonspecific thalamic nucleus, not the specific nuclei, is involved in novelty detection in an auditory mismatch negativity (MMN) paradigm. *Data:* Extracellular recordings to standard stimulus (2300 Hz, thin line) and deviant stimulus (2450 Hz, thick line) obtained from the caudomedial portion of the nonspecific medial geniculate body (MGcm) in guinea pigs (Kraus et al., 1994). Significant differences between the responses to the standard and deviant stimuli are indicated in the box under the difference wave. Significant negative deflections (at 30–80 ms and 135–170 ms) were identified in the nonspecific MGcm but not in the specific medial geniculate body (MGv). *Simulation:* a complete corticothalamic module was used in 300 ms simulation epochs, and the potential of the nonspecific thalamic nucleus cell was recorded. Stimulation of a layer 6^{II} cell that has previously learned a horizontal stimulus provides top-down feedback to the thalamus, where it mismatches a vertically oriented bottom-up input. The mismatch corresponds to the MMN condition, in which a repetitive stimulus builds up top-down expectations that are mismatched when a novel stimulus is presented. The first increase in the nonspecific nucleus firing rate is caused by the release from inhibition from the TRN due to the reduced firing of the primary thalamic nucleus, whereas the second increase in firing rate is caused by thalamocortical layer 6^{II} feedback, in turn caused by the synchronized layer 5 firing that is caused by activation of the nonspecific thalamus during a mismatch, followed by widespread activation of cortical layer 1, including the dendrites of layer 5 cells. (d) Simulation of all layer 5 cells firing synchronously in response to the increased nonspecific thalamic input. In these simulations the top-down feedback (stimulation of a layer 6^{II} cell with horizontal top-down thalamocortical receptive field) is kept on for one second, during which the top-down feedback mismatches the vertically oriented bottom-up input.

2.3. *Attentive matching in the specific thalamus*

The SMART model proposes functional roles for both the specific and nonspecific projections of the TRN (Figs. 2b and e). The specific inhibitory projections of the TRN to the LGN (Guillery et al., 1998; Guillery and Harting, 2003) provide a detailed anatomical realization of the ART matching process that suppresses bottom-up inputs that mismatch cortical top-down excitatory expectations. In particular, the top-down excitatory on-center, adaptive pathway from layer 6^{II} to LGN core cells is supplemented by an TRN-mediated inhibitory off-surround (Figs. 2b and 7).

LGN cells that receive only top-down excitatory inputs are inhibited by the model TRN (balanced excitation and inhibition; one-against-one), whereas cells that receive sufficiently large simultaneous bottom-up and top-down excitatory inputs can offset TRN inhibition and fire (two-against-one). A perfect match occurs when the same subset of LGN cells receives bottom-up excitation and top-down excitatory modulatory priming signals from cortical layer 6^{II}; e.g., they both represent the same horizontal bar, as in Fig. 7a. These matched LGN cells fire tonic action potentials that activate layers 4 and 6^{I} of the target cortical area. The tonic firing mode preserves a linear input–output relationship in LGN cells, and relays information better than burst firing (Sherman and Guillery, 2002). A sufficiently big mismatch, such as the top-down horizontal bar expectation matched against the vertical bar bottom-up input in Fig. 7b, hyperpolarizes LGN cells via

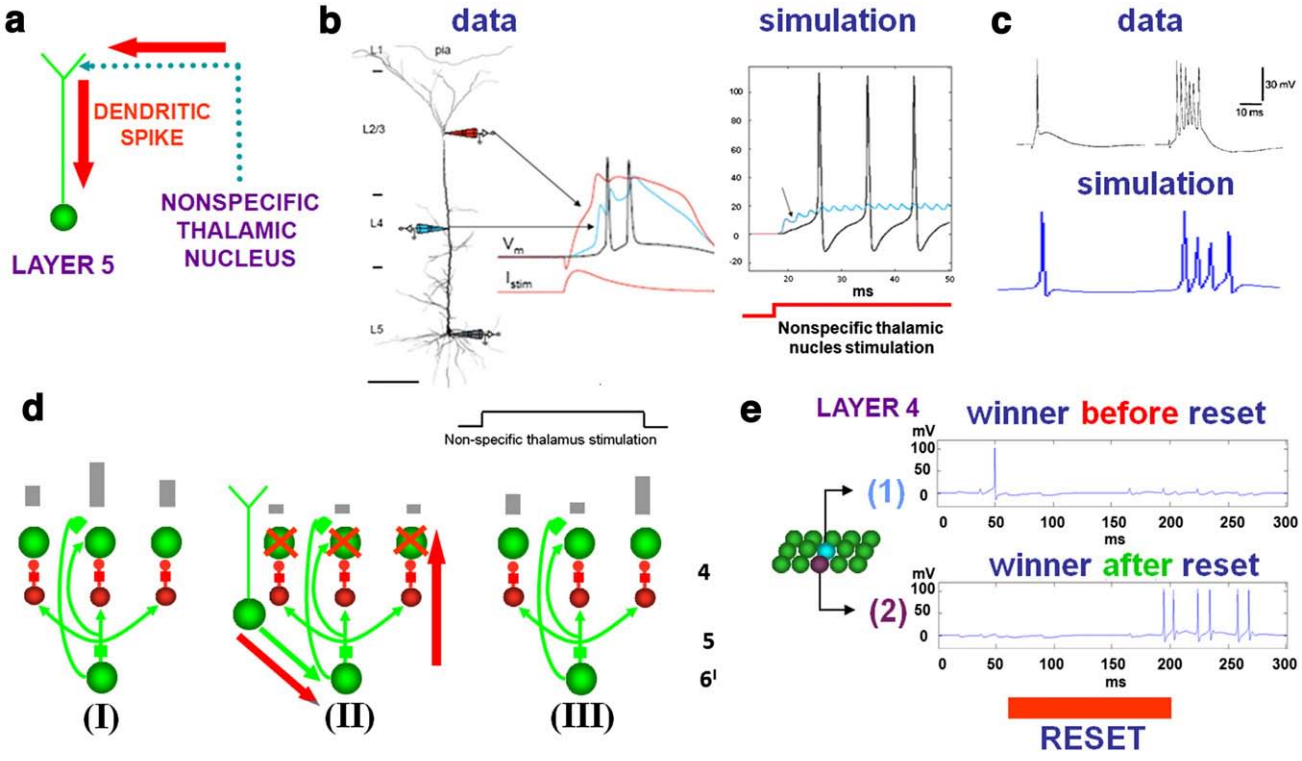

Fig. 10 – (a) In the model, an increase in nonspecific thalamic firing rate during a mismatch nonspecifically activates layer 1, including apical dendrites of layer 5 cells, where dendritic spikes are triggered that can cause layer 4 somatic action potentials. (b) Input to the apical dendrite of layer 5 pyramidal neurons results in action potentials recorded at the soma. *Data*: recordings of a layer 5 pyramidal neuron (rats, *in vitro*) show apical (red), proximal (blue) dendritic and somatic (black) potentials during stimulation of the apical dendrite (modified with permission from Larkum et al., 1999). *Simulation*: stimulation of the apical dendrites of an isolated simulated layer 5 pyramidal cell via the nonspecific thalamic nucleus produces a stream of action potentials at the soma. The arrow indicates the recording from the intermediate section of the dendrite of the simulated neuron, located at 400 μm from the soma, which is equivalent to the L4 recording electrode in the data. The voltage oscillations recorded at the proximal dendrite are caused by dendritic spikes occurring at the cell's apical dendrite, and propagated towards the soma. (c) *Data: in vitro* (rat) recordings of layer 5 pyramidal cells show that neuronal firing in response to extracellular synaptic excitation can consists of single spikes or burst firing (modified from Williams and Stuart, 1999) *Simulation:* recordings from a layer 5 pyramidal neuron during a mismatch episode. Depending on the presence of a layer 2/3 input, the cell can either respond with a single spike (no layer 2/3 input) or a burst of spikes (layer 2/3 input). (dI) Layer 6^{I}→4 on-center off-surround network normalizes and primes layer 4 cells activities. Neurotransmitter depletion (green squares) does not bias the competition in layer 4 until a reset occurs. (dII) A reset is driven by mismatch-mediated layer 6^{I} firing in response to a burst of layer 1 nonspecific activation. (dIII) The reset unmasks previously inactive cells that are favored by higher levels of neurotransmitters which have accumulated in non-depleted layer 6^{I}→4 synapses. (e) Before a reset occurs, a "wrong" winning layer 4 cell spikes (1). Reset (red bar) favors the activation of previously inhibited cells (2).

layer 6^{II}→TRN→LGN feedback, and then voltage-dependent T (transient) type Ca^{+} currents causing burst firing (Sherman and Guillery, 2001). The model exhibits both the tonic and the burst firing modes that are found in the data (Fig. 8).

Consistent with Sherman and Guillery (2002), SMART clarifies how burst firing might help to switch attention to a modality where a sudden bottom-up stimulus occurs, as when a sudden visual cue occurs while paying attention to an auditory stimulus. This mechanism complements the nonspecific thalamus-mediated mismatch, which can use vigilance control to cause mismatches across multiple modalities. Indeed, using vigilance control, even if a modality experiences a match that is good enough to predict an outcome elsewhere in the brain (e.g., seeing a visual object predicts its name), a mismatch with this outcome can raises vigilance enough to drive a search within the original modality for a recognition category that can predict the outcome better in the future (see Section 2.8).

2.4. *Attentive priming via corticocortical and corticothalamic feedback connections*

As noted above, the STDP rule (Fig. 6a; see Methods) is used to learn the top-down corticocortical attentive connection from V2 layer 6^{II} cells to layer 1 apical dendrites of V1 layer 5 cortical cells during presentation of a bottom-up input (Fig. 6d). This learning correlates V2 layer 6^{II} cell outputs with *retrograde dendritic spikes* from V1 layer 5 cells to their layer 1 dendrites (Gorchetchnikov and Grossberg, 2007; Grossberg, 1975, 1982; Johnston et al., 1999). Such learning subsequently allows the V2 layer 6^{II} cell to fire the associated V1 layer 5 cell, and from there the corresponding V1 layer 6^{I} cell, which in turn primes V1 layer 4 via the modulatory on-center, off-surround layer 6^{I}→4 network. This top-down circuit mediates attention in the network. It embodies the concept of "folded feedback" whereby top-down signals are folded into the bottom-up flow of

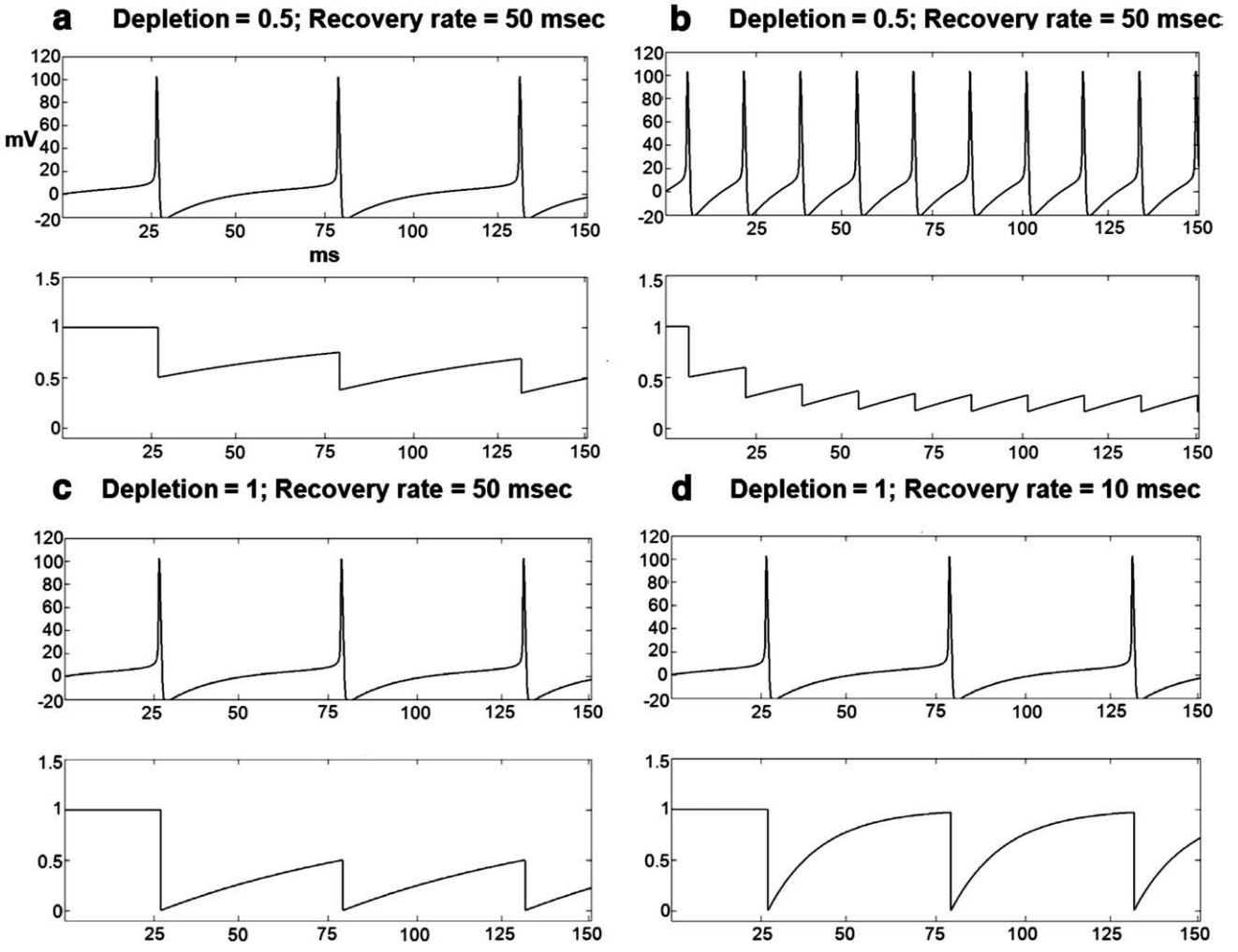

Fig. 11 – Neurotransmitter dynamics with different values of depletion (inactivation, habituation) and recovery rate (ε and τ, respectively, see Eq. (7) in Methods) and different pre-synaptic firing frequencies in an isolated layer 6^{I} cell. Stimulation was induced by current injection until firing rates of 23 Hz (panels a, c) or 70 Hz (panels b, d) were generated. Each panel shows the pre-synaptic cell membrane potential (top) and the level of neurotransmitter at the synapse (bottom). (a, b) Higher firing rates cause larger and quicker neurotransmitter depletion due to the mass action (Eq. (7) in Methods), all else being equal. (c) Increasing the depletion rate ε from 0.5 to 1 results in larger neurotransmitter depletion. (d) A faster recovery rate τ counterbalances the effect of depletion.

information from layer 6^{I} to 4, where they can attentionally enhance or suppress bottom-up signals (Grossberg, 1999a).

A key prediction of the model is that the excitatory on-center of the $6^{I}\rightarrow 4$ pathway is modulatory, or subthreshold. This prediction is consistent with the data showing that layer 4 excitatory post-synaptic potentials (EPSPs) elicited by layer 6 stimulation are much weaker than those caused by stimulation of LGN axons (Stratford et al., 1996), and also with the finding that binocular layer 6 neurons synapse onto monocular layer 4 cells without reducing the monocularity of the target layer 4 cells (Callaway, 1998).

Corticothalamic feedback is also modulatory, and provides excitatory priming of target thalamic cells. Fig. 9a (top left panel) shows neurophysiological data illustrating modulatory priming in the specific somatosensory thalamus caused by layer 6 stimulation (Jones, 2002), and simulated model thalamic cell modulation (bottom left panel) during top-down layer 6^{II} priming of the model LGN. Fig. 9b shows simulated subthreshold activation of a V1 layer 4 cell after learning top-down feedback from a V2 layer 6^{II} cell to the apical dendrites of V1 layer 5 cells. In the figure, the effect of top-down feedback is simulated by direct layer 5 stimulation. These experimental and modeling results are consistent with ART predictions that top-down attentive signals are typically, by themselves, modulatory and insufficient to fully activate their target cells. See Grossberg (2000) for an analysis of how top-down signals can elicit suprathreshold responses during percepts of visual imagery and hallucinations when the excitatory and inhibitory signals become imbalanced.

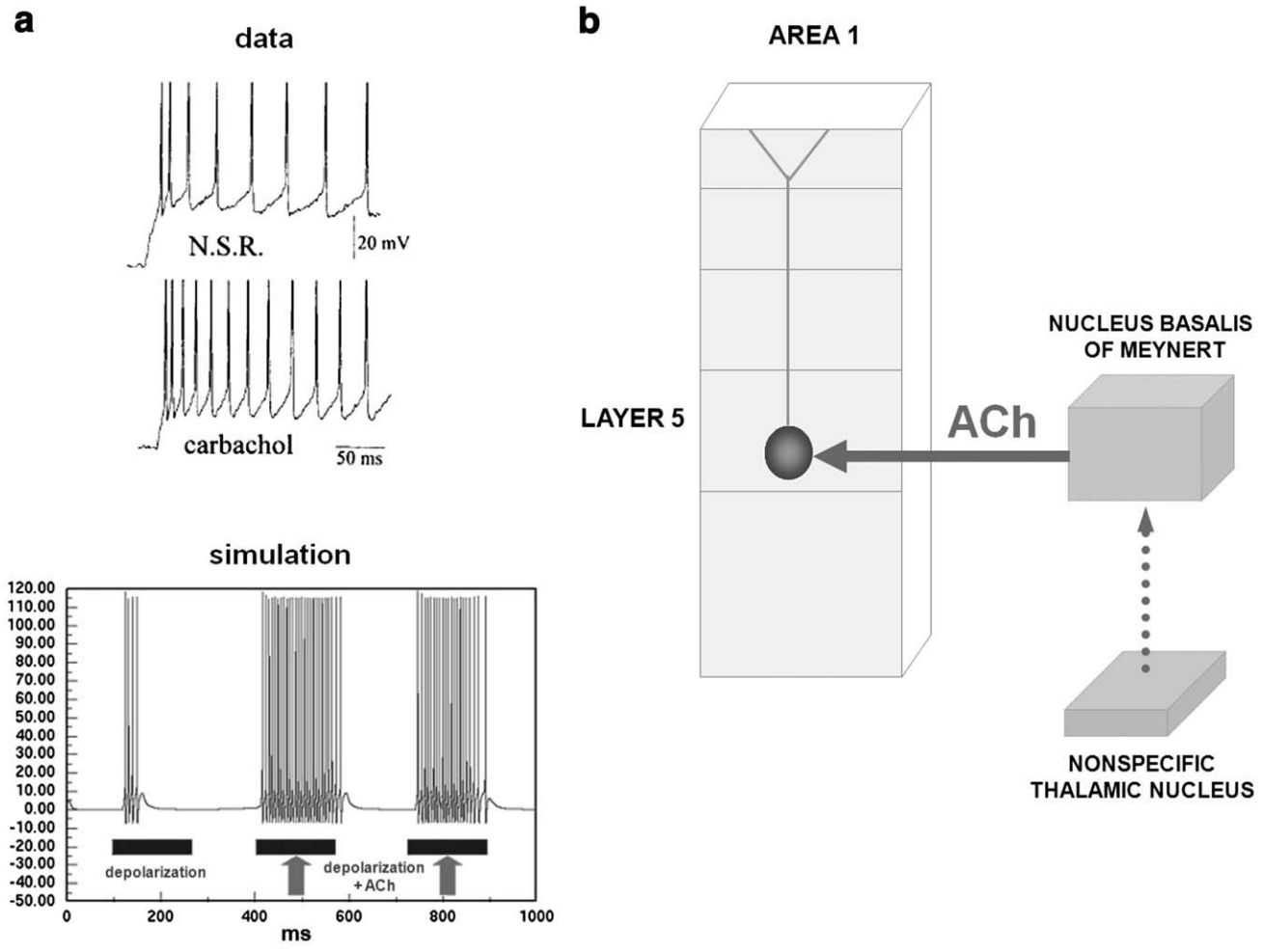

Fig. 12 – Interactions between nonspecific thalamic glutamatergic transmission, ACh and after-hyperpolarization (AHP) (a) ACh may modulate reset by regulating AHP currents and cell excitability in layer 5 cortical cells. *Data:* Intracellular recordings *in vitro* show that the ACh agonist carbachol reduces firing adaptation in layer 2 neurons in response to a constant current step injection (modified with permission from Saar et al., 2001). *Simulation:* an isolated, 3-compartment-layer 5 pyramidal cell is simulated, and a constant current injection is provided to the soma in order to produce a stream of action potentials at 80 Hz. The AHP current at the soma is characterized by a long-lasting hyperpolarizing K^{+} current, which slows down and eventually prevents spiking activity. ACh activation is represented as the 100 ms stimulation of a single cholinergic neuron terminating on the soma of the layer 5 pyramidal cell. The activation of the cholinergic nucleus opens a conductance (multiplicative gating variable, Eq. (7)) in Section 4.4) which reduces the conductance of the AHP current, therefore reducing spiking adaptation. (b) The nonspecific thalamic nucleus may control the cortical release of ACh via its terminations in the Nucleus Basalis of Meynert (van Der Werf et al., 2002).

2.5. *Nonspecific thalamic nucleus, cortical arousal regulation, and mismatch negativity*

The matching process in the specific thalamic nuclei is predicted to regulate the activity of the nonspecific thalamic nucleus. In particular, a match decreases the firing rate, or cortical arousal, from the nonspecific nucleus, whereas a mismatch increases it (Fig. 7). How does the nonspecific thalamus become sensitive to the degree of match in the specific thalamus?

The total convergent bottom-up excitatory input to a nonspecific thalamic nucleus is unchanged by the matching process (van Der Werf et al., 2002; Jones, 2002; Fig. 7). When a match occurs, the TRN receives stronger excitation via bottom-up thalamocortical collaterals than during a mismatch (Sherman and Guillery, 2001, 2002; Fig. 7a vs. 5b). During a match, this leads to strong, convergent inhibition to the nonspecific thalamic nucleus that can balance the total excitatory input that it receives. During a mismatch, reduced specific thalamus spiking causes decreased inhibition by TRN of the nonspecific thalamus, and a consequent increase in nonspecific thalamus firing rate, or arousal, that is proportional to the degree of mismatch (Fig. 7c).

The human mismatch negativity (MMN) event-related potential has features that are consistent with these predicted properties. Physically deviant stimuli trigger a MMN roughly 200 ms after stimulus onset (Näätänen et al., 1978). Kraus et al. (1994) demonstrated involvement of nonspecific, but not specific, thalamic nuclei in the MMN (Fig. 9c), with differences

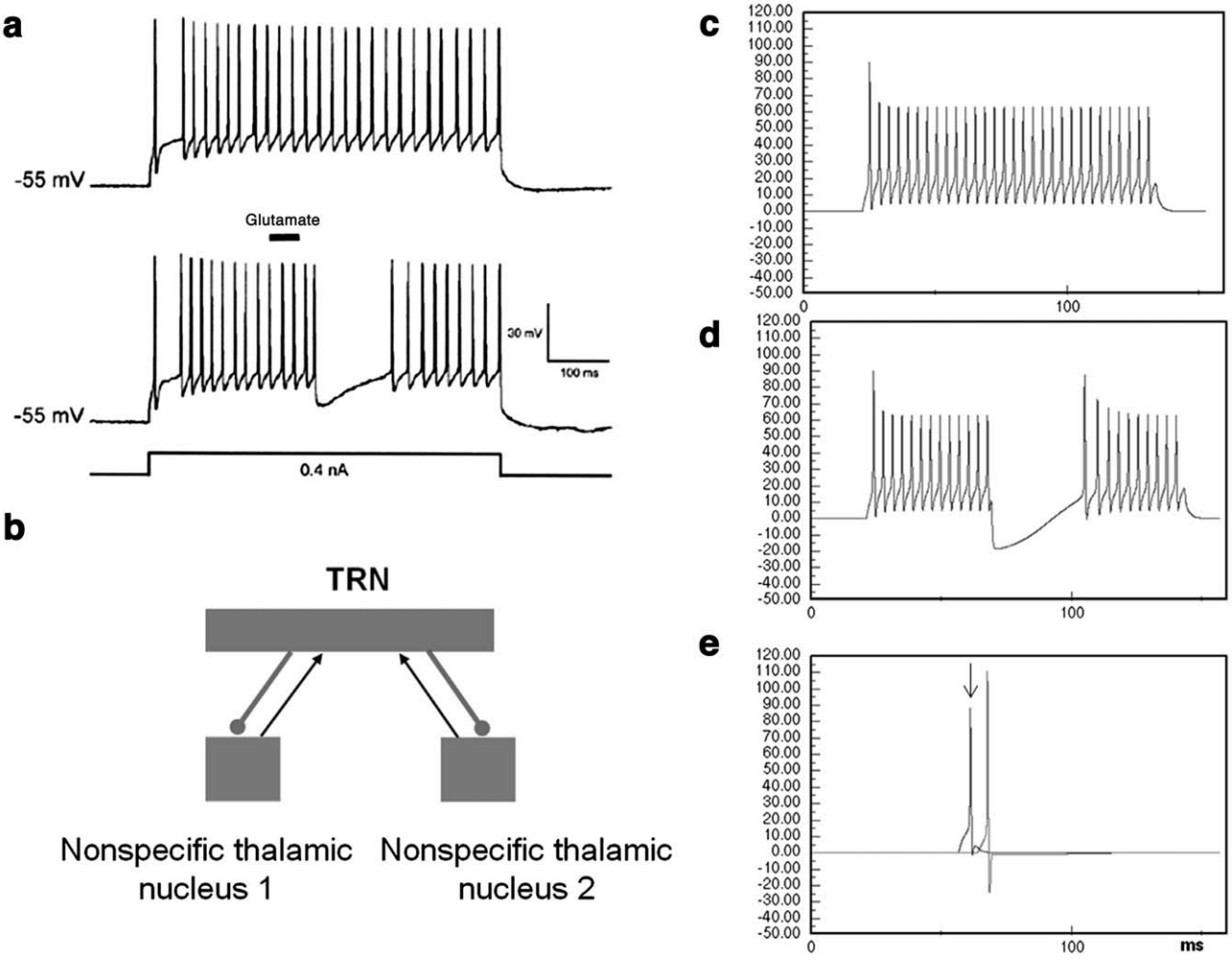

Fig. 13 – (a) Stimulation of one nonspecific thalamic nucleus interrupts a train of action potentials in another nonspecific thalamic nucleus. When held close to –55 mV, a rostral intralaminar nucleus (RIL) cell responds with a train of action potentials (top recording) to a depolarizing 0.4 *n*A current pulse (bottom, square wave). A train of action potentials (bottom recording) in the RIL cell in response to the depolarizing current pulse was interrupted by glutamate stimulation (black bar) in the caudal intralaminar nucleus (CIL, modified with permission from Crabtree and Isaac, 2002). (b) Model simulation includes two nonspecific thalamic nuclei and a TRN, all simulated as 1-neuron populations, with the TRN receiving excitation from the nonspecific thalamic nuclei, and inhibiting them with GABA projections. Cell activation was recorded at the nonspecific thalamic nucleus 2. (c) Constant stimulation of the nonspecific thalamic nucleus 2 gives rise to a train of action potentials (tonic firing) at 187 Hz. (d) Stimulation of nonspecific thalamic nucleus 1 causes a TRN-mediated IPSP in the nonspecific thalamic nucleus 2. (e) Stimulation of the nonspecific thalamic nucleus 1 (blue) causes a spike in the TRN (red), which in turn inhibits the nonspecific thalamic nucleus 2.

between novel and standard stimuli at 30–80 ms and 135–170 ms after stimulus onset. The late latency suggests a cortical contribution, which involves superficial cortical layers (Karmos et al., 1986).

The SMART model explains and simulates these earlier thalamic and later cortical components using the following properties: Mismatch increases nonspecific thalamic nucleus firing at around 50 ms after stimulus onset (Kraus et al., 1994; Fig. 9c), reaching cortical layer 1 and causing synchronized firing in layer 5 (Fig. 9d). The timing of the first MMN component in SMART is due to synaptic delays and spiking dynamics of the polysynaptic cycle that links LGN and the cortical circuit. During a mismatch, layer 5 apical dendrites accumulate the incoming EPSPs generated by the nonspecific thalamic nucleus burst until synchronized dendritic spiking occurs in all layer 5 cells. This layer 5 wave then excites layer 6^{II} (Fig. 3c), which in turn reactivates the nonspecific thalamic nucleus at around 150 ms after stimulus onset, thereby causing the second MMN component. Low threshold Ca^+ currents (see Eqs. (21)–(27) in the Methods) in the nonspecific thalamic nucleus generate an additional burst of spikes. This spiking pattern occurs when a hyperpolarized thalamic cell with low-threshold Ca^+ T-current is activated by an excitatory stimulus (Sherman and Guillery, 2001, 2002; Shipp, 2003). These simulation results provide an indirect confirmation of the Karmos et al. (1986) proposal of the cortical origin of the second component in the MMN.

The SMART model discussion of MMN is related to an earlier prediction about the interpretation of the ART search cycle that is summarized in Fig. 4; namely, that the mismatch, arousal, and STM reset events that are summarized in Figs. 4b and c correspond to different human scalp-recorded Event Related Potentials, or ERPs, and that these events should tend to co-occur, as they do in the ART search cycle, if they occur at all. In particular, as ART gradually developed, it predicted that the Processing Negativity, N200 (a component of which is MMN), and P300 ERPs correspond to match, arousal, and STM reset events at various levels of thalamocortical processing (Grossberg, 1978, 1980, 1984). This prediction was supported by ERP experiments using an oddball paradigm with a choice reaction time task, in which

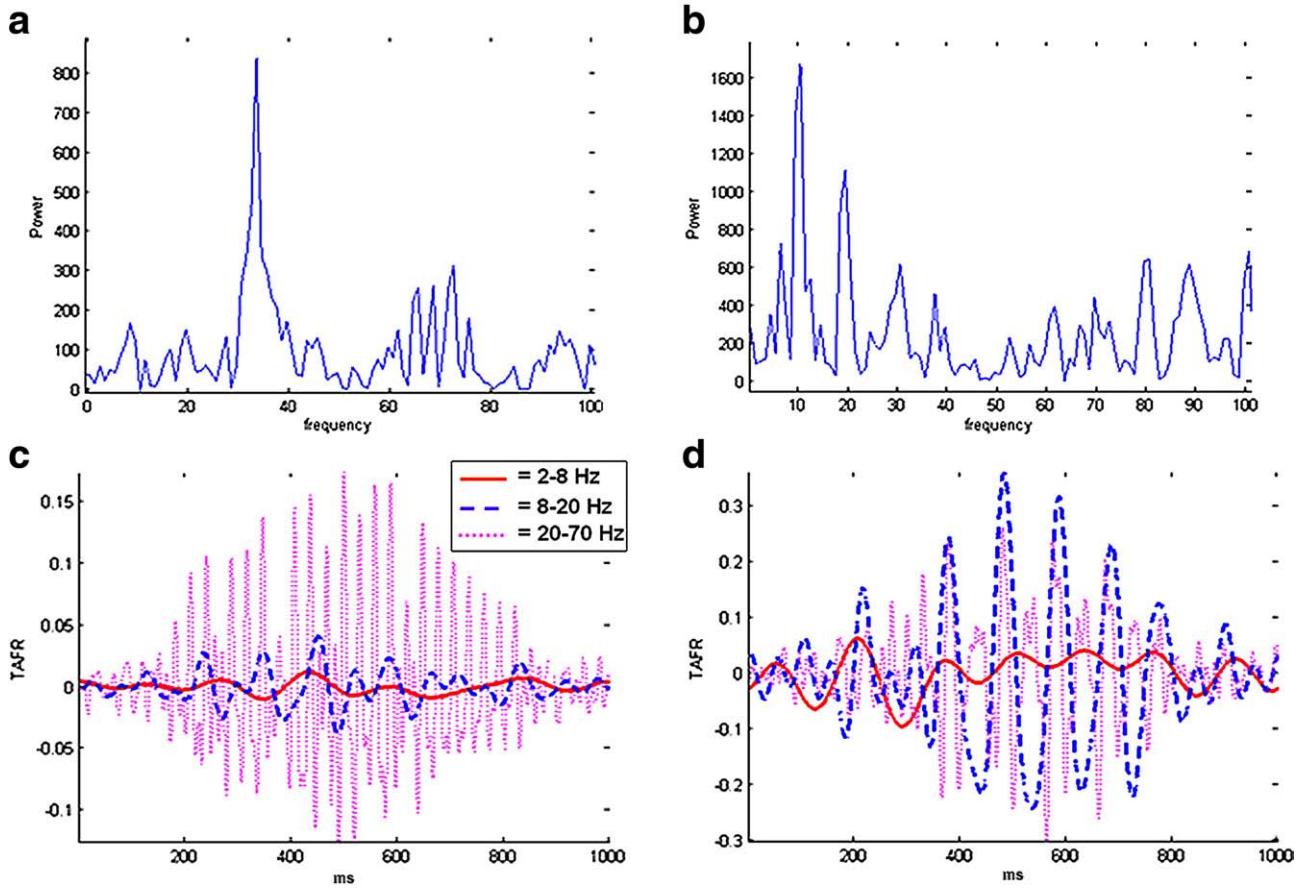

Fig. 14 – Power spectra of cumulative spike histograms of a laminar primary sensory cortical area during presentation of a stimulus (horizontal bar, 5 thalamic relay nuclei activated for 1000 ms) during match (a) and mismatch (b) conditions show a peak in the slow γ frequency band (20–70 Hz) in case of match, and lower frequencies in case of mismatch. The histograms were analyzed into three frequency bands (δ and θ, 2–8 Hz; α and β, 8–20 Hz; γ, 20–70 Hz) to highlight the separate contribution of different oscillation frequencies is a match (c) and mismatch (d). Notably, γ oscillations are drastically reduced in a mismatch in favor of lower-frequency oscillations.

correlated components of the P120, N200, and P300 behaved like the predicted mismatch, arousal, and STM reset events (Banquet and Grossberg, 1987).

2.6. *Layer 5 regulation of cortical reset*

Larkum et al. (1999) found that layer 5 cell dendrites can produce action potentials that actively propagate to layer 5 cell bodies and cause somatic action potentials (Figs. 10a and b). Until now, there has been no functional explanation of these regenerative dendritic potentials. Figs. 10b and 10c compare *in vitro* recordings of layer 5 pyramidal apical dendrites and soma, and model layer 5 cell simulations during match and mismatch episodes.

2.7. *Predictive search using mismatch-mediated arousal and habituative synapses*

How does a mismatch-mediated layer 5 reset signal choose a new cortical representation that can lead to a better match, and thus a better prediction? How can reset do this without an external teacher? How can it be done given that, at the moment of reset, the correct answer is not known, and at the location where reset occurs, there is no knowledge of which active thalamocortical representations caused the reset? A proposed solution to this problem (Grossberg, 1980) is herein realized using known laminar corticocortical and thalamocortical circuits. This solution predicts that the pathway which mediates reset utilizes habituative transmitter gates, also called depressing synapses (Grossberg, 1976, 1980; Carpenter and Grossberg, 1990; Abbott et al., 1997; Tsodyks and Markram, 1997). In particular, when a bottom-up input from a layer 6^I cell activates its excitatory parthway to layer 4, and its layer 6^I-to-4 inhibitory interneurons, an activity-dependent fraction of neurotransmitter in these pathways is released to activate layer 4 target cells (Fig. 11; see Methods). The transmitter recovery rate in these pathways is slow relative to its release rate (see Fig. 11). Thus the net EPSP recorded at a post-synaptic site decreases through time to a habituated level of firing after an initial burst of activation (Beierlein et al., 2002). Despite this reduction, synaptic transmission remains unbiased, and stronger inputs produce bigger steady-state EPSPs even as the corresponding transmitters habituate (Grossberg, 1980; Fig. 10d(I)).

When a layer 5-mediated reset wave later hits layer 6^I (Fig. 10d(II)), this arousal burst changes the balance of total input to layer 4 cells. Simulations (Fig. 10e) and mathematical proofs (Grossberg, 1980; Grossberg and Seidman, 2006) show how layer 4 cells reset based on their prior activation and the reset wave size, to favor previously inactive or weakly active layer 4 cells (Fig. 10d(III)).

2.8. *Acetylcholine neuromodulation controls vigilance, learning, and generalization*

How is the concreteness or abstractness of recognition categories controlled in a task-sensitive manner? A clue is provided by the fact that the nonspecific thalamic nucleus controls the excitability of layer 5, and therefore when reset and search for a new recognition category occurs. If the

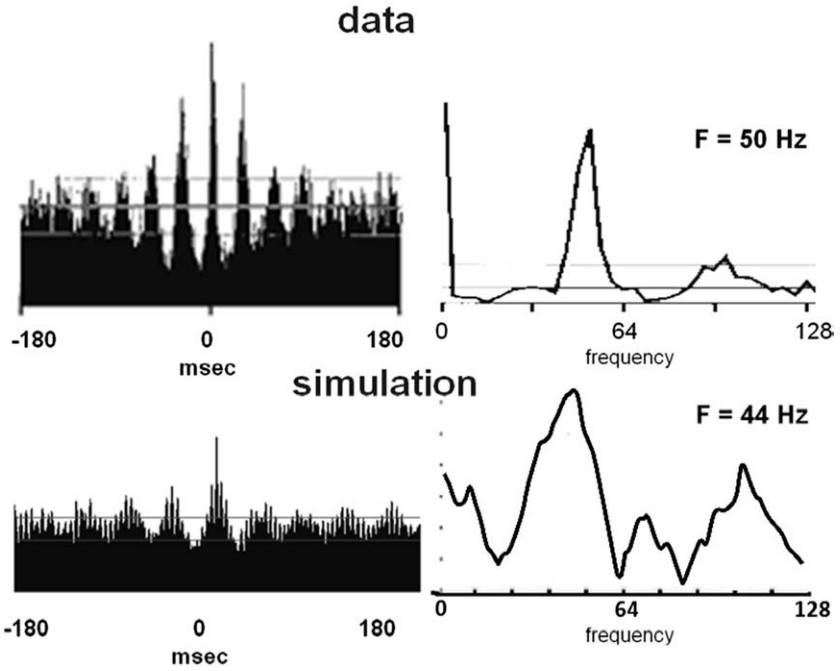

Fig. 15 – Example of short range (300μm), single unit–single unit correlation of cells with overlapping receptive fields and similar orientation preference in V1; *top, left*: cross-correlation computed from the two spike trains during the response to the stimulus. *top, right*: power spectrum of the cross-correlation shown on the left, which shows a peak around 50 Hz. Modified from Friedman-Hill et al. (2000). *Bottom, left*: cross-correlation computed from the spike trains of two nearby simulated layer 4 cells during stimulation of a learned stimulus (lines show the 95% confidence limit). *Bottom, right*: power spectrum of the cross-correlogram shown on the left.

sensitivity of layer 5 to arousal bursts from nonspecific thalamus can be modulated by predictive success, then the concreteness or abstractness of learned recognition categories can be controlled.

Fig. 12a summarizes data compatible with this hypothesis. ACh release occurs in the cortex from the nucleus basalis of Meynert. SMART predicts that increased ACh release occurs in the cortex from the nucleus basalis of Meynert following a predictive mismatch (Fig. 12b). In both *in vitro* data (Saar et al., 2001) and isolated model layer 5 pyramidal cells, ACh regulates AHP currents and cell excitability in layer 5 cortical cells. More specifically, Fig. 12a (top) shows that a steady depolarization current causes rat pyramidal cell firing to rapidly habituate, whereas injection of the ACh agonist carbachol reduces the adaptation (Saar et al., 2001). Fig. 12a (bottom) shows the simulation results for an isolated layer 5 pyramidal cell which include AHP currents in its somatic compartment, before and after ACh stimulation. Data and simulations show that the release of ACh can modulate, through the reduction of AHP and the prevention of spike adaptation, the excitability of layer 5 pyramidal neurons, and consequently the amount of thalamic mismatch that can be tolerated by the cortical area. High levels of ACh may increase vigilance by reducing spiking adaptation, facilitating reset and therefore requiring a higher degree of match between bottom-up and top-down representations.

Given this mechanism, suppose that bottom-up and top-down information are well enough matched in one cortical area to activate a category which generates a prediction elsewhere in the brain. If this prediction causes a predictive mismatch with, say, environmental feedback, then increased ACh release can trigger reset and search throughout the cortex, including the cortical region that accepted the previous match as sufficient to make the prediction. Reset can rapidly shut off the previously active recognition category before it can become engaged in erroneous new learning, and the ensuing search can discover either a new recognition category, or a familiar one, that makes a good enough mismatch to prevent prediction disconfirmation. The new recognition category will be learned, or the familiar category will be refined, to incorporate the new constraints imposed by the bottom-up data. ACh hereby makes the cortex more "vigilant." High vigilance forces learning of more precisely matched, and thus more concrete, categories than low vigilance.

2.9. *Intramodal attention and nonspecific thalamus*

Crabtree and Isaac (2002) have shown that activation of cells in one nonspecific thalamic nucleus leads to a TRN-mediated IPSP that temporarily switches off tonic firing of action potentials in cells of another nonspecific thalamic nucleus (Fig. 13a). A simulation of these results was carried out in an isolated circuit comprising two nonspecific thalamic cells and a TRN cell (Fig. 13b). Constant stimulation of a nonspecific thalamic nucleus cells caused a tonic stream of action potentials (Fig. 13c) which was interrupted by

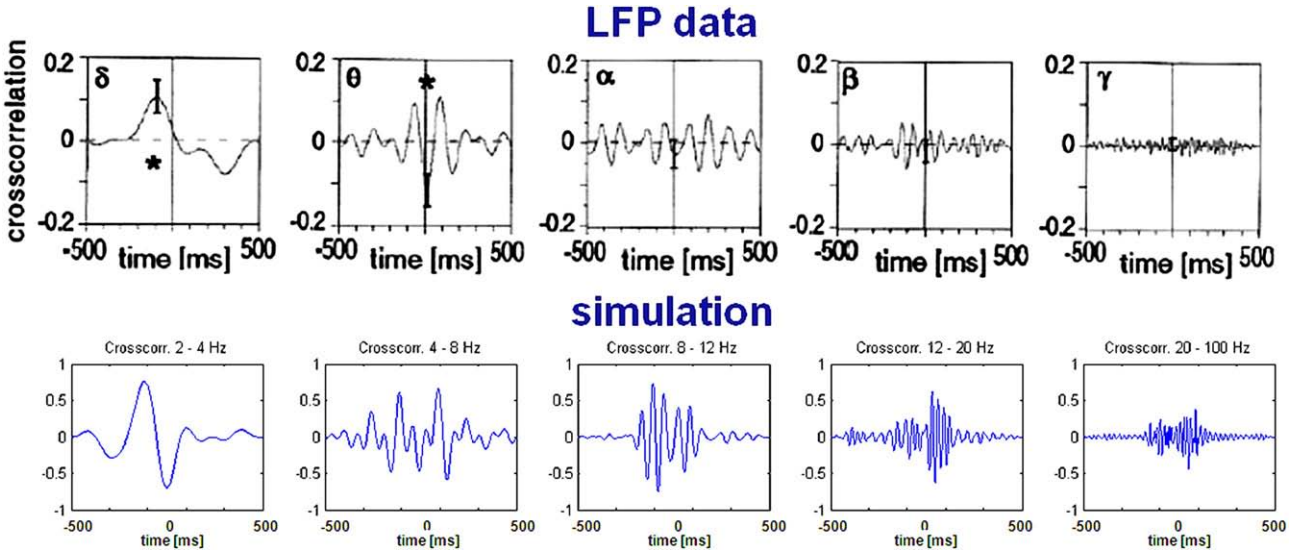

Fig. 16 – *Data:* Cross-correlation functions of local field potentials (LFP) from the middle layer of area 17 (primary visual cortical area) and lower layers of area 7 (higher-order visual area) during presentation of a no-go stimulus in behaving cats (reprinted with permission from Von Stein et al., 2000). *Simulation:* The activity of two thalamocortical loops was simulated, with a synaptic delay between layer 2/3 of the first-order cortical area and layer 4 of the second-order cortical area set at 10 ms. Epochs of 1000 ms were aligned to onset of a learned bottom-up stimulus that was presented for 1 s prior to the beginning of the recording. Analysis was performed on a LFP recorder from two simulated 54-tip-electrodes from the two cortical areas, and data were separated in five different frequency ranges in accordance with classical electroencephalogram conventions: 2–4, 4–8, 8–12, 12–20, and 20–100 Hz. The data were Fourier transformed and multiplied with the complex conjugate, and the inverse transformation was performed for selected frequency bins (corresponding to one "band") to obtain cross-correlation functions for separate frequency ranges. Cross-correlation functions at different frequency bands was performed between LFP produced in the lower 0.3 mm of the higher cortical area and the upper 0.3 mm of the lower cortical area (both areas are 1.2 mm thick).

the stimulation of a competing nonspecific thalamic cell (Fig. 13d). Crabtree and Isaac (2002) suggested that this effect is due to the TRN, as confirmed by our simulation results in Fig. 13e.

2.10. *Synchronous oscillation frequency reflects match and mismatch*

Gamma (γ, 20–70 Hz) and beta (β, 12–30 Hz) oscillations are observed in visual cortex during various cognitive, perceptual and attentive states (Singer, 1999; Engel et al., 2001; Hermann et al., 2004; Grossberg, 1976, 2003). Beta oscillations often correlate with long-range synchronous activity of neocortical regions (Roelfsema et al., 1997), and gamma is restricted to sites within an area (Friedman-Hill et al., 2000) or between two areas with strong monosynaptic connections (Von Stein et al., 2000). Gamma and beta oscillation frequencies in the model reflect match and mismatch dynamics, respectively.

Gamma oscillations are amplified between cells of an input population, and between cells of an input and a receiving population, when a top-down expectation matches its bottom-up input pattern (Figs. 14a and c). During mismatch within lower cortical layers, beta oscillations prevail (Figs. 14b and d) due to the low frequency, widespread synchronized firing of layer 5 cells, as illustrated in Fig. 9d. Layer 1 apical dendritic potentials slowly depolarize layer 5 cell bodies, causing the low frequency, synchronized spikes of layer 5 cells. This frequency component dominates the power spectrum of the cumulative spike histogram in cases of mismatches, as illustrated in Figs. 14b and d.

Buffalo, et al. (2004) have reported that gamma oscillations are more frequent in superficial cortical layers, whereas beta oscillations are found more in deeper cortical layers, consistent with the prediction that the beta oscillations may be due to the initiation of reset in the deeper layers. Their data would seem to be due to temporal averaging, since during sustained periods of match, one might expect all the cortical layers to synchronize with the same oscillation frequency due to interlaminar feedback connections (cf., Yazdanbakhsh and Grossberg, 2004). This functional interpretation of the gamma/beta differential may be testable by varying the relative number of reset events per unit time.

The SMART model also simulates data about short and long-range synchrony. Friedman-Hill et al. (2000) showed gamma synchronization between two adjacent macaque V1 cells with overlapping receptive fields in response to a preferred stimulus (Fig. 15 top). Model V1 layer 4 cells during match of a learned stimulus (Fig. 15 bottom) show a similar cross-correlation power spectrum. These results are consistent with the intuition that cells with a shared bottom-up input would tend to spike in close temporal proximity, and therefore express high gamma synchronization when no strong low-frequency synchronization is imposed by mismatch-mediated, synchronized layer 5 discharges.

Von Stein et al. (2000) showed (Fig. 16, top) that synchronization between distant cortical areas (middle layers of cortical area 17 and lower layers of area 7 in cats) is prevalent in the lower and middle frequency ranges, whereas local interactions (within areas 17 and 7) show gamma band dominance. The model simulates these properties (Fig. 16, bottom), showing that synchrony between distant cortical areas is mediated mostly by lower-frequency oscillations. These simulations support the hypothesis that monosynaptically connected cells, such as cells within an area or between nearby areas, can synchronize at gamma frequency bands (Fig. 15), which is compatible with STDP. Top-down interactions between lower layers of higher-order and upper levels of lower-order cortical areas are mostly modulatory. Therefore, upper pyramidal layers of lower-order areas should *not necessarily* fire in response to a top-down modulatory influence from higher cortical areas, and should *not necessarily* express gamma frequency synchronization, unless bottom-up and top-down signals match.

3. Discussion

This article describes a model that functionally links single-cell properties, such as spiking dynamics, STDP, and ACh modulation; detailed laminar thalamic and cortical circuit designs and their interactions; aggregate cell recordings, such as current source densities and local field potentials; and single-cell and large-scale inter-areal oscillations in the gamma and beta frequency domains, as an expression of the cognitive processing requirements that are needed to regulate fast learning and stable memory of brain representations. As a result of this wide descriptive range, the model proposes many testable predictions that link these various levels of brain organization as manifestations of how bottom-up adaptive filters and top-down expectations may be learned, matched, and stably remembered during thalamocortical and corticocortical STDP learning. In particular, the model simulates how specific and nonspecific thalamic nuclei regulate learning via temporal cycles of match/resonance and mismatch/reset, wherein learning is facilitated during match/resonance states and reduced during mismatch/reset states. The predicted involvement of the nonspecific thalamus in learning is consistent with lesion studies showing a role for the nonspecific intralaminar/midline thalamic nuclei in declarative memory (van Der Werf et al., 2003). Moreover, Kraus et al. (1994) have shown that the nonspecific thalamic nuclei, but not the specific thalamic nuclei, show significant differential activation in states of match vs. mismatch, consistently with the model prediction that the nonspecific pathway is sensitive to the degree of mismatch between bottom-up and top-down cortical signals.

Simulations (Figs. 13c–e) and experimental results (Crabtree and Isaac, 2002; Fig. 13a) show that the nonspecific thalamic nuclei innervating different cortical areas compete via TRN-mediated inhibitory interactions. The model predicts that competition in the nonspecific pathway does not interfere with bottom-up processing in the specific pathway, but rather transiently decreases the activation of some layer 5 cells, therefore preventing the corresponding cortical area from further influencing thalamic and cortical areas in the cortical hierarchy. The model suggests that this mechanism might be a subcortical substrate of cross-modality switching and competitive deployment of attentional resources. This prediction complements the observation (Zeki and Shipp, 1988; Sillito et al., 1994) that top-down, layer 6-mediated

attention has similar modulatory effects on target cortical and subcortical areas even in the absence of bottom-up input (Grossberg, 1999a; Raizada and Grossberg, 2003). In particular, simulation results (Figs. 9a and b) show how layer 6-mediated top-down corticothalamic feedback causes both fast priming excitation and slower inhibitory effects, as has been reported in experimental data (Jones, 2002).

A novel role for the neurotransmitter acetylcholine is postulated, linking levels of cortical ACh release to layer 5 excitability and layer 4 reset. Experimental results (Singer and Rauschecker, 1982; Kilgard and Merzenich, 1998) and modeling work (Hasselmo, 1993; Sánchez-Montañés et al., 2000) have shown that cholinergic modulation is an essential ingredient in cortical plasticity. The model predicts how strong ACh release, such as during repeated mismatches, or as a consequence of an environmental stressor, can influence the sharpness of the neural code, by altering the degree of match required for bottom-up and top-down matches to prevent reset. Lower levels of ACh favors coarser codes, because higher levels of mismatch can be tolerated by the system, thereby enabling more variable bottom-up input patterns to be associated with the same active recognition category without causing recoding.

The model for the first time mechanistically links cognitive mechanisms with brain oscillations, notably in the gamma (γ) and beta (β) frequency ranges, recorded from a variety of cortical and subcortical structures. Kopell et al. (2000) proposed that γ and β oscillations might subserve different functional roles. Their simulations showed that β oscillations are more robust in synchronizing areas separated by larger transmission delays, whereas γ oscillations tend to be dispersed when significant delays are interposed. Olufsen et al. (2003) have shown that β oscillations allow a different separation between "leading" and "suppressed" cell assemblies than do γ oscillations. Gamma oscillations promote a sharp dichotomy between active/inactive assemblies, a situation similar to a "choice". The SMART model shows how β oscillations can become a signature of modulatory top-down feedback and reset. Top-down processing, in both experimental and model results (Fig. 16), shows prevalence of lower-frequency oscillations, consistent with their modulatory nature (Olufsen et al., 2003) and their computational role of priming (Raizada and Grossberg, 2003; Siegel et al., 2000). In accordance with the present results, a computational study by Siegel et al. (2000) has shown that top-down feedback is accompanied by an overall increase of power in the low-frequency domain in the target neural population.

The SMART model extends previous modeling work by explaining how gamma oscillations emerge when modulatory top-down expectations are matched by consistent bottom-up input patterns. Such a match allows cells to more efficiently cross their spiking threshold to fire action potentials, leading to an overall increase in local gamma frequency synchronization among cells sharing common top-down priming modulation.

The SMART model also links the role of different oscillation frequencies with STDP. Learning episodes tend to be restricted to match conditions, when on average presynaptic and postsynaptic cells spike within 10–20 ms, namely within the STDP learning window, consistent with experimental results (Wespatat et al., 2004). The model predicts that STDP further reinforces synchronous activation of related cortical and subcortical areas, and that the effect of spurious synchronizations on long-term memory weights in a fast learning regimen can be prevented or rapidly reversed by a synchronous resonance during a match state. Gamma oscillations, amplified in case of a match, may favor propagation of spikes through the cortical hierarchy by packing pre-synaptic spikes within a narrow temporal window. This prediction is consistent with the observation that the efficacy of pairs of presynaptic LGN spikes on generating post-synaptic activation in the visual cortex falls off rapidly in time with the increase of the interspike interval (Usrey, 2002).

The different oscillation frequencies associated with match/resonance (gamma frequency) and mismatch/reset (beta frequency) link these frequencies not only to selective learning, but also to the active search process that can discover cortical substrates upon which to base new learning. The fact that mismatch is also predicted to be expressed in components of the N200 ERP points to new experiments that combine ERP and oscillation frequency as indices of the cognitive processes that actively regulate learning.

SMART predicts how the nonspecific thalamic nucleus may play a crucial role in processing match/mismatch of sensory information and cortical expectations. However, the nonspecific thalamic nucleus is not the only structure involved in processing novelty. The hippocampus has long been implicated as a neural substrate that is sensitive to stimulus novelty; e.g., Deadwyler, West, and Lynch (1979), Deadwyler, West, and Robinson (1981); O'Keefe and Nadel (1978); Otto and Eichenbaum (1992); Vinogradova (1975); see Kumaran and Maguire (2007a) for a review. Previous modeling work (Grossberg and Schmajuk, 1989; Grossberg and Merrill, 1992, 1996) has proposed how the hippocampus may modulate recognition learning and reinforcement learning by an adaptively-timed inhibition of orienting responses in delayed non-match to sample paradigms where both temporal delays between cues and novelty-sensitive recognition processes are involved. This proposed role of the hippocampus as a structure involved in bridging temporal gaps between temporally-disjoint representations is consistent with animal (Solomon et al., 1986) and human (Clark and Squire, 1998; Büchel et al., 1999) studies showing that the hippocampus may maintain a memory trace between the offset of the conditioned stimulus and the delayed onset of the unconditioned stimulus to enable associative learning in trace conditioning. The hippocampus has also been related to sequence novelty, a type of associative novelty where familiar items appear in a new temporal order (Kumaran and Maguire, 2007b).

SMART explains data consistent with the hypothesis that fine-grained matches between bottom-up sensory information and top-down cognitive expectations may occur in the thalamocortical system. The hippocampal role in adaptive timing, spatial navigation, and declarative (notably, episodic) memory supplements the thalamocortical system with temporally and spatially-related expectations (cf. Gorchetchnikov and Grossberg, 2007). When these hippocampal processes are dependent on sensory and cognitive recognition events, the hippocampus might be a recipient, rather than a generator, of a mismatch response. This hypothesis is consistent with

anatomical data showing connections from nonspecific thalamus to hippocampus (Pakhomova, 1981). The MMN literature provides additional evidence that an early generator of mismatch is located in the nonspecific thalamic nucleus (Kraus et al., 1994). This hypothesis is partially supported by a recent ERP study where Rosburg et al. (2007) recorded from human hippocampus and rhinal cortex in an oddball paradigm. Both in the rhinal cortex and hippocampus, the amplitudes of ERP components elicited by deviants exceeded those of standard tones. The study showed a negative component in the rhinal cortex with a latency of about 200 ms and a positive component with a latency of about 400 ms, and a large negative component in the hippocampus with a latency of about 300–400 ms. The authors concluded that, based on the temporal order of deviance-related ERP activity, "…the information of sound deviance goes from the auditory cortex via the rhinal cortex to the hippocampus" (p. 7). These findings are consistent with the proposal that sensory mismatches occur early in the thalamocortical system, but further studies are needed to systematically explore the relative timing of novelty-generated signals in the thalamus and hippocampus across species, and the functional differences that these novelty signals represent.

Additional cortical areas, such as the anterior cingulate cortex (ACC) are known play a role in reward-sensitive error detection (Bush et al., 2000; Holroyd et al., 2004; Luu and Pederson, 2004). Among other possible functions, ACC may be activated by reward-sensitive instrumental mismatches and thereby help to reset the active reward-sensitive and action-sensitive representations that led to predictive failure, much as mismatches within the nonspecific thalamic nuclei and hippocampus may reset a hierarchy of sensory, cognitive, spatial, timing, and sequential planning-related representations.

Finally, the SMART model advances a computational framework that allows testing and further development of how computations on multiple organizational levels in cortical and subcortical networks of spiking neurons may provide additional insights into how the brain learns to predict and control an increasingly complex and changing environment in a stable way through time.

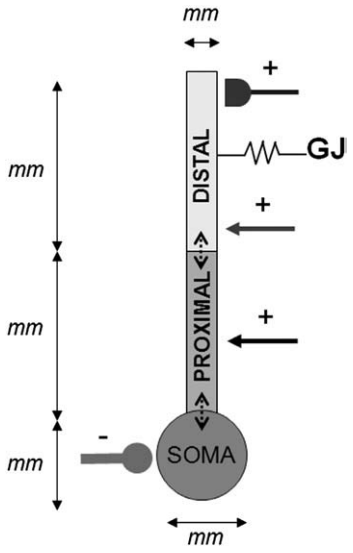

Fig. 17 – The generic neuron model. The neuron depicted above is a 3-compartment-cell with a soma, a proximal and a distal dendrite. Excitatory driving (arrow terminating in the proximal dendrite,+), modulatory (arrow terminating in the distal dendrite,+), plastic (half-ellipse terminating in the distal dendrite,+), as well as inhibitory (rounded arrow terminating in the soma,–) connections can terminate in each cell compartment, which are in turn linked by passive leakage currents (vertical dotted arrows). Electrical coupling between different cell compartments (gap junctions, GJ) can also be present (in the figure, in the distal dendrite).

4. Experimental procedures

4.1. *Model overview*

The SMART model (Figs. 2 and 3) includes two hierarchically-organized thalamocortical loops: a first-order primary loop (analogous to the LGN-V1) and a higher-order loop (analogous to the PULV-V2). Each thalamocortical loop simulates a 1.2 mm thick, 6-layered cortical module with cortical excitatory and inhibitory neurons, a thalamic nucleus composed of core and matrix cells (Jones, 2002) and local inhibitory interneurons, and a GABAergic thalamic reticular nucleus (TRN). The primary thalamocortical loop also includes a nonspecific thalamic nucleus. All cortical and subcortical layers are organized in 9×9 neural sheets, with the exception of the nonspecific thalamic nucleus and matrix thalamic cells that are simulated as single populations. Units are implemented as multi-compartment neurons obeying Hodgkin–Huxley-type dynamics (Hodgkin and Huxley, 1952). The minimal numbers of compartments and currents needed to produce the desired network properties is used in each neuron's unbranched cable sections (Rall, 1962). The model implements online spike-timing-dependent plasticity (STDP) learning (Gorchetchnikov et al., 2005a), and the plastic synaptic weights, as well as each neuron's compartmental currents, are recorded to allow off-line local field potentials (LFP), current source densities (CSD), and oscillation frequency/synchrony analysis (Versace et al., 2007). Stimuli are horizontally or vertically oriented bars that enable testing of model hypotheses about match/mismatch dynamics and learning.

4.2. *Neuron description*

Excitatory neurons (thalamic core, matrix, and nonspecific, cortical layers 4, 2/3, 5 and 6) and inhibitory interneurons (TRN and thalamic interneurons, cortical layers 4 and 2/3 interneurons), as well as their connections, were constructed according to known anatomical and biophysical data from primarily rats and cats. When unavailable, cell parameters were chosen in order to obtain the desired functional properties. Each of the two simulated thalamocortical loops consists of 732 multi-compartmental neurons (Fig. 17), 2,106 compartments, and is described by 17,415 differential equations. Fig. 18 shows the spatial arrangement and cell sizes of the populations composing the simulated 1.2 mm thick laminar cortical sheet.

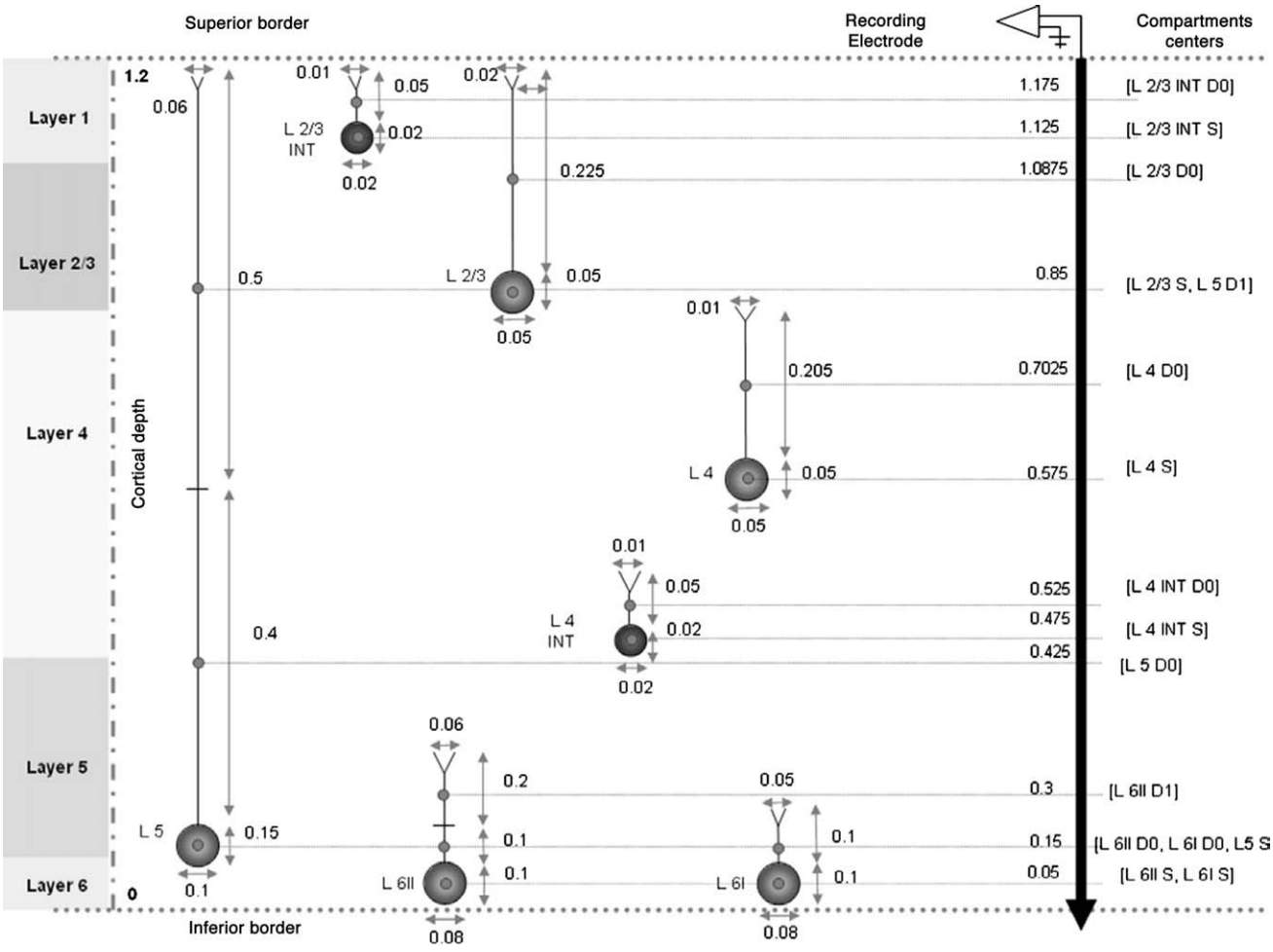

Fig. 18 – Spatial arrangement and cell sizes of the populations composing the 1.2 mm thick laminar cortical sheet. A multi-compartment model with a spatially explicit structure allows to calculate trans-membrane currents, which can be employed to derive aggregate cell recordings such as Local Field Potentials (LFP) and Current Source Densities (CSD). The activity of dendrites and cell somas of the populations can be recorded by an electrode with variable number of tips (black thick downward arrow, right). Since each compartment is treated as electrically uniform, the center of the compartment is the physical point at which the current source/sink is calculated (thick dot at the center of soma/dendrite). Cell bodies and dendrites are vertically aligned parallel to the recording electrode. For each layer, cells are displaced at random distance from the recording electrode. The distance of the electrode to the selected cell in the population is drawn from a uniform distribution on the interval [10–200] μm, whereas the distance to all other cells in the population is drawn from a uniform distribution on the interval [10–1000] μm. In the figure, only one cell for each population is shown. Abbreviations: L=layer; S=soma; D=dendrite (D0=proximal dendrite; D1=distal dendrite), INT=interneurons. All measurements are in mm.

Each compartmental membrane potential V[mV] is described by:

$$C_M \frac{dV}{dt} = \sum_i I_i. \quad (1)$$

In Eq. (1), C_M [μF·cm^2] is the membrane capacitance. Ionic or chemically-gated channels and inter-compartmental currents are described by the current density I_i [μA/cm^2] equation:

$$I_i = g_{Ch}(V^{EQ} - V), \quad (2)$$

where the channel conductance g_{Ch} and the equilibrium voltage V^{EQ} [mV] change according to the nature of the current. Inter-compartmental currents from compartment m to compartment l are described by Eq. (2), where $g_{Ch}=g_{ml}D_l/4L_l^2$ [kΩcm], g_{ml} is the conductance between compartments m and l, D_l [mm] and L_l [mm] are the diameter and length of membrane compartment l, respectively, and $V^{EQ}=V_m$ and $V=V_l$ are potentials of the neighboring compartments. Table 3 lists dimensions, passive cable properties, and ionic channels (such as sodium (Na^{++}), potassium (K^+) and leakage channels) parameters.

In chemically gated channels (AMPA, GABA, etc.) between neurons j and k, $V^{EQ}=E_i$[mV] is the reversal potential of the channel, and the conductance $g_{Ch}=w_{jk}\,\bar{g}_{jk}\,g(t)$, where w_{jk} is the synaptic weight connecting neurons j and k, and $\bar{g}_{jk}$ [pS] is the maximal channel conductance of the synaptic weight w_{jk}. The synaptic weight $w_{jk} = \frac{N_i}{\pi DL}\left[\frac{10^6}{cm^2}\right]$ corresponds to the density of receptors (millions of channels per membrane cm^2). The conductance $g(t)$ is defined as a dual exponential factor describing the time course of the excitatory or inhibitory post-synaptic

Table 3 – Dimensions, passive cable properties and ionic channels parameters of each cellular stage of the thalamocortical circuit

Cell	Compartment diameter	Compartment length	Axial resistance	E_L	g_L	g_{Na}	g_K	g_{Ca}
Units	mm	mm	KΩ cm	mV	mS/cm^2	mS/cm^2	mS/cm^2	mS/cm^2
First-order thalamic relay								
Soma	0.05	0.06	8	−60	0.01	100	100	–
Dendrite 0	0.005	0.008	8	−60	0.01	–	–	10
Dentric 1	0.005	0.008	8	−60	0.01	–	–	10
First-order thalamic (matrix)								
Soma	0.05	0.06	8	−60	0.01	100	100	–
Dendrite 0	0.005	0.008	8	−60	0.01	–	–	10
Dentric 1	0.005	0.008	8	−60	0.01	–	–	10
First-order thalamic interneurons								
Soma	0.02	0.02	60	−49	0.01	50	30	–
Dendrite 0	0.001	0.1	60	−49	0.01	–	–	–
TRN								
Soma	0.05	0.05	10	−69	0.1	100	100	–
Dendrite 0	0.01	0.05	10	−69	0.1	–	–	10
Dentric 1	0.01	0.05	10	−69	0.1	–	–	10
Thalamic nonspecific								
Soma	0.08	0.08	10	−64	0.09	100	100	–
Dendrite 0	0.015	0.1	10	−64	0.1	–	–	250
Dentric 1	0.015	0.1	10	−64	0.1	–	–	250
Layer 4 Excitory								
Soma	0.05	0.05	40	−65	0.01	50	30	–
Dendrite 0	0.01	0.25	40	−65	0.01	–	–	–
Layer 4 inhibitory								
Soma	0.02	0.02	100	−50	0.01	50	30	–
Dendrite 0	0.01	0.05	100	−50	0.01	–	–	–
Layer 2/3 excitory								
Soma	0.05	0.05	100	−65	0.05	50	30	–
Dendrite 0	0.02	0.225	100	−65	0.05	–	–	–
Layer 2/3 inhibitory								
Soma	0.02	0.02	60	−49	0.01	50	30	–
Dendrite 0	0.01	0.05	60	−49	0.01	–	–	–
Layer 5								
Soma	0.1	0.15	5	−72	0.1	50	30	–
Dendrite 0	0.06	0.4	5	−72	0.03	–	–	–
Dentrite 1	0.06	0.5	5	−72	0.03	50	30	–
Layer 6^{-I}								
Soma	0.08	0.1	80	−70	0.15	50	30	–
Dendrite 0	0.05	0.1	80	−70	0.9	–	–	–
Layer 6^{II}								
Soma	0.06	0.1	25	−64	0.1	50	30	–
Dendrite 0	0.08	0.1	25	−64	0.03	–	–	–
Dentric 1	0.08	0.2	25	−64	0.03	–	–	–

E_L and g_L represent the leakage currents equilibrium potential and conductance, respectively. Cell morphologies are the same for cells in the first-order and second-order thalamocortical loop.

potentials (EPSP and IPSP, respectively) triggered by the pre-synaptic spike:

$$g(t) = \begin{cases} \frac{p}{\tau_f - \tau_r}\left(e^{-\frac{t}{\tau_f}} - e^{-\frac{t}{\tau_r}}\right) & \text{if} \quad \tau_f \neq \tau_r \\ \frac{t}{\tau_f} e^{\left(1-\frac{t}{\tau_f}\right)} & \text{if} \quad \tau_f = \tau_r \end{cases}, \tag{3}$$

where t is the time since the onset of a pre-synaptic spike, p is a normalizing coefficient that ensures:

$$\max\left(\frac{p}{\tau_f - \tau_r}\left(e^{-\frac{t}{\tau_f}} - e^{-\frac{t}{\tau_r}}\right)\right) = 1 \tag{4}$$

and τ_r and τ_f are the EPSP and IPSP rise and fall time constants, respectively. See Supplementary Table 4 online for parameters of chemically-gated channels.

Unless otherwise specified, simulations were implemented in a full first-order thalamocortical sector including a six-layered cortical structure (V1), a TRN sector, a first-order thalamic nucleus (LGN), and a nonspecific thalamic nucleus. Eqs. (1)–(27) and (29) below describe the cell properties of the first-order thalamocortical sector, whereas Eq. (28) is used only in producing the results illustrated in Figs. 12 and 19. The passive properties of the cells describing each cellular stage in the first-order thalamocortical sector are listed in Table 3,

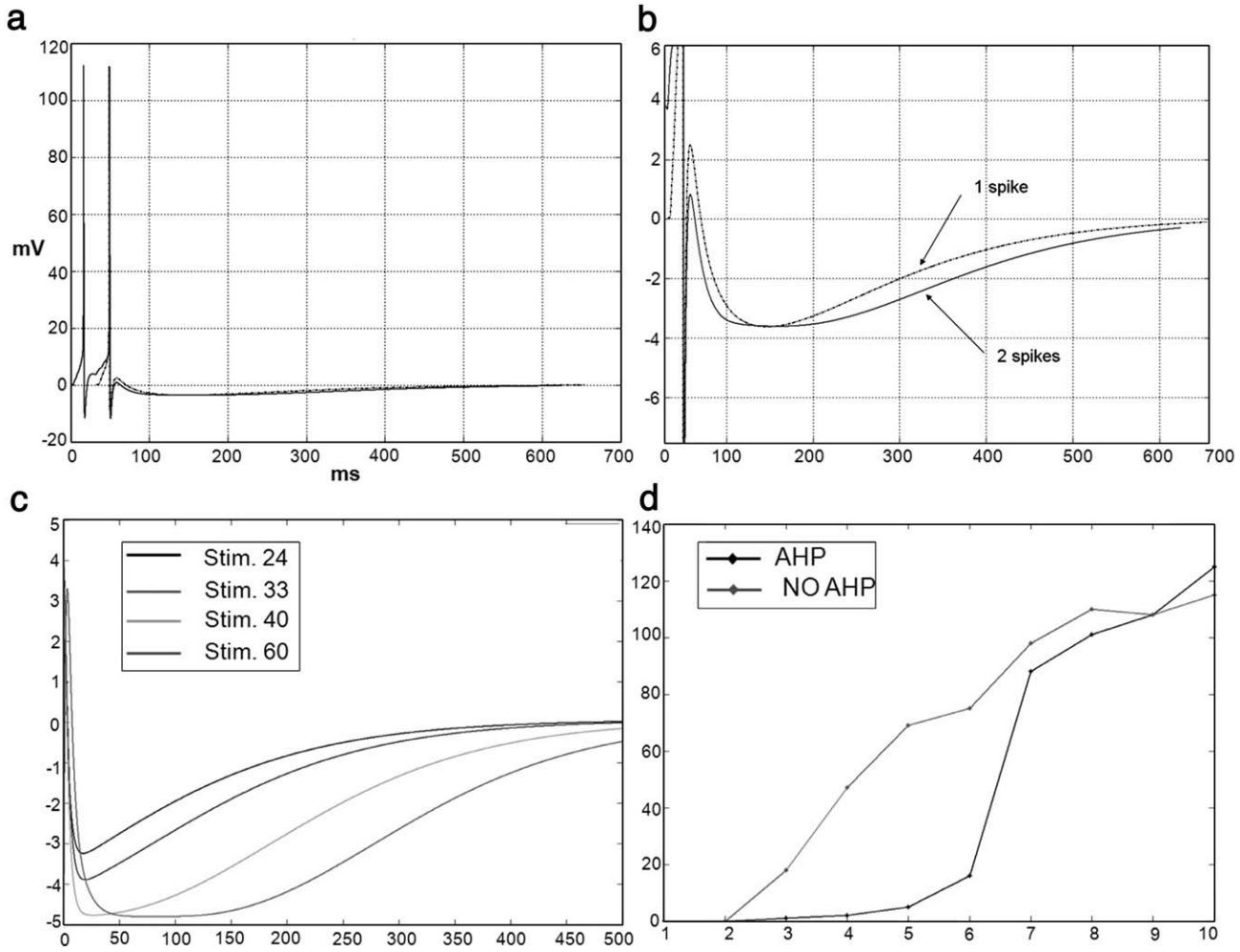

Fig. 19 – AHP-controlled inhibitory currents are spike-dependent. (a) Effect of cell spiking frequency on the membrane potential in the presence of AHP. The membrane potential of an isolated layer 5 pyramidal cell is plotted after emitting one (dotted trace) or two (continuous trace) spikes. Stimulation was induced by a 10 ms current injection until one or two spikes were generated. In order to allow direct comparison of the membrane voltage, the second spike in the "two-spikes" condition and the only spike in the "one-spike" condition were aligned for comparison. (b) Magnification of (a) shows the different time course and amplitude of the membrane potential in the two conditions. (c) Higher firing rates, caused by higher currents injections of 24, 33, 40, and 60 mV cause longer-lasting and deeper cell hyperpolarization, almost fully recovering after 500 ms. (d) Firing rate (output) vs. input intensity (voltage clamp of 3, 9, 15, 24, 33, 40, 60, 72, 77 mV) in a pyramidal cell with (black) and without (red) AHP. Firing rates of cells with active AHP are generally lower from those with blocked AHP. Cells with active or inactive AHP also differ on the shape by their input/output function.

whereas chemical and electrical synapses properties are listed in the Supplementary Table 4 online. Simulations of isolated cells in the network are performed by preserving all passive electrical properties of the simulated cell as listed in Table 3, whereas all synaptic conductances of other cell stages are set to zero to prevent any interaction with the isolated cell. More details on the simulation methods for isolated cells are provided in the pertinent figure captions.

4.3. *Synaptic plasticity*

Plasticity in the synaptic weight w_{jk} modulates the post-synaptic conductance $\bar{g}_{jk}\, g(t)$ by varying the density of post-synaptic channels, therefore influencing the impact of a spike on the magnitude of the current I_i. Learning in synaptic weights obeys a gated learning law (Grossberg, 1980; Gorchetchnikov et al., 2005a):

$$\frac{dw_{jk}}{dt} = \lambda f_G(V_k, g_{jk})\left(g_{jk} f_N(V_k)\left(\breve{w} - \hat{w}\right) + w_0 - w_{jk}\right), \tag{5}$$

where λ is the learning rate, $f_G(V_k,g_{jk})$ is a gating signal that turns learning on and off, $\breve{w}$ and $\hat{w}$ are the minimum and maximum weight, and w_0 stands for the baseline weight achieved when there is no correlation between presynaptic and postsynaptic firing. The gating function $f_G(V_k)$ is described as:

$$f_G(V_k) = \begin{cases} D+1 & \text{if} \quad V_k \geq V_k^{\theta} \\ -10(t-s)+D+1 & \text{if} \quad s<t<s+0.1\ \text{ms} \\ \dfrac{-D}{25}(t-s-0.1\ \text{ms})+D & \text{if} \quad s+0.1\ \text{ms} \leq t < s+25.1\ \text{ms} \\ 0 & \text{otherwise} \end{cases}, \tag{6}$$

where V_k^{θ} is the spiking threshold potential, t is time, s is the moment of the postsynaptic spike, and $D = \left(\breve{w} - w_0\right)/\left(\hat{w} - \breve{w}\right)$. This scaling function is a non-negative function of pre- and postsynaptic activity and allows synaptic change to occur only when pre- and postsynaptic cell are simultaneously active. See Gorchetchnikov et al. (2005a) for the derivation and the detailed discussion of the rule.

Two forms of gating are used: post-synaptic and dual-AND gating. Post-synaptic gating, where $f_G(V_k, g_{jk}) = (V_k)^2$, is implemented in specific thalamic projections terminating in layer 4 (bottom-up adaptive weights) and allows the winning layer 4 cells to learn the LGN spatio-temporal pattern of activation. Dual-AND gating, where $f_G(V_k, g_{jk}) = g_{jk}(V_k)^2$, is implemented in layer 6^{II} projections terminating in the specific thalamus and in layer 1 apical dendrites of layer 5 cells of a previous cortical stage (top-down adaptive weights). This gating allows V2 layer 6^{II} cells sending feedback projections to V1 layer 5 cells to prime, and then learn the activation pattern of, active layer 5 cells.

4.4. *Neurotransmitter release*

The neurotransmitter released by the pre-synaptic terminal scales the EPSP or IPSP triggered at the post-synaptic site. The accumulation and depletion (inactivation, habituation) of neurotransmitter z_{jk} at a synapse between neurons j and k is described by (Grossberg, 1980):

$$\frac{dz_{jk}}{dt} = \frac{(B - z_{jk})}{\tau} - \varepsilon\delta(t)z_{jk}, \tag{7}$$

where $B=1$ is the target level of neurotransmitter at rest, $0<\varepsilon<1$ is the depletion coefficient that can scale the amount of neurotransmitter released at every spike, and $0.1<\tau<500$ is the recovery rate (in ms) regulating the rate of neurotransmitter accumulation. A spike $\delta(t)$ is defined as:

$$\delta(t) = \begin{cases} 1 & \text{if } V(t)<0 \text{ and } V(t-\Delta t)>V^{\theta} \\ 0 & \text{otherwise} \end{cases}, \tag{8}$$

where $V(t)$ is the soma membrane voltage at time t, V^{θ} is the voltage threshold that is invariably crossed during spikes (30 mV), $V(t-\delta t)$ is the soma membrane voltage at time $t-\delta t$ that precedes the soma voltage crossing 0 mV. In Eq. (7), the neurotransmitter z_{jk} accumulates towards B at a rate inversely proportional to the recovery rate τ, and habituates, or is depleted, by $-\varepsilon\delta(t)z_{jk}$ every time a spike occurs. Neurotransmitter depletion allows the EPSP and IPSP to be multiplicatively gated by the amount of neurotransmitter available, while still ensuring that $0<g_{jk}z_{jk}<B$ (for all simulations, $B=1$). Fig. 11 shows how neurotransmitter level varies with different values of ε and τ and different pre-synaptic firing frequencies.

4.5. *Ionic currents*

Potassium (K^+) and Sodium (Na^{++}) currents I_k and I_{Na} in Eq. (1) are derived from Traub and Miles (2001), and are described as:

$$I_K = \overline{g}_K n^4 (E_K - V), \tag{9}$$

where

$$\frac{dn}{dt} = \alpha(1-n) - \beta n, \tag{10}$$

$$\alpha = \frac{.032(15 - V)}{e^{\frac{15-V}{5}} - 1}, \tag{11}$$

$$\beta = .5e\frac{10 - V}{40}, \tag{12}$$

and

$$I_{Na} = m^3 h \overline{g}_{Na}(E_{Na} - V), \tag{13}$$

where

$$\frac{dm}{dt} = \alpha(1-m) - \beta m, \tag{14}$$

$$\alpha = \frac{.032(13 - V)}{e^{\frac{13-V}{4}} - 1}, \tag{15}$$

$$\beta = \frac{-.28(40 - V)}{e^{\frac{40-V}{-5}} - 1}, \tag{16}$$

$$\frac{dh}{dt} = \alpha(1-h) - \beta h, \tag{17}$$

$$\alpha = .128e^{\frac{27-V}{18}}, \tag{18}$$

and

$$\beta = \frac{4}{e^{\frac{40-V}{5}} + 1}. \tag{19}$$

For all neurons, $E_K=-90$ mV and $E_{Na}=50$ mV. Leakage current I_{leak} is defined as:

$$I_{leak} = -\frac{g_{leak}N_{leak}}{\pi DL}V, \tag{20}$$

where g_{leak} is the conductance of the leakage channel, $\frac{N_{leak}}{\pi DL}$ is the channel density, and $E_{leak}=0$ mV.

4.6 *Calcium currents in thalamic cells*

Low-Threshold *T-Type* currents (Destexhe, 2000) are implemented in thalamic matrix, core, TRN and nonspecific thalamic cells, and are described as:

$$I_{Ca} = \overline{g}_{Ca} m^3 h (E_{Ca} - V), \tag{21}$$

where

$$\frac{dm}{dt} = \frac{1}{\tau_m}(m_{\infty} - m), \tag{22}$$

$$\tau_m = \frac{1}{e^{\frac{-63-V}{7.8}} + 1}, \tag{23}$$

$$m_{\infty} = 2.44 + 2.506 \cdot 10^{-2} e^{-9.84 \cdot 10^{-2} V}, \tag{24}$$

$$\frac{dh}{dt} = \frac{1}{\tau_h}(h_{\infty} - h), \tag{25}$$

$$\tau_h = \frac{1}{\frac{-83-V}{6.3} + 1}, \tag{26}$$

and

$$h_{\infty} = 19.5 + 7.171 \cdot 10^{-2} e^{-10.54 \cdot 10^{-2} V}. \tag{27}$$

For all neurons with Ca^{++} currents, $\overline{g}_{Ca} = 250$ mS/cm^2, and $E_{Ca}=180$ mV.

4.7. *Cholinergic modulation and after-hyperpolarization currents (AHP)*

Pharmacological and physiological studies have demonstrated that ACh has facilitatory effects on cortical pyramidal neurons (McCormick and Prince, 1985), and rat cortical layer 5 cells seem to be a preferential target for cholinergic innervation (Turrini et al., 2001). The known electrophysiological excitatory action is thought to be mediated by binding of ACh to muscarinic and/or nicotinic receptors on pyramidal neurons. This causes a reduction of membrane K^+ conductance in cortical neurons, enhancing depolarization in response to glutamatergic input (McCormick and Prince, 1985) and reducing spike adaptation due to the after-hyperpolarization current (AHP, Hille, 2001) based on a slow and long-lasting increase in K^+ conductance.

AHP and its modulation by acetylcholine are modeled by:

$$I_i = g_{Ch}(V^{EQ} - V),$$

where the AHP current conductance $g_{Ch} = g^* \overline{g}_{AHP} g(t)$ is modulated by the conductance g^* controlled by the cholinergic presynaptic spike, and $\overline{g}_{AHP}$[nS] is the maximal K^+ conductance of the AHP channel. The AHP conductance $g(t)$ is described by Eq. (3):

$$g(t) = \begin{cases} \frac{p}{\tau_f - \tau_r}\left(e^{-\frac{t}{\tau_f}} - e^{-\frac{t}{\tau_r}}\right) & \text{if} \quad \tau_f \neq \tau_r \\ \frac{t}{\tau_f} e^{\left(1-\frac{t}{\tau_f}\right)} & \text{if} \quad \tau_f = \tau_r \end{cases}$$

where t is time since the action potential of a modulatory cell; p is the scaling coefficient described in Eq. (4). For the AHP used in these simulations τ^r and τ^f, namely the rise and fall time constants, respectively, are τ^r=80 ms and τ^f=100 ms. The K^+ channels responsible for the AHP are opened by any cell's axonal output. If there is no spike, $t=\infty$, therefore $g=0$. If there is a spike, $t=0$, causing g to rise. The effect of a cell's spike on the soma membrane potential in the presence of AHP is illustrated in Fig. 19.

The cholinergic modulation conductance g^* is described by

$$g^* = \begin{cases} 1 - \frac{p}{\tau_f - \tau_r}\left(e^{-\frac{t}{\tau_f}} - e^{-\frac{t}{\tau_r}}\right) & \text{if} \quad \tau_f \neq \tau_r \\ 1 - \frac{t}{\tau_f} e^{\left(1-\frac{t}{\tau_f}\right)} & \text{if} \quad \tau_f = \tau_r \end{cases}, \qquad (28)$$

where τ^r=5 ms and τ^f=6 ms, and t is the time since the presynaptic cholinergic cell spikes (nucleus basalis of Maynert). These simulations investigate only the fast cholinergic dynamics, and do not address longer-lasting effect of ACh on target neural populations (Hasselmo, 1995). The cholinergic input acts by closing the normally open gate g^*, therefore limiting the total AHP conductance when ACh modulation is active.

4.8. *Network connectivity*

Connections between and within cell populations link a presynaptic cell with a given postsynaptic cell compartment target of the axonal projection, and can be categorized as: 1-to-1, 1-to-many, or many-to-1 projections. Synaptic weights w_{ij} can be defined between and within layers according to:

$$w_{ij} = \frac{1}{\sqrt{2\pi\sigma^2}} e^{-(x-\mu)^2/2\sigma^2}, \qquad (29)$$

where μ is the mean and σ is the standard deviation. Each axonal pathway can be considered as a delay line, which adds an additional component of delay between pre- and post-synaptic spike, aside from the time required by EPSPs to trigger an action potential. Axonal delays were chosen to be consistent with both known transmission delays in cortical and subcortical areas, and with the spatial conformation of the model, and are summarized in Supplementary Table 4 online. In general, inhibitory to excitatory connections have small delays, intra-cortical feedforward connections have longer delays (Dinse and Kruger, 1994), and feedback connections (both corticocortial and corticothalamic) have even longer delays (Schmolesky et al., 1998; Miller, 1996).

The model accounts for the driving vs. modulatory nature of synaptic connections by exploiting both the magnitude of the synaptic weight *and* the passive neuron cable properties. An EPSP occurring at the distal dendrite tends to be attenuated with respect to the one occurring at the proximal dendrite or the soma depending on compartmental length and diameter. Inter-compartmental currents are described by Eq. (2), where $g_{Ch}=g_{ml}\cdot D_l/4L_l^2$ [kΩ^*cm], and where V^{EQ} and V represent the voltage of neighboring compartments. The longer and smaller the dendrite, the more attenuated the post-synaptic current will be at the soma. Differential dendritic termination and synaptic weight magnitudes can be used to simulate the proposed functional differentiation between driving, large, round (R-type) thalamic vesicles occurring at retinothalamic and thalamocortical synapses, and elongated, small vesicles that characterize many corticothalamic terminations (Rockland, 1998; Sherman and Guillery, 2001). Elongated and round-type synapses also widely occur a the level of corticocortial synapses (Rockland, 2002). Besides the different morphology of synaptic boutons, inputs to thalamic relay cells are not distributed evenly on their dendrites (Guillery, 1969; Wilson et al., 1984; Erişir et al., 1997). Retinal and parabrachial inputs are limited to proximal dendrites, while cortical inputs are located more distally. The SMART model captures these morphological and functional characteristics by concentrating driving connections in proximal dendrites, and modulatory connections with smaller synaptic weights in distal dendrites of the target cell. These characteristics are realized between neurons in the on-center/off-surround architecture implemented by inhibitory interneurons in cortical and thalamic areas.

4.9. *Stimuli and initial conditions*

Each cell compartment is initialized at the respective resting membrane potential (see Table 3 online for passive cable properties and ionic channels conductances). Bottom-up stimuli consist of static vertical or horizontal bars centered on the 9×9 receptor grid, and implemented via fixed depolarizing voltage clamp (holding potential=−12 mV; membrane resting potential/leakage=−60 mV) to 5 vertically or horizontally aligned thalamic specific relay neurons until a

stream of action potential is induced at a firing rate of 40 Hz. When indicated, top-down feedback is induced by injecting a stimulating current to the soma of a layer 6^{II} cortical cell. A typical run of the model consists of 100 ms epoch, or 1000 ms in recording of neural synchrony, with the membrane potentials of all neuronal compartments recorded along with the plastic synaptic weights configuration before and after the run.

4.10. Oscillations analysis

Power analysis of single or collective neural signals allows the extraction of information contained in different frequency ranges. Where indicated, analysis of 1000 ms epochs is performed separately in three different frequency ranges: 2–8 (delta and theta, δ and θ), 8–10 (alpha and beta, α and β) and 20–70 Hz (gamma, γ). The mean firing rate is subtracted from the data, and a Hamming window of 200 ms is applied to smooth the resulting values. The results are then Fourier transformed and multiplied with the complex conjugate (cross- and auto-components), and the inverse transformation is performed for selected, continuous frequency bins (corresponding to one "band"). In this way, it is possible to reconstruct a time-averaged firing rate for selected frequency ranges. These values can then be used to compute cross- and auto-correlations at different frequency ranges (Von Stein et al., 2000).

4.11. Local Field Potential and Current Source Density analysis

Cortical LFP and CSD are recorded via a simulated 54-tip-electrode. The distance of the electrode to the selected cell in the population is drawn from a uniform random distribution in the interval [10–200] μm, whereas the distance to all other cells in the layer is drawn from a uniform random distribution in the interval [10–1000] μm. An extracellular inward current flow towards the interior of the cell creates a current *sink*, while an outside flow creates a current *source* in a particular membrane section. Assuming an extracellular fluid with constant conductance, the potential generated by such current dipole is:

$$V_e = \frac{1}{4\pi\sigma}\left(\frac{I^+}{r^+} + \frac{I^-}{r^-}\right), \tag{30}$$

where *I*-s and *r*-s are currents and distances between the electrode and the point where the respective current flows through the membrane (approximated by the center of the compartment), respectively,+ and – mark the attributes of source and sink, respectively, and $\sigma = 15$ [mS/cm] is the extracellular conductivity. In the case of more complex cells with many possible sources and sinks, V_e becomes:

$$V_e = \frac{1}{4\pi\sigma}\sum_l \frac{I_l}{r_l}. \tag{31}$$

Compartmental trans-membrane currents I_l[μA] are expressed in terms of:

$$\begin{aligned} I_l = J_l S_l &= -\frac{g_l D_l}{4L_l^2}(V_l - V_{l\pm1})\left(2\frac{\pi D_l^2}{4} + \pi D_l L_l\right) \\ &= -\frac{g_l \pi D_l^2}{4L_l^2}(V_l - V_{l\pm1})\left(\frac{D_l}{2} + L_l\right). \end{aligned} \tag{32}$$

Since CSD and LFP can be measured with multiple electrodes, for each electrode tip the distance r_l to the compartment center is different. CSD is calculated both in experimental studies and in the present work by linear approximation of the second derivative of the voltage:

$$CSD = \frac{V_{e+1} + V_{e-1} - 2V_e}{\Delta x}, \tag{33}$$

where Δx is the distance between neighboring electrode tips.

4.12. Simulation environment

The model is implemented in KInNeSS (KDE Integrated NeuroSimulation Software, www.kinness.net), a software package that allows the simulation of single neurons with multiple compartments as well as large networks of such elements (Versace et al., 2007). All off-line data analysis is implemented in Matlab (Mathworks Inc.). Simulations are run on 2.80 GHz Intel CPU, 1 GB of RAM, under Linux operating system. The network is described in Neuro Markup Language code (NeuroML, http://www.neuroml.org/). NeuroML is a variation of XML designed for modeling different aspects and levels of neural systems, from intracellular mechanisms and ion channel kinetics to the dynamics of networks of reconstructed neurons. The code is downloadable in the Research section at http://www.kinness.net/.

Appendix A. Supplementary Table 4

Supplementary Table 4 associated with this article can be found, in the online version, at doi:10.1016/j.brainres.2008.04.024.

REFERENCES

Abbott, L.F., Sen, K., Varela, J.A., Nelson, S.B., 1997. Synaptic depression and cortical gain control. Science 275, 220–222.
Ahissar, M., Hochstein, S., 2002. View from the top: herarchies and reverse hierarchies in the visual system. Neuron 36, 791–804.
Ahmed, B., Anderson, J.C., Martin, K.A.C., Nelson, J.C., 1997. Map of the synapses onto layer 4 basket cells of the primary visual cortex of the cat. J. Comp. Neurol. 380, 230–242.
Alonso, J.M., Usrey, W.M., Redi, R.C., 2001. Rules of connectivity between geniculate cells and simple cells in cat primary visual cortex. J. Neurosci. 21, 4002–4015.
Banquet, J.P., Grossberg, S., 1987. Probing cognitive processes through the structure of event-related potentials during learning: An experimental and theoretical analysis. Appl. Opt. 26, 4931–4946.
Bazhenov, M., Timofeev, I., Steriade, M., Sejnowski, T.J., 1998. Computational models of thalamocortical augmenting responses. J. Neurosci. 18, 6444–6465.
Beierlein, M., Fall, C.P., Rinzel, J., Yuste, R., 2002. Thalamocortical bursts trigger recurrent activity in neocortical networks: layer 4 as a frequency-dependent gate. J. Neurosci. 22, 9885–9894.
Bi, G.Q., Poo, M., 2001. Synaptic modification by correlated activity: Hebb's postulate revisited. Annu. Rev. Neurosci. 24, 139–166.
Blasdel, G.G., Lund, J.S., 1983. Termination of afferent axons in macaque striate cortex. J. Neurosci. 3, 1389–1413.
Bosking, W., Zhang, Y., Schofield, B., Fitzpatrick, D., 1997. Orientation selectivity and the arrangement of horizontal

connections in tree shrew striate cortex. J. Neurosci. 17, 2112–2127.
Büchel, C., Dolan, R.J., Armony, J.L., Friston, K.J., 1999. Amygdala-hippocampal involvement in human aversive trace conditioning revealed through event-related functional magnetic resonance imaging. J. Neurosci. 19, 10869–10876.
Buffalo, E.A., Fries, P., Desimone, R., 2004. Layer-specific attentional modulation in early visual areas. Soc. Neurosci. Abstr. 30, 717–6.
Bullier, J., McCourt, M.E., Henry, G.H., 1988. Physiological studies on the feedback connection to the striate cortex from cortical areas 18 and 19 of the cat. Exp. Brain Res. 70, 90–98.
Bush, G., Luu, P., Posner, M.I., 2000. Cognitive and emotional influences in anterior cingulate cortex. Trends Cogn. Sci. 4, 215–222.
Callaway, E.M., 1998. Local cicrcuits in primary visual cortex of the macaque monkey. Annu. Rev. Neurosci. 21, 47–74.
Callaway, E.M., Wiser, A.K., 1996. Contributions of individual layer 2–5 spiny neurons to local circuits in macaque primary visual cortex. Vis. Neurosci. 13, 907–922.
Cao, Y., Grossberg, S., 2005. A laminar cortical model of stereopsis and 3D surface perception: Closure and da Vinci stereopsis. Spatial Vis. 18, 515–578.
Carpenter, G.A., Grossberg, S., 1987. A massively parallel architecture for a self-organizing neural pattern recognition machine. Comp. Vis. Graph. Image Proc. 37, 54–115.
Carpenter, G.A., Grossberg, S., 1990. ART 3: Hierarchical search using chemical transmitters in self-organizing pattern recognition architectures. Neural Netw. 3, 129–152.
Carpenter, G.A., Grossberg, S., 1991. Pattern Recognition by Self-organizing Neural Networks. MIT Press, Cambridge, MA.
Carpenter, G.A., Grossberg, S., 1993. Normal and amnesic learning recognition, and memory by a neural model of cortico-hippocampal interactions. Trends Neurosci. 16, 131–137.
Carpenter, G.A., Grossberg, S., Reynolds, J.H., 1991. ARTMAP: supervised real-time learning and classification of nonstationary data by a self-organizing neural network. Neural Netw. 4, 565–588.
Carpenter, G.A., Grossberg, S., Markuzon, N., Reynolds, J.H., Rosen, D.B., 1992. Fuzzy ARTMAP: a neural network architecture for incremental supervised learning of analog multidimensional maps. IEEE Trans. Neural Netw. 3, 698–713.
Carpenter, G.A., Martens, S., Ogas, O.J., 2005. Self-Organizing information fusion and hierarchical knowledge discovery: a new framework using ARTMAP neural networks. Neural Netw. 18, 287–295.
Cauller, L.J., 1995. Layer I of primary sensory neocortex: where top-down converges upon bottom-up. Behav. Brain Res. 71, 163–170.
Cauller, L.J., Connors, B.W., 1994. Synaptic physiology of horizontal afferents to layer I in slices of rat SI neocortex. J. Neurosci. 14, 751–762.
Cauller, L.J., Connors, B.W., 2001. Synaptic physiology of horizontal afferents to Layer I in slices of rat SI neocortex. J. Neurosci. 14, 751–762.
Clark, R.E., Squire, L.R., 1998. Classical conditioning and brain systems: the role of awareness. Science 280, 77–81.
Crabtree, J.W., Isaac, J.T., 2002. New intrathalamic pathways allowing modality-related and cross-modality switching in the dorsal thalamus. J. Neurosci. 22, 8754–8761.
Crick, F., 1984. Function of the thalamic reticular complex: the searchlight hypothesis. Proc. Natl. Acad. Sci. U. S. A. 81, 4586–4590.
Deadwyler, S.A., West, M.O., Lynch, G., 1979. Activity of dentate granule cells during learning: Differentiation of perforant path inputs. Brain Res. 169, 29–43.
Deadwyler, S.A., West, M.O., Robinson, J.H., 1981. Entorhinal and septal inputs differentially control sensory-evoked responses in the rate dentate gyrus. Science. 211, 1181–1183.
Desimone, R., 1998. Visual attention mediated by biased competition in extrastriate visual cortex. Phil. Trans. R. Soc. Lond. B. 353, 1245–1255.
Desimone, R., Duncan, J., 1995. Neural mechanisms of selective visual attention. Annu. Rev. Neurosci. 18, 193–222.
Destexhe, A., 2000. Modelling corticothalamic feedback and the gating of the thalamus by the cerebral cortex. J. Physiol. (Paris) 94, 391–410.
Destexhe, A., Contreras, D., Steriade, M., 1999. Cortically-induced coherence of a thalamic-generated oscillation. Neuroscience 92, 427–443.
Dinse, H.R., Kruger, K., 1994. The timing of processing along the visual pathway in the cat. Neuroreport 5, 893–897.
Douglas, R.J., Koch, C., Mahowald, M., Martin, K.A.C., Suarez, H.H., 1995. Recurrent excitation in neocortical circuits. Science 269, 981–985.
Engel, A.K., Fries, P., Singer, W., 2001. Dynamic predictions: oscillations and synchrony in top-down processing. Nat. Rev. Neurosci. 2, 704–716.
Erişir, A., Van Horn, S.C., Bickford, M.E., Sherman, S.M., 1997. Immunocytochemistry and distribution of parabrachial terminals in the lateral geniculate nucleus of the cat: a comparison with corticogeniculate terminals. J. Comp. Neurol. 377, 35–49.
Facon, E., Steriade, M., Wertheim, N., 1958. Prolonged hypersomnia caused by bilateral lesions of the medial activator system; thrombotic syndrome of the bifurcation of the basilar trunk. Rev. neurol. (Paris) 98, 117–133.
Fitzpatrick, D., Lund, J.S., Blasdel, G.G., 1985. Intrinsic connections of macaque striate cortex: afferent and efferent connections of lamina 4C. J. Neurosci. 5, 3329–3349.
Friedman-Hill, S., Maldonado, P.E., Gray, C.M., 2000. Dynamics of striate cortical activity in the alert macaque: I. Incidence and stimulus-dependence of gamma-band neuronal oscillations. Cereb. Cortex 10, 1105–1116.
Fries, P., Reynolds, J.H., Rorie, A.E., Desimone, R., 2001. Modulation of oscillatory neuronal synchronization by selective visual attention. Science 291, 1560–1563.
Gao, E., Suga, N., 1998. Experience-dependent corticofugal adjustment of midbrain frequency map in bat auditory system. Proc. Natl. Acad. Sci. U. S. A. 95, 12663–12670.
Gorchetchnikov, A., Grossberg, S., 2007. Space, time, and learning in the hippocampus: how fine spatial and temporal scales are expanded into population codes for behavioral control. Neural Netw. 20, 182–193.
Gorchetchnikov, A., Versace, M., Hasselmo, M.E., 2005a. A model of STDP based on spatially and temporally local information: derivation and combination with gated decay. Neural Netw. 18, 458–466.
Gorchetchnikov, A., Versace, M., Hasselmo, M.E., 2005b. Spatially and temporally local spike-timing-dependent plasticity rule. Proc. Int. Jt. Conf. Neural Netw. 1568, 390–396.
Gove, A., Mingolla, E., Grossberg, S., 1995. Brightness perception, illusory contours, and corticogeniculate feedback. Vis. Neurosci. 12, 1027–1052.
Grieve, K.L., Sillito, A.M., 1991. The length summation properties of layer VI cells in the visual cortex and hypercomplex cell end zone inhibition. Exp. Brain. Res. 84, 319–325.
Grossberg, S., 1975. A neural model of attention, reinforcement, and discrimination learning. Internatl. Rev. Neurobiol. 18, 263–327.
Grossberg, S., 1976. Adaptive pattern classification and universal recoding, II: Feedback, expectation, olfaction, and illusions. Biol. Cybern. 20, 69–98.
Grossberg, S., 1978. A theory of human memory: self-organization and performance of sensory-motor

codes, maps, and plans. In: Rosen, R., Snell, F. (Eds.), Progress in theoretical biology, Volume 5. Academic Press, NY, pp. 233–374.
Grossberg, S., 1980. How does a brain build a cognitive code? Psych. Rev. 87, 1–51.
Grossberg, S., 1982. A psychophysiological theory of reinforcement, drive, motivation, and attention. J. Theoret. Neurobiol. 1, 286–369.
Grossberg, S., 1984. Some psychophysiological and pharmacological correlates of a developmental, cognitive, and motivational theory. In: Karrer, R., Cohen, J., Tueting, P. (Eds.), Brain and Information: Event Related Potentials. NY Acad. Sci. pp. 58–142. New York.
Grossberg, S., 1994. 3-D vision and figure-ground separation by visual cortex. Percept. Psychophys. 55, 48–120.
Grossberg, S., 1995. The attentive brain. Amer. Scientist, 83, 438–449.
Grossberg, S., 1999a. How does the cerebral cortex work? Learning, attention, and grouping by the laminar circuits of visual cortex. Spat. Vis. 12, 163–187.
Grossberg, S., 1999b. The link between brain learning, attention, and consciousness. Conscious. Cogn. 8, 1–44.
Grossberg, S., 2000. How hallucinations may arise from brain mechanisms of learning, attention, and volution. J. Int. Neuropsych. Soc. 6, 579–588.
Grossberg, S., 2003. How does the cerebral cortex work? Development, learning, attention, and 3D vision by laminar circuits of visual cortex. Behav. Cogn. Neur. Rev. 2, 47–76.
Grossberg, S., Stone, G.O., 1986. Neural dynamics of word recognition and recall: attentional priming, learning, and resonance. Psych. Rev. 93, 46–74.
Grossberg, S., Schmajuk, N.A., 1989. Neural dynamics of adaptive timing and temporal discrimination during associative learning. Neural Netw. 2, 79–102.
Grossberg, S., Merrill, J.W.L., 1992. A neural network model of adaptively timed reinforcement learning and hippocampal dynamics. Cog. Brain Res. 1, 3–38.
Grossberg, S., Merrill, J.W.L., 1996. The hippocampus and cerebellum in adaptively timed learning, recognition, and movement. J. Cogn. Neurosci. 8, 257–277.
Grossberg, S., Yazdanbakhsh, A., 2005. Laminar cortical dynamics of 3D surface perception: stratification, transparency, and neon color spreading. Vision Res. 45, 1725–1743.
Grossberg, S., Seidman, D., 2006. Neural dynamics of autistic behaviors: Cognitive, emotional, and timing substrates. Psych. Rev. 113, 483–525.
Guillery, R.W., 1969. An abnormal retinogeniculate projection in Siamese cats. Brain Res. 3, 739–741.
Guillery, R.W., Harting, J.K., 2003. Structure and connections of the thalamic reticular nucleus: advancing views over half a century. J. Comp. Neurol. 463, 360–371.
Guillery, R.W., Feig, S.L., Lozsadi, D.A., 1998. Paying attention to the thalamic reticular nucleus. Trends Neurosci. 21, 28–32.
Hasselmo, M.E., 1993. Acetylcholine and learning in a cortical associative memory. Neural Comput. 5, 32–44.
Hasselmo, M.E., 1995. Neuromodulation and cortical function: modeling the physiological basis of behavior. Behav. Brain Res. 67, 1–27.
Heeger, D.J., 1992. Normalization of cell responses in cat striate cortex. Vis. Neurosci. 9, 181–197.
Heilman, K.M., Bowers, D., Valenstein, E., Watson, R.T., 1993. Disorders of visual attention. Baillière's clin. neurol. 2, 389–413.
Herrmann, C.S., Munk, M.H.J., Engel, A., 2004. Cognitive functions of gamma-band activity: memory match and utilization. Trends Cognit. Sci. 8, 347–355.
Hille, B., 2001. Ion Channels of Excitable Membranes, Third Edition. Sinauer Associates, MA, USA.
Hodgkin, A.L., Huxley, A.F., 1952. A quantitative description of membrane current and its application to conduction and excitation in nerve. J. Neurophysiol. 117, 500–544.
Holroyd, C.B., Nieuwenhuis, S., Mars, R.B., Coles, M.G.H., 2004. Anterior cingulate cortex, selection for action, and error processing. In: Posner, M.I. (Ed.), Cognitive Neuroscience of Attention. Guilford Publication, Inc, New York, pp. 219–231.
Ichinohe, N., Fujiyama, F., Kaneko, T., Rockland, K.S., 2003. Honeycomb-like mosaic at the border of layers 1 and 2 in the cerebral cortex. J. Neurosci. 23, 1372–1382.
Johnston, D., Hoffman, D.A., Colbert, C.M., Magee, J.C., 1999. Regulation of back-propagating action potentials in hippocampal neurons. Curr. Opin. Neurobiol. 9, 288–292.
Jones, E.G., 2002. Thalamic circuitry and thalamocortical synchrony. Phil. Trans. R. Soc. Lond. B. 357, 1659–1673.
Karmos, G., Molnár, M., Csépe, V., Winkler, I., 1986. Evoked potential components in the layers of the auditory cortex of the cat. Acta neurobiol. exp. 46, 227–236.
Kilgard, M.P., Merzenich, M.M., 1998. Cortical map reorganization enabled by nucleus basalis activity. Science. 279, 1714–1718.
Kolmac, C.I., Mitrofanis, J., 1997. Organisation of the reticular thalamic projection to the intralaminar and midline nuclei in rats. J. Comp. Neurol. 377, 165–178.
Kopell, N., Ermentrout, G.B., Whittington, M.A., Traub, R.D., 2000. Gamma rhythms and beta rhythms have different synchronization properties. Proc. Natl. Acad. Sci. U. S. A. 15, 1867–1872.
Kraus, N., McGee, T., Littman, T., Nicol, T., King, C., 1994. Nonprimary auditory thalamic representation of acoustic change. J. Neurophysiol. 72, 1270–1277.
Krupa, D.J., Ghazanfar, A.A., Nicolelis, M.A.L., 1999. Immediate thalamic sensory plasticity depends on corticothalamic feedback. Proc. Natl. Acad. Sci. U. S. A. 96, 8200–8205.
Kumaran, D., Maguire, E.A., 2007a. Which computational mechanisms operate in the hippocampus during novelty detection? Hippocampus. 17, 735–748.
Kumaran, D., Maguire, E.A., 2007b. Match–mismatch processes underlie human hippocampal responses to associative novelty. J. Neurosci. 27, 8517–8524.
Landisman, C.E., Long, M.E., Beierlein, M., Deans, M.R., Paul, D.L., Connors, B.W., 2002. Electrical synapses in the thalamic reticular nucleus. J. Neurosci. 22, 1002–1009.
Larkum, M.E., Zhu, J.J., 2002. Signaling of Layer 1 and whisker-evoked Ca^{++} and Na^{++} action potentials in distal and terminal dendrites of rat neocortical pyramidal neurons in vitro and in vivo. J. Neurosci. 22, 6991–7005.
Larkum, M.E., Zhu, J.J., Sakmann, B.A., 1999. A new cellular mechanism for coupling inputs arriving at different cortical layers. Nature. 398, 338–341.
Larkum, M.E., Zhu, J.J., Sakmann, B.A., 2002. Signaling of Layer 1 and whisker-evoked Ca^{++} and Na^{++} action potentials in distal and terminal dendrites of rat neocortical pyramidal neurons in vitro and in vivo. J. Neurosci. 22, 6991–7005.
Larkum, M.E., Senn, W., Lusher, H.R., 2004. Top-down dendritic input increases the gain of layer 5 pyramidal neurons. Cereb. Cortex 14, 1059–1070.
Levy, W.B., Steward, O., 1983. Temporal contiguity requirements for long-term associative potentiation/depression in the hippocampus. Neuroscience 8, 791–797.
Llinas, R.R., Pare, D., 1991. Of dreaming and wakefulness. Neuroscience 44, 521–535.
Llinas, R.R., Leznik, E., Urbano, F.J., 2002. Temporal binding via cortical coincidence detection of specific and nonspecific thalamocortical inputs: a voltage-dependent dye-imaging study in mouse brain slices. Proc. Natl. Acad. Sci. U. S. A. 99, 449–454.
Lumer, E.D., Edelman, G.M., Tononi, G., 1997. Neural dynamics in a model of the thalamocortical system I. Layers, loops and the emergence of fast synchronous rhythms. Cereb. Cortex 7, 207–227.

Luu, P., Pederson, S.M., 2004. The anterior cingulate cortex: regulating actions in context. In: Posner, M.I. (Ed.), Cognitive neuroscience of attention. Guilford Publication, Inc, New York.
Markram, H., Lubke, J., Frotscher, M., Sakmann, B., 1997. Regulation of synaptic efficacy by coincidence of postsynaptic APs and EPSPs. Science 275, 213–215.
Markram, H., Toledo-Rodriguez, M., Wang, Y., Gupta, A., Silberberg, G., Wu, C., 2004. Interneurons of the neocortical inhibitory system. Nat. Rev. Neurosci. 5, 793–807.
Maunsell, J.H.R., Van Essen, D.C., 1983. Anatomical connections of the middle temporal visual area in the macaque monkey and their relationship to a hierarchy of cortical areas. J. Neurosci. 3, 2563–2586.
McCormick, D.A., Prince, D.A., 1985. Two types of muscarinic response to acetylcholine in mammalian cortical neurones. Proc. Natl. Acad. Sci. U. S. A. 82, 6344–6349.
McGuire, B.A., Hornung, J.P., Gilbert, C.D., Wiesel, T.N., 1984. Patterns of synaptic input to layer 4 of cat striate cortex. J. Neurosci. 4, 3021–3033.
McGuire, B.A., Gilbert, C.D., Rivlin, P.K., Wiesel, T.N., 1991. Targets of horizontal connections in macaque primary visual cortex. J. Comp. Neurol. 305, 370–392.
Miller, R., 1996. Corticothalamic interplay and the security of operation of neural assemblies and temporal chains in the cerebral cortex. Biol. Cybern. 75, 263–275.
Miller, J.M., Benevento, L.A., 1979. Demonstration of a direct projection from the intralaminar central lateral nucleus to the primary visual cortex. Neurosci. Lett. 14, 229–234.
Montero, V.M., 1997. C-fos induction in sensory pathways of rats exploring a novel environment: shifts of active thalamic reticular sectors by predominant sensory cues. Neuroscience 76, 1069–1081.
Murphy, P.C., Duckett, S.G., Sillito, A.M., 1999. Feedback connections to the lateral geniculate nucleus and cortical response properties. Science 286, 1552–1554.
Näätänen, R., Gaillard, A.W.K., Mäntysalo, S., 1978. Early selective attention effect on evoked potential reinterpreted. Acta psychol. 42, 313–329.
Nicolelis, M.A., Fanselow, E.E., 2002. Dynamic shifting in thalamocortical processing during different behavioural states. Phil. Trans. R. Soc. Lond. B. 357, 1753–1758.
O'Keefe, J., Nadel, L., 1978. The Hippocampus as a Cognitive Map. Oxford University Press, New York.
Olufsen, M.S., Whittington, M.A., Camperi, M., Kopell, N., 2003. New roles for the gamma rhythm: population tuning and preprocessing for the beta rhythm. J. Comput. Neurosci. 14, 33–54.
Otto, T., Eichenbaum, H., 1992. Neuronal activity in the hippocampus during delayed non-match to sample performance in rats: evidence for hippocamp processing in recognition memory. Hippocampus. 2, 323–334.
Pakhomova, A.S., 1981. Neurophysiol. 13, 267–273.
Pinault, D., Deschenes, M., 1998. Anatomical evidence for a mechanism of lateral inhibition in the rat thalamus. E. J. Neurosci., 10, 3462–3469.
Pollen, D.A., 1999. On the neural correlates of visual perception. Cereb. Cortex 9, 4–19.
Raizada, R.D.S., Grossberg, S., 2003. Towards a theory of the laminar architecture of cerebral cortex: computational clues from the visual system. Cereb. Cortex. 13, 100–113.
Rall, W., 1962. Theory of physiological properties of dendrites. Ann. N. Y. Acad. Sci. 96, 1071–1092.
Reid, R.C., Alonso, J.M., 1995. Specificity of monosynaptic connections from thalamus to visual cortex. Nature 378, 281–284.
Rockland, K.S., 1996. Two types of cortico-pulvinar terminations: round, type 2 and elongate, type 1. J. Comp. Neurol. 368, 57–87.
Rockland, K.S., 1998. Convergence and branching patterns of round, Type 2 corticopulvinar axons. J. Comp. Neurol. 390, 515–536.
Rockland, K.S., 2002. Visual cortical organization at the single axon level: a beginning. Neurosci. res. 42, 155–166.
Rockland, K.S., Virga, A., 1989. Terminal arbors of individual "feedback" axons projecting from area V2 to V1 in the macaque monkey: a study using immunohistochemistry of anterogradelly transported *Phaseolus vulgaris* leucoagglutinin. J. Comp. Neurol. 285, 54–72.
Rockland, K.S., Andresen, J., Cowie, R.J., Robinson, D.L., 1999. Single axon analysis of pulvinocortical connections to several visual areas in the macaque. J. Comp. Neurol. 406, 221–250.
Roelfsema, P.R., Engel, A.K., König, P., Singer, W., 1997. Visuomotor integration is associated with zero time-lag synchronization among cortical areas. Nature 385, 157–161.
Rosburg, T., Trautner, P., Ludowig, E., Schaller, C., Kurthen, M., Elger, C.E., Boutros, N.N., 2007. Hippocampal event-related potentials to tone duration deviance in a passive oddball paradigm in humans. Neuroimage 37, 274–281.
Rouiller, E.M., Welker, E., 2000. A comparative analysis of the morphology of corticothalamic projections in mammals. Brain Res. Bull. 53, 727–741.
Saar, D., Grossman, Y., Barkai, E., 2001. Long-lasting cholinergic modulation underlies rule learning in rats. J. Neurosci. 21, 1385–1392.
Salin, P.A., Bullier, J., 1995. Corticocortical connections in the visual system: structure and function. Physiol. Rev. 75, 107–154.
Sánchez-Montañés, M.A., Verschure, P.F.M.J., König, P., 2000. Local and global gating of synaptic plasticity. Neural Comput. 13, 543–552.
Schmidt, K.E., Goebel, R., Löwel, S., Singer, W., 1997. The perceptual grouping criterion of colinearity is reflected by anisotropies of connections in the primary visual cortex. Eur. J. Neurosci. 9, 1083–1089.
Schmolesky, M.T., Wang, Y., Hanes, D.P., Thompson, K.G., Leutgeb, S., Schall, J.D., Leventhal, A.G., 1998. Signal timing across the macaque visual system. J. Neurophysiol. 6, 3272–3278.
Sherman, S.M., Guillery, R., 2001. Exploring the Thalamus. Academic Press, San Diego.
Sherman, S.M., Guillery, R.W., 2002. The role of the thalamus in the flow of information to the cortex. Phil. Trans. R. Soc. Lond. B. 357, 1695–1708.
Shipp, S., 2003. The functional logic of cortico-pulvinar connections. Phil. Trans. R. Soc. Lond. B. 358, 1605–1624.
Siegel, M., Körding, K.P., König, P., 2000. Integrating top-down and bottom-up sensory processing by somato-dendritic interactions. J. Comput. Neurosci. 8, 161–173.
Sillito, A.M., Jones, H.E., Gerstein, G.L., West, D.C., 1994. Feature-linked synchronization of thalamic relay cell firing induced by feedback from the visual cortex. Nature 369, 479–482.
Singer, W., 1999. Neuronal synchrony: a versatile code for the definition of relations? Neuron 24, 49–65.
Singer, W., Rauschecker, J.P., 1982. Central core control of development plasticity in the kitten visual cortex. II: Electrical activation of mesencephalic and diencephalic projections. Exp. Brain. Res. 47, 223–233.
Soares, J.G.M., Diogo, A.C.M., Fiorani, M., Souza, A.P.B., Gattass, R., 2004. Effects of inactivation of the lateral pulvinar on response properties of second visual area cells in cebus monkeys. Clin. Exp. Pharmacol. Physiol. 31, 580–590.
Sohal, V.S., Huguenard, J.R., 2003. Inhibitory interconnections control burst pattern and emergent network synchrony in reticular thalamus. J. Neurosci. 23, 8978–8988.
Solomon, P.R., Vander Schaaf, E.R., Thompson, R.F., Weisz, D.J., 1986. Hippocampus and trace conditioning of the rabbit's

classically conditioned nictitating membrane response. Behav. Neurosci. 100, 729–744.
Steriade, M., Contreras, D., Curro Dossi, R., Nunez, A., 1993. The slow,<1 Hz oscillation in reticular thalamic and thalamocortical neurons: scenario of sleep rhythm generation in interacting thalamic and neocortical networks. J. Neurosci. 13, 3284–3299.
Stratford, K.J., Tarczy-Hornoch, K., Martin, K.A.C., Bannister, N.J., Jack, J.J.B., 1996. Excitatory synaptic inputs to spiny stellate cells in cat visual cortex. Nature 382, 258–261.
Swadlow, H.A., Gusev, A.G., Bezdudnaya, T., 2002. Activation of a cortical column by a thalamocortical impulse. J. Neurosci. 22, 7766–7773.
Tamas, G., Somogyi, P., Buhl, E.H., 1998. Differentially interconnected networks of GABAergic interneurons in the visual cortex of the cat. J. Neurosci. 18, 4255–4270.
Traub, R.D., Miles, R., 2001. Neuronal networks of the hippocampus. Cambridge University Press, Cambridge, UK.
Traub, R.D., Spruston, N., Soltesz, I., Konnerth, A., Whittington, M.A., Jefferys, G.R., 1998. Gamma-frequency oscillations: a neuronal population phenomenon, regulated by synaptic and intrinsic cellular processes, and inducing synaptic plasticity. Prog. Neurobiol. 55, 563–575.
Tsodyks, M., Markram, H., 1997. The neural code between neocortical pyramidal neurons depends on neurotransmitter release probability. Proc. Natl. Acad. Sci. U. S. A. 94, 719–723.
Turrini, P., Casu, M.A., Wong, T.P., De Koninck, Y., Ribeiro-da-Silva, A., Cuello, A.C., 2001. Cholinergic nerve terminals establish classical synapses in the rat cerebral cortex: synaptic pattern and age-related atrophy. Neuroscience. 105, 277–285.
Usrey, W.M., 2002. The role of spike timing for thalamocortical processing. Curr. Opin. Neurobiol. 12, 411–417.
van Der Werf, Y.D., Witter, M.P., Groenewegen, H.J., 2002. The intralaminar and midline nuclei of the thalamus. Anatomical and functional evidence for participation in processes of arousal and awareness. Brain res. Brain Res. Rev. 39, 107–140.
van Der Werf, Y.D., Scheltens, P., Lindeboom, J., Witter, M.P., Uylings, H.B., Jolles, J., 2003. Deficits of memory, executive functioning and attention following infarction in the thalamus; a study of 22 cases with localised lesions. Neuropsychologia 41, 1330–1344.
Van Essen, D.C., Newsome, W.T., Maunsell, J.H., Bixby, J.L., 1986. The projections from striate cortex, V1 to areas V2 and V3 in the macaque monkey: asymmetries, areal boundaries, and patchy connections. J. Comp. Neurol. 244, 451–480.
Versace, M., Ames, A., Leveille, J., Fortenberry, B., Mhatre, H., Gorchetchnikov, A., 2007. KInNeSS: A modular framework for computational neuroscience. CAS/CNSTR-07-007. Submitted to Neuroinformatics.
Vinogradova, O.S., 1975. Functional organization of the limbic system in the process of registration of information: Facts and hypotheses. In: Isaacson, R.L., Pribram, K.H. (Eds.), The Hippocampus, vol. 2. Plenum, New York, pp. 3–69.
Vogt, B.A., 1991. The role of layer I in cortical function. In: Peters, A., Jones, E. (Eds.), Cerebral Cortex. Plenum, New York,pp. 49–79.
Von Stein, A., Chiang, C., König, P., 2000. Top-down processing mediated by interareal synchronization. Proc. Natl. Acad. Sci. U. S. A. 97, 14748–14753.
Wang, S., Eisenback, M.A., Bickford, M.E., 2002. Relative distribution of synapses in the pulvinar nucleus of the cat: implications regarding the "driver/modulator" theory of thalamic function. J. Comp. Neurol. 454, 482–494.
Weese, G.D., Phillips, J.M., Brown, V.J., 1999. Attentional orienting is impaired by unilateral lesions of the thalamic reticular nucleus in the rat. J. Neurosci. 19, 1035–10139.
Wespatat, V., Tennigkeit, F., Singer, W., 2004. Phase sensitivity of synaptic modifications in oscillating cells of rat visual cortex. J. Neurosci. 24, 9067–9075.
Williams, S.R., Stuart, G.J., 1999. Mechanisms and consequences of action potential burst firing in rat neocortical pyramidal neurons. J. Neurophysiol. 521, 467–482.
Wilson, J.R., Friedlander, M.J., Sherman, S.M., 1984. Fine structural morphology of identified X-and Y-cells in the cat's lateral geniculate nucleus. Phil. Trans. R. Soc. Lond. B. 221, 411–436.
Yazdanbakhsh, A., Grossberg, S., 2004. Fast synchronization of perceptual grouping in laminar visual cortical circuits. Neural Netw. 17, 707–718.
Zeki, S., Shipp, S., 1988. The functional logic of cortical connections. Nature 335, 311–317.
Zhang, Y.Q., Lu, S.G., Ji, J.P., Zhao, Z.Q., Mei, J., 2004. Electrophysiological and pharmacological properties of nucleus basalis magnocellularis neurons in rats. Acta pharmacologica Sinica 25, 161–170.